

Electronic Theses and Dissertations, 2004-2019

2005

Adapting The Modified Cam Clay Constitutive Model To The Computational Analysis Of Dense Granular Soils

Jose Arvelo
University of Central Florida

 Part of the [Civil Engineering Commons](#)
Find similar works at: <https://stars.library.ucf.edu/etd>
University of Central Florida Libraries <http://library.ucf.edu>

This Masters Thesis (Open Access) is brought to you for free and open access by STARS. It has been accepted for inclusion in Electronic Theses and Dissertations, 2004-2019 by an authorized administrator of STARS. For more information, please contact STARS@ucf.edu.

STARS Citation

Arvelo, Jose, "Adapting The Modified Cam Clay Constitutive Model To The Computational Analysis Of Dense Granular Soils" (2005). *Electronic Theses and Dissertations, 2004-2019*. 526.
<https://stars.library.ucf.edu/etd/526>

ADAPTING THE MODIFIED CAM CLAY CONSTITUTIVE MODEL TO THE
COMPUTATIONAL ANALYSIS OF DENSE GRANULAR SOILS

by

JOSE ALEJANDRO ARVELO G.
B.S. Catholic Andres Bello University, 1994

A thesis submitted in partial fulfillment of the requirements
for the degree of Master of Science
in the department of Civil and Environmental Engineering
in the college of Engineering and Computer Science
at the University of Central Florida
Orlando, Florida

Fall Term
2005

ABSTRACT

The computational constitutive Modified Cam Clay Model (MCCM) was developed at Cambridge to study the behavior of clays and has been proven to be effective. In this study, this model is extended to the case of dense sands to analyze the accuracy of the stress-strain behavior. This analysis is based on triaxial test data applied to remolded and compacted sand samples under drained conditions.

The laboratory triaxial tests were performed by the Florida Department of Transportation to research the permeability effect in sandy soils compacted up to 95% of maximum unit weight at the optimum moisture content. Each soil sample was tested using different stress paths. In addition, these data were also used to obtain the soil parameters. These soil parameters are used as input data for the Modified Cam Clay Model.

Moreover, a computer program in MATLAB was developed based on the MCCM constitutive theory and application in order to predict the stress-strain response for overconsolidated soils under drained condition. Based on observations of the qualitative behavior of these soils, a modification is proposed in this thesis to the original constitutive model to improve the predicted stress-strain behavior.

The results of the computer program are typically presented in the deviatoric stress versus shear strain and the stress path plane (deviatoric stress versus mean effective stress). These are the principal plots used for the behavior prediction of soil specimens. Furthermore, the results of the computer program were compared to the laboratory

triaxial test data. In general, it is may be concluded that, MCCM with some modification, is applicable to dense sands.

To my Parents, Brothers, and specially My Wife and Son

ACKNOWLEDGMENTS

I would like to express my sincere gratitude to my advisor, Professor Dr. Manoj B. Chopra, who patiently guided and encouraged me during the course of this thesis. I also want to thank Mr. Ben Watson of Florida Department of Transportation (FDOT) for his kindness to support the essential data used in this thesis.

Special thank is due to Dr. Frank Townsend of University of Florida for his contribution with additional triaxial test data. I wish to thank Mr. Sergio Sanchez for his participation during the computer program work in this research. Finally, I am grateful to my colleagues that have encouraged me and brought their knowledge during the course of this thesis.

TABLE OF CONTENTS

LIST OF TABLES	ix
LIST OF FIGURES	x
CHAPTER I INTRODUCTION.....	119
SCOPE OF WORK.....	120
CHAPTER II FUNDAMNETAL CONCEPTS IN SOIL MECHANICS	122
CRITICAL STATE SOIL MECHANICS.....	122
CRITICAL STATE LINE AND QUALITATIVE SOIL RESPONSE IN SANDS AND OTHER GRANULAR MATERIALS.....	126
PEAK STRENGTHS FOR SAND	128
MOHR-COULOMB FAILURE CRITERIA	130
THE ROSCOE SURFACE	131
ELASTIC-PLASTIC MODEL FOR SOILS	133
<i>Elastic Volumetric and Shear Strains</i>	134
<i>Plastic Volumetric Strains and Plastic Hardening</i>	137
<i>Plastic Shear Strains</i>	140
<i>Plastic Potentials</i>	140
<i>Normality or Associated Flow</i>	142
SUMMARY	143
CHAPTER III COMPUTATIONAL MODEL FOR DENSE SANDS	145
GENERAL	145
MODIFIED CAM-CLAY MODEL (MCCM)	146

<i>The Modified Cam Clay Predictions for Conventional Triaxial Tests</i>	150
<i>Predictions for Conventional Triaxial Compression Test under Drained Condition</i>	151
<i>Predictions on Highly Over Consolidated Soils</i>	152
THE MODIFIED CAM CLAY MODEL IN MATLAB	154
ADAPTING MCCM TO PREDICTION OF DENSE GRANULAR SOIL BEHAVIOR	158
CHAPTER IV TEST RESULTS	166
GENERAL	166
MATERIAL PROPERTIES	166
<i>Internal Angle of Friction (ϕ')</i>	167
<i>Initial Void Ratio (e_0)</i>	169
<i>Past Maximum Effective Pressure (σ'_{max})</i>	170
<i>Swelling Index (κ)</i>	172
<i>Compression Index (λ)</i>	174
<i>Poisson's Ratio (ν)</i>	175
<i>Young's Modulus (E')</i>	177
TRIAXIAL TEST RESULTS	179
DATA ANALYSIS AND COMPUTATION	182
ANALYSIS OF THE TEST RESULTS	183
<i>Stress Invariants "q and p"</i>	184
<i>Shear Strain (ϵ_q) Prediction</i>	199
CHAPTER V CONCLUSIONS AND RECOMMENDATIONS	225

Summary and Conclusions	225
Recommendations for Future Work.....	227
Appendix A.....	229
Appendix B.....	255
Appendix C.....	327
REFERENCES	338

LIST OF TABLES

TABLE 1	INTERNAL FRICTION ANGLES (ϕ')	169
TABLE 2	INITIAL VOID RATIO (e_0)	170
TABLE 3	PAST MAXIMUM EFFECTIVE PRESSURE (σ'_{MAX}).....	172
TABLE 4	COMPRESSION AND SWELLING INDEXES	176
TABLE 5	YOUNG'S MODULUS (E').....	178
TABLE 6	STRESS INVARIANTS	181
TABLE 7	PEAK AND FAILURE STRESSES	188
TABLE 8	SHEAR STRAIN (MCCM PREDICTION).....	201
TABLE 9	SHEAR STRAIN (ADAPTED MODEL)	207

LIST OF FIGURES

FIGURE 1: THREE-DIMENSIONAL VIEW OF NORMAL COMPRESSION LINE (NCL), CRITICAL STATE LINE (CSL), AND SERIES OF CAM CLAY YIELD LOCI (MODIFIED FROM WOOD, 1990).....	123
FIGURE 2: CRITICAL STATE LINE IN THE (Q:P') PLANE (MODIFIED FROM WOOD, 1990) ..	124
FIGURE 3: THE CRITICAL STATE LINE ON THE V-LN(P') SPACE (MODIFIED FROM WOOD, 1990).....	125
FIGURE 4: EFFECT OF SHEARING ON THE VOLUME OF DENSE AND LOOSE SANDS. (MODIFIED FROM LANCELLOTTA,1995)	127
FIGURE 5: POINTS OF PEAK DEVIATOR STRESSES "Q" IN CONVENTIONAL DRAINED TRIAXIAL COMPRESSION TESTS ON ISOTROPICALLY OVERCONSOLIDATED SAMPLES. (LANCELLOTTA,1995)	129
FIGURE 6: MOHR-COULOMB FAILURE CRITERION IN TERMS OF "Q AND P'"	131
FIGURE 7: PROJECTION OF ROSCOE, HVORSLEV, AND TENSILE FAILURE SURFACE IN 3-D SPACE	132
FIGURE 8: PROJECTION OF ROSCOE SURFACE IN "Q- P'" SPACE	133
FIGURE 9: YIELD SURFACE IN "Q - P'" SPACE (MODIFIED FROM WOOD, 1990)	135
FIGURE 10: NORMAL COMPRESSION LINE AND UNLOADING-RELOADING LINE IN SEMI-LOGARITHMIC PLOT (MODIFIED FROM WOOD, 1990).....	136
FIGURE 11: EXPANSION OF YIELD LOCUS AND CHANGE IN VOLUME ASSOCIATED (MODIFIED FROM WOOD 1990).....	138
FIGURE 12: PLASTIC STRAIN INCREMENT VECTOR NORMAL TO PLASTIC POTENTIAL CURVES (MODIFIED FROM WOOD, 1990).....	141
FIGURE 13: FAMILIES OF PLASTIC POTENTIAL (DASHED) AND YIELD LOCUS (SOLID) (MODIFIED FROM WOOD,1990).....	142
FIGURE 14: NORMALITY OR ASSOCIATED FLOW RULE(MODIFIED FROM WOOD 1990) ...	143
FIGURE 15: MODIFIED CAM CLAY MODEL (AFTER WOOD, 2000).....	148
FIGURE 16: STRESS PATH "Q - P'" SPACE FOR DRAINED CONDITIONS (AFTER WOOD, 1990)	152
FIGURE 17: TYPICAL PLOTS UNDER DRAINED CONDITIONS IN HIGHLY OVERCONSOLIDATED SOILS (AFTER WOOD, 1990)	153
FIGURE 18: FLOW CHART 1	157
FIGURE 19: TYPICAL "E VS. Q" PLOT IN DENSE SAND	159
FIGURE 20: TYPICAL "E VS. E _Q " PLOT IN DENSE SAND	159
FIGURE 21: TYPICAL "N VS. E _Q " PLOT IN DENSE SAND.....	160
FIGURE 22: TYPICAL "E _A VS. E _N " PLOT FOR DENSE SANDS DURING SOFTENING	162
FIGURE 23: TYPICAL "E VS. LN(P ₀ ')" PLOT FOR DENSE SANDS DURING SOFTENING.....	162
FIGURE 24: FLOW CHART 2.....	165
FIGURE 25: MOHR-COULOMB ENVELOPE AND Kf FAILURE ENVELOPE	168
FIGURE 26: CAM CLAY ELLIPSE AND "Q VS. P'" STRESS PATH.....	171
FIGURE 27: TYPICAL "E-LN(P') " PLOT	173
FIGURE 28: TYPICAL "E-LNP'" PLOT FOR DENSE SANDS.....	174
FIGURE 29: TYPICAL "E-LNP ₀ '" PLOT FOR DENSE SANDS	175
FIGURE 30: TYPICAL "Q- E _A " PLOT FOR DENSE SANDS	177

FIGURE 31: MCCM TYPICAL PLOTS UNDER DRAINED CONDITIONS IN HIGHLY OVERCONSOLIDATED SOILS (AFTER WOOD, 1990)	179
FIGURE 32: “Q- ϵ_Q ” VALUES AT PEAK AND FAILURE POINTS.....	182
FIGURE 33: TYPICAL PLOTS FOR DENSE SANDS	184
FIGURE 34: PEAK SHAPE EFFECT	186
FIGURE 35: ULTIMATE OR FAILURE DEVIATOR STRESS	186
FIGURE 36: STRESS PATH, PEAK AND ULTIMATE OR FAILURE STRESSES	189
FIGURE 37: STRESS PATH, PEAK AND ULTIMATE OR FAILURE STRESSES	190
FIGURE 38: STRESS PATH, PEAK AND ULTIMATE OR FAILURE STRESSES	191
FIGURE 39: STRESS PATH, PEAK AND ULTIMATE OR FAILURE STRESSES	192
FIGURE 40: STRESS PATH, PEAK AND ULTIMATE OR FAILURE STRESSES	193
FIGURE 41: STRESS PATH, PEAK AND ULTIMATE OR FAILURE STRESSES	194
FIGURE 42: STRESS PATH, PEAK AND ULTIMATE OR FAILURE STRESSES	195
FIGURE 43: STRESS PATH, PEAK AND ULTIMATE OR FAILURE STRESSES	196
FIGURE 44: STRESS PATH, PEAK AND ULTIMATE OR FAILURE STRESSES	197
FIGURE 45: STRESS PATH, PEAK AND ULTIMATE OR FAILURE STRESSES	198
FIGURE 46: MCCM VOLUMETRIC DEFORMATION ON HIGHLY OVERCONSOLIDATED SOILS	202
FIGURE 47: TYPICAL VOLUMETRIC DEFORMATION ON DENSE SANDS	202
FIGURE 48: EXPANSION VOLUMETRIC AND DEVIATOR STRESS ON DENSE SANDS	203
FIGURE 49: COMPRESSION INDEX AND EXPANSION INDEX COMPARISON	204
FIGURE 50: TYPICAL “Q- ϵ_Q ” FOR HIGHILY OVERCONSOLIDATED SOILS (MCCM) AND DENSE SANDS	208
FIGURE 51: “Q- ϵ_Q ” PLOT	209
FIGURE 52: “Q- ϵ_Q ” PLOT	210
FIGURE 53: “Q- ϵ_Q ” PLOT	211
FIGURE 54: “Q- ϵ_Q ” PLOT	212
FIGURE 55: “Q- ϵ_Q ” PLOT	213
FIGURE 56: “Q- ϵ_Q ” PLOT	214
FIGURE 57: “Q- ϵ_Q ” PLOT	215
FIGURE 58: “Q- ϵ_Q ” PLOT	216
FIGURE 59: “Q- ϵ_Q ” PLOT	217
FIGURE 60: “Q- ϵ_Q ” PLOT	218
FIGURE 61: “Q- ϵ_Q ” PLOT	219
FIGURE 62: “Q- ϵ_Q ” PLOT	220
FIGURE 63: “Q- ϵ_Q ” PLOT	221
FIGURE 64: “Q- ϵ_Q ” PLOT	222
FIGURE 65: “Q- ϵ_Q ” PLOT	223
FIGURE 66: “Q- ϵ_Q ” PLOT	224

CHAPTER I

INTRODUCTION

Soil mechanics is an old discipline that began with our ancestor's knowledge. Initially, this discipline was more practical than theoretical, and the practical knowledge was found by the process of trial and error involving many construction projects. Early engineers designed with empirical techniques that nowadays have been functional.

Theoretical information arose when disciplines such as Mathematics, Physics, Chemistry and others were applied to study the behavior of many phenomena. The implementation of these related disciplines in relation to soil mechanics has been necessary to define and establish mechanisms or models that simulate the soil behavior.

In addition, modeling has become a branch of the soil mechanics that has emerged and been increasingly used to find answers for a variety of unknowns in soil mechanics. Constitutive models of soil behavior are considered a relatively new branch in soil mechanics. These models describe the soil behavior in terms of constitutive equations, which have been idealized from mechanisms. Modified Cam-Clay Model (MCCM), proposed by Roscoe and Burland (1968), is considered an idealized model which forms the basis of several soil mechanic analytical theories.

Modified Cam-Clay Model is based on few and simple postulates that predict the stress-strain behavior of soils. These postulates were made in relation to the soil behavior under conventional triaxial test. It is also important to note that this theoretical analysis considers additional and significant investigations such as the generalization of Terzaghi's effective stress theory.

Even though this model's name seems to work only for clayey soils, it may also be applicable to other materials such as granular soils. Because granular materials have an important role in soil mechanics, particularly for states like Florida, the applicability of these constitutive models to define and predict the soil behavior of granular soils has been an important concern to improve the analysis of soil mechanics. This is addressed in the present thesis.

Scope of work

The applicability of the Modified Cam Clay Model to predict and simulate the behavior of dense granular soils is the focus of this work. Also, this investigation will verify some analytical studies commonly found in geotechnical engineering involving granular materials.

The results of a group of conventional triaxial tests, supplied by the Florida Department of Transportation (FDOT), will be used for comparison to the numerical prediction of the proposed model. These triaxial tests are defined by a conventional strain-controlled triaxial test, specifically under compression consolidation and drained condition. The properties from the tests on the soil samples are analyzed and then applied to the prediction model. Then, some modifications are proposed to the MCCM to improve the predictions.

Before the presentation of the experimental plan and results, a review in the first few chapters explains the basis of the critical state in soil mechanics and the Modified Cam Clay Model principles. This also serves as a platform for the computational analysis and modeling for granular materials. Chapter 2 presents the details of the Fundamental

Concepts in Soil Mechanics. Chapter 3 describes the basis of the Modified Cam Clay Model and the prediction consideration. Then, it is explained the application of this model in Matlab program and the proposed modification for dense granular soils. On Chapter 4 is presented the results of the analysis based on the model invariants. Finally, Chapter 5 shows a summary with the conclusions and recommendations for future investigations.

CHAPTER II

FUNDAMNETAL CONCEPTS IN SOIL MECHANICS

The following sections present a general discussion on fundamental concepts in soil mechanics based on theoretical background compiled by David Muir Wood in his work *Soil Behaviour and Critical State Soil Mechanics* (1990) based on the work of Roscoe and Burland (1968). This discussion was included in order to aid in the understanding of soil modeling founded on constitutive relations. Also, these concepts form the basis of the computational program presented later.

Critical State Soil Mechanics

The Critical State of a material corresponds to a point in which plastic shearing could continue indefinitely without more effective stresses and volume changes. Casagrande (1936) contemplated, while performing analysis of sand, that a critical void ratio is reached if no volume change occurs during a shear test under drained conditions. This effect of perfect plasticity is expressed by the following equation:

$$\partial p' / \partial \varepsilon_q = \partial q / \partial \varepsilon_q = \partial v / \partial \varepsilon_q = 0 \quad (1)$$

where q and p' represent the deviator stress and the mean effective stress respectively, v is the specific volume, and ε_q denotes the volumetric strain.

These stress invariants parameters can be calculated in terms of the principal stresses of the conventional triaxial test, and according to Cambridge University, p' and q are expressed as:

$$q = (\sigma_1' - \sigma_3') \quad (2)$$

$$p' = (2\sigma_3' + \sigma_1')/3 \quad (3)$$

where σ_1' is the effective vertical stress, and σ_3' represents the effective lateral pressure in the triaxial test.

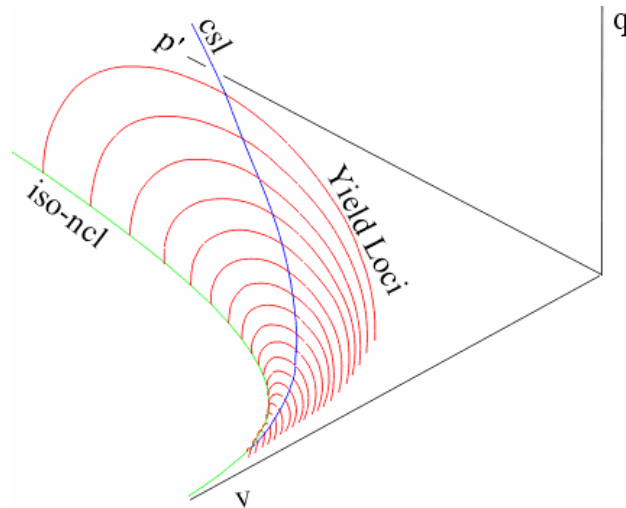


Figure 1: Three-dimensional View of Normal Compression Line (ncl), Critical State Line (csl), and Series of Cam Clay Yield Loci (Modified from Wood, 1990)

It is possible to characterize the complex behavior of soils by a certain combinations of isotropic consolidation responses and stress paths, limited to the triaxial plane ($p':q: v$) as shown in Figure 1. It is asserted that there is a unique relationship between shear stress (q), the mean effective stress (p'), and the void ratio (e) or the specific volume (v) at failure or critical state.

The concept of critical state in soil mechanics has a fundamental aspect called the critical state line. This line has the property to predict the failure location of initially isotropically consolidated soils when the stress state of the samples reaches this line,

irrespective of the test path followed by the samples on their way to the critical state. This failure is observed to occur in conventional triaxial compression tests for both drained and undrained. In addition, the projection of the critical state line (CSL) onto the p' - q space, Figure 2, may be expressed as:

$$q = Mp' \quad (4)$$

where “ M ” represents the slope of the critical state line. It may also be represented in the v - p' space, Figure 3, by:

$$v = -\Gamma / \ln p' \quad (5)$$

where “ Γ ” is the specific volume (v) corresponding to $p' = 1 \text{ kN/m}^2$ or lb/in^2 on the critical state line.

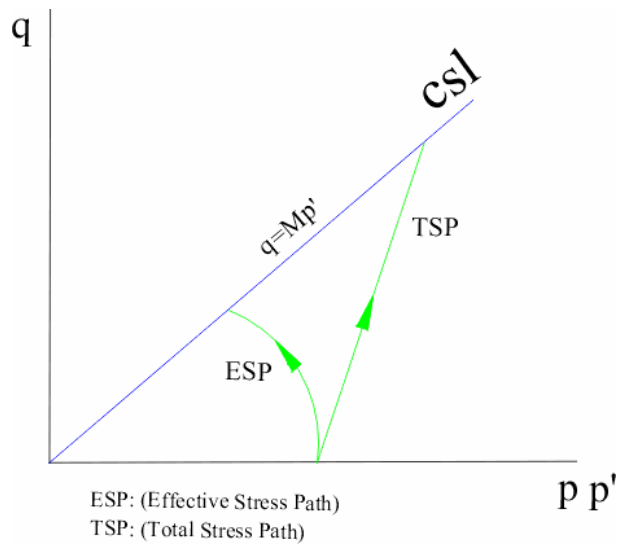


Figure 2: Critical State Line in the ($q:p'$) Plane (Modified from Wood, 1990)

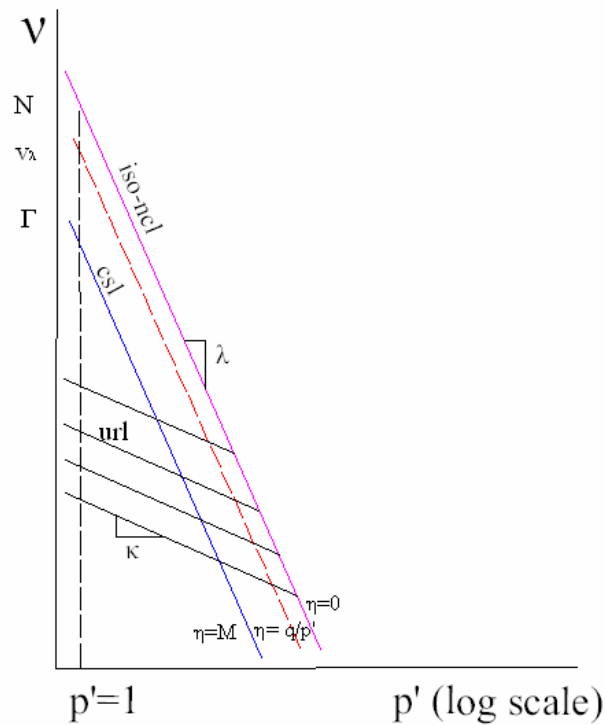


Figure 3: The Critical State Line on the v - $\ln(p')$ Space (Modified from Wood, 1990)

Also, it is important to denote that the establishment of the principle of effective stress by Terzaghi (1936) is a fundamental consideration to understand the magnitude of the effective stresses carried by the soil skeleton through the interparticle contact forces. Therefore, if the soil is saturated of water, the total stresses applied must be reduced for the effect of the water pressure to really obtain the effective stresses supported by the soil particles, thus:

$$p' = p - u \quad (6)$$

where “ p ” represents the total stresses and “ u ” is the water pressure. However, if the loading rates are slow such that the water is able to drain through the soil pores when any stress increment is applied to the soil, this phenomena is considered as a drained

condition. No water pressure must be considered, $u=0$ in drained situations. In general, granular soils are considered to have drained conditions when stress increments are applied due to the high permeability rates.

Critical State Line and Qualitative Soil Response in Sands and Other Granular Materials

The recognition of the critical state line to estimate the expected qualitative response of soils in triaxial compression tests is a significant consideration for soil mechanics. It is important to note that the term “Qualitative”, expressed previously, is the medium that constitutive models use to make powerful quantitative statements in accordance with the expected patterns of soil behavior.

An important phenomenon known as dilatancy, or the change in volume associated with distortion of granular materials, must be considered to understand the behavior of granular materials. This effect is related to soil density, as shown in Figure 4. According to Casagrande (1936), every granular material has a specific critical void ratio. When this specific void ratio is reached during a test, the stresses remain constant even if the test is continued with the application of more loads. Moreover, during a shear test in medium to loose granular material, the stresses increase until the sand reaches the specific critical void ratio. In addition, a soil compaction is observed with the reduction of the initial void ratio into the critical void ratio. This compaction effect is due to the rearrangement of the soil particles into the void spaces.

On the other hand, if the shearing test is conducted on a dense granular material, it shows that the stress increments reach a peak value followed by a continuous stress

reduction. It is important to note that dense granular soils during a shear test show increments of the volume due to the lack of void spaces to rearrange the soil particle.

This effect can also be observed on Figure 4.

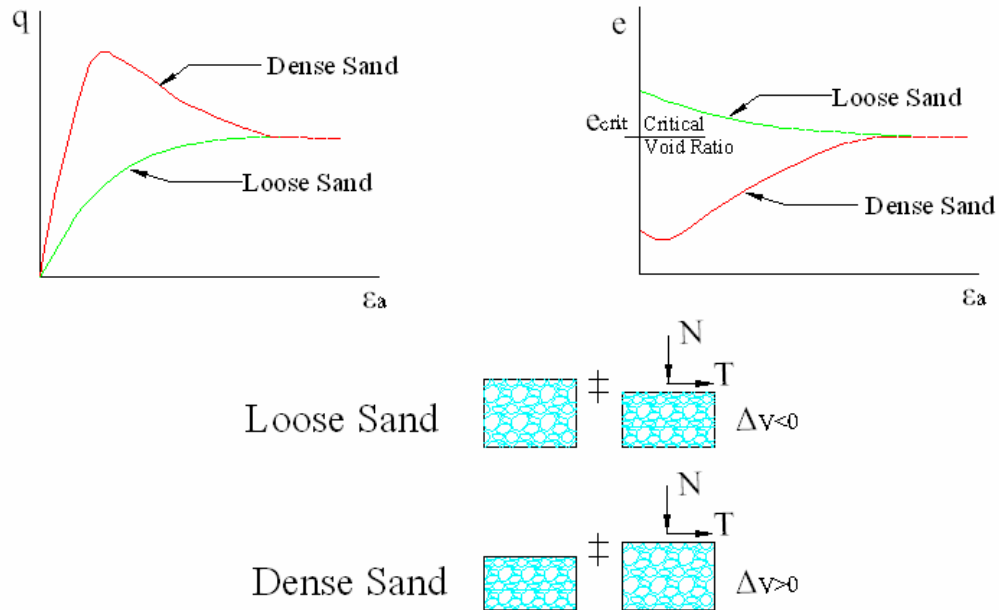


Figure 4: Effect of Shearing on the Volume of Dense and Loose Sands. (Modified from Lancellotta,1995)

From a diversity of research in granular materials, it is possible to note that dense sand initially contracts its volume, then it expands to a critical void ratio. The frictional capacity between soil particles defines the peak value of the shear strength of the cohesionless materials.

Furthermore, “Particle Crushing” is an important effect to consider in granular soils. The intensity of this effect depends on not only the high confining pressures submitted to the soil during the shear deformation but also the density of the soil. For example, dense sands densify when the soil particles crush in fragments, and the resulting fragments rearrange the void spaces. Also, it is important to notice that the amount of crushing in a soil raise when the confining pressure is increased.

Peak Strengths for Sand

Peak strength pattern of dense sand was introduced in last section, and the purpose of this section is to further explain this effect. This peak pattern occurs because of the connection among the dense soil particles. This causes a frictional force that increases up to a stress state where the soil particles start moving to different positions reducing the frictional capacity of the soil. In addition, another effect that intervenes in the stress capacity is particles crushing. Even though this effect was not considered by the MCCM, it may affect the soil properties.

According to MCCM prediction, the peak effect of the stresses is considered because the stress path has to reach the yield locus, which is located above the critical state line, and then it returns to the critical state line. Also, it is important to recall that this behavior in dense sand is similar to overconsolidated clays when the overconsolidation ratio is greater than two. In Figure 5, the yield locus is represented by any point between “B” and “C” which represents the peak of the deviator stress value, and then it drops to the critical state line, which is considered the ultimate strength value.

Furthermore, from the beginning of the drained triaxial compression test until the yield locus is reached, any deformation of the soil is associated with elastic behavior, and the return to the critical state line is related to a softening pattern governed by plastic deformation behavior.

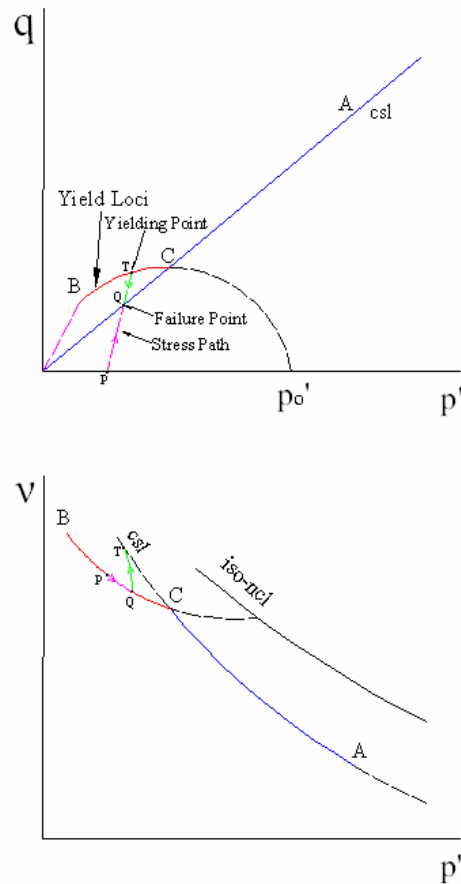


Figure 5: Points of Peak Deviator Stresses “q” in Conventional Drained Triaxial Compression Tests on Isotropically Overconsolidated Samples. (Lancellotta,1995)

Mohr-Coulomb Failure Criteria

Soil failure states may be determined with the application of the Mohr-Coulomb Failure criterion. It establishes that failure on any plane of a soil mass will occur when the applied shear stress reaches or exceeds a maximum critical value, which is defined by the following equation:

$$\tau = \pm(c' + \sigma' \tan \phi') \quad (7)$$

where c' represents the cohesion component of the soil, and the second term is related to the frictional resistance of the soil depending on the effective normal stress (σ'), and the friction angle (ϕ').

Equation (7) may be redefined in terms of principal stresses. Moreover, if the principal stresses are expressed in terms of the invariants q and p' , as defined previously in equations (2) and (3) of this chapter, and considering frictional behavior is assumed with a neglected cohesion, it is possible to solve for the property “ M ”, which is the slope of the Critical State Line, as:

$$M = 6 \sin \phi' / (3 - \sin \phi') \quad (8)$$

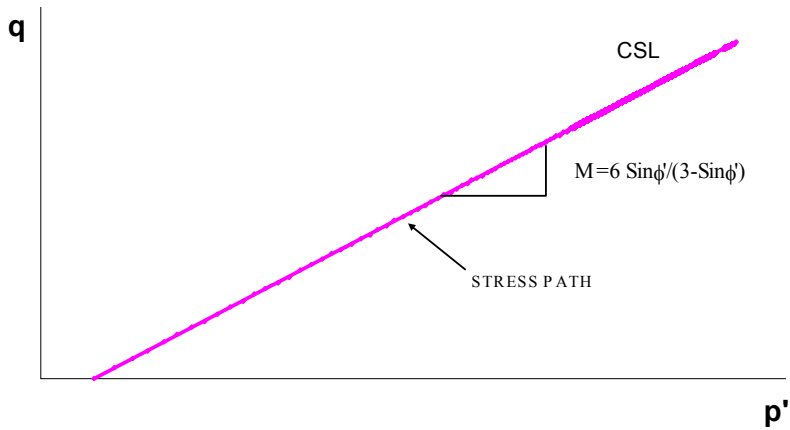


Figure 6: Mohr-Coulomb Failure Criterion in Terms of “q and p”

The Roscoe Surface

Constitutive models in soil mechanics consider the existence of a yield loci that marks the changes of the behavior of soils. To illustrate the parameters and the shape of a specific yield surface, the yield surface is obtained based on a qualitative analysis of laboratory research. For example, The Roscoe, Hvorslev, and Tensile failure surface by Wood (1990) define the boundaries which confine the possible stress states for a given soil, and it is presented in Figure 7.

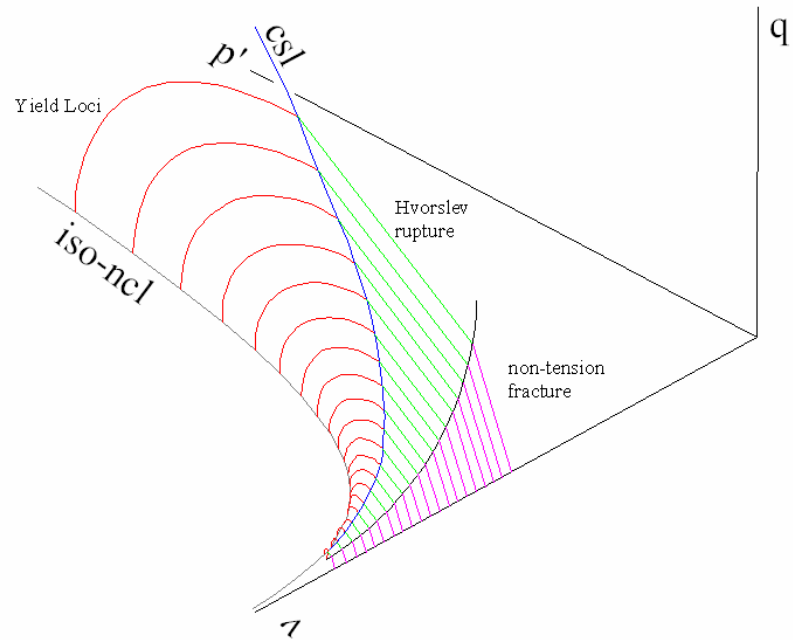


Figure 7: Projection of Roscoe, Hvorslev, and Tensile Failure Surface in 3-D Space

Figure 8 shows the Roscoe projection of undrained and drained yield surface in a two-dimensional space $q-p'$. It is clear that the contours from drained and undrained tests have a similar tendency and are consistent with each other. The assumption that all isotropically normally consolidated clay specimens behave in a similar manner gives rise to what is known as the “Roscoe Surface”.

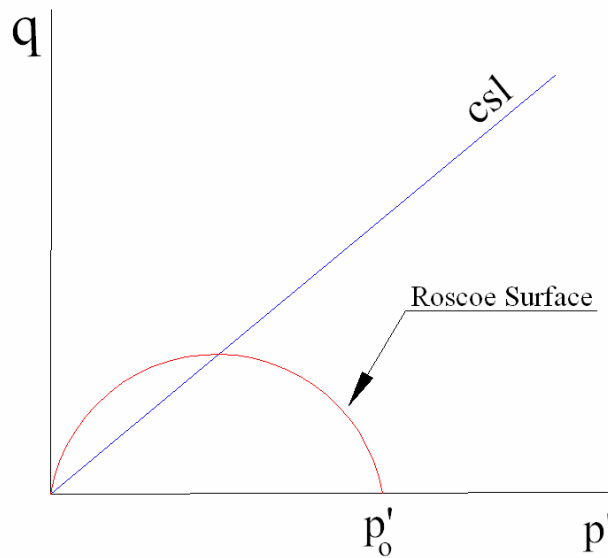


Figure 8: Projection of Roscoe Surface in “q- p” Space

Elastic-Plastic Model for Soils

Recognizing that yield surfaces exist for soils, the next element to consider is the behavior of soils in reference to the yield surface. The model states that stress changes inside the yield surface will be considered under elastic behavior. Once the stress state reaches the current yield surface, a combination of elastic and plastic responses will result. It is important to determine the magnitude and the direction of the plastic deformation in relation with the change in size of the yield surface.

Discussion of the elastic-plastic model for soil in this chapter will be limited to the cases of stress and strain for conventional triaxial tests. Furthermore, the model will be described in terms of the triaxial stress invariants (p' , q) and strain invariants (ϵ_q , ϵ_p , and ϵ_a).

Elastic Volumetric and Shear Strains

Recoverable deformations are linked to any stress changes within the yield surface. These elastic deformations may be related to elastic stress-strain characteristics for each soil. In order to simplify the treatment, one may assume that the material is initially in an isotropic condition. The elastic stress-strain relationship may be expressed as:

$$\delta\varepsilon_p^e = (1/G')\delta q \quad (9)$$

$$\delta\varepsilon_q^e = (1/K')\delta p' \quad (10)$$

where K' and G' are the bulk and shear modulus of the soil respectively, in terms of effective stress condition. It is worth noting that in expressions (9) and (10), recoverable changes in volume are associated only with changes in the mean stress p' .

A yield locus of a soil in the $q-p'$ space is illustrated in Figure 9. For a given state of stress, the specific volume (v) may be determined by projecting the point into the $v-p'$ space. Deformation from one point to another point within the yield surface will be determined under elastic theory.

The loading history of a soil has a direct influence on the position, shape, and size of the yield surface. Figure 9 shows the stress path for a soil that is loaded along one-dimensional compression and the associated elastic deformation observed in the $v-p'$ space. It should be noted that in the $v-p'$ plane, the normally consolidated line is the plastic deformation curve, and the unload-reload line is the elastic response

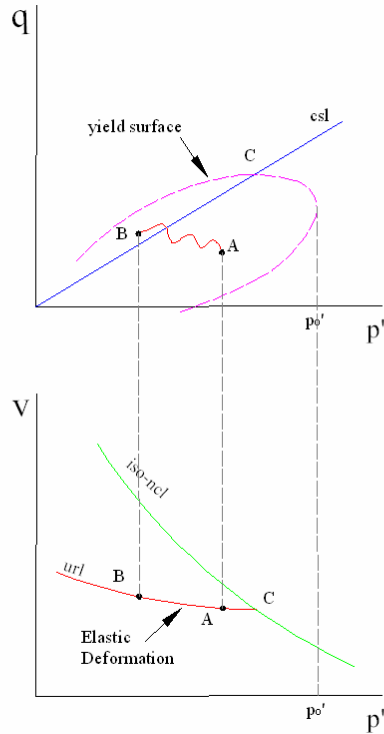


Figure 9: Yield Surface in “ $q - p'$ ” Space (Modified from Wood, 1990)

curve. Another feature of this $v-p'$ diagram is that if one plots it in a semi-logarithmic scale as shown in Figure 10, instead of an arithmetic scale, one obtains a straight line response similar to the consolidation test results in conventional $e-\log\sigma'_v$ analyses.

Because of the $e-\log\sigma'_v$ plot linear behavior, the equation for the normal compression line turns into:

$$v = v_{\lambda} - \lambda \ln p' \quad (11)$$

and the expression for the unloading-reloading line becomes

$$v = v_{\kappa} - \kappa \ln p' \quad (12)$$

where “ λ ” is the slope of the normal compression line, or known as the compression index, and “ κ ” represents the slope of the unloading-reloading line, also called the

swelling index. Also, v_λ and v_κ are the specific volumes at $p' = 1$ kPa or lb/in². Note that the values of these last two parameters are dependent on the units selected to measure stress.

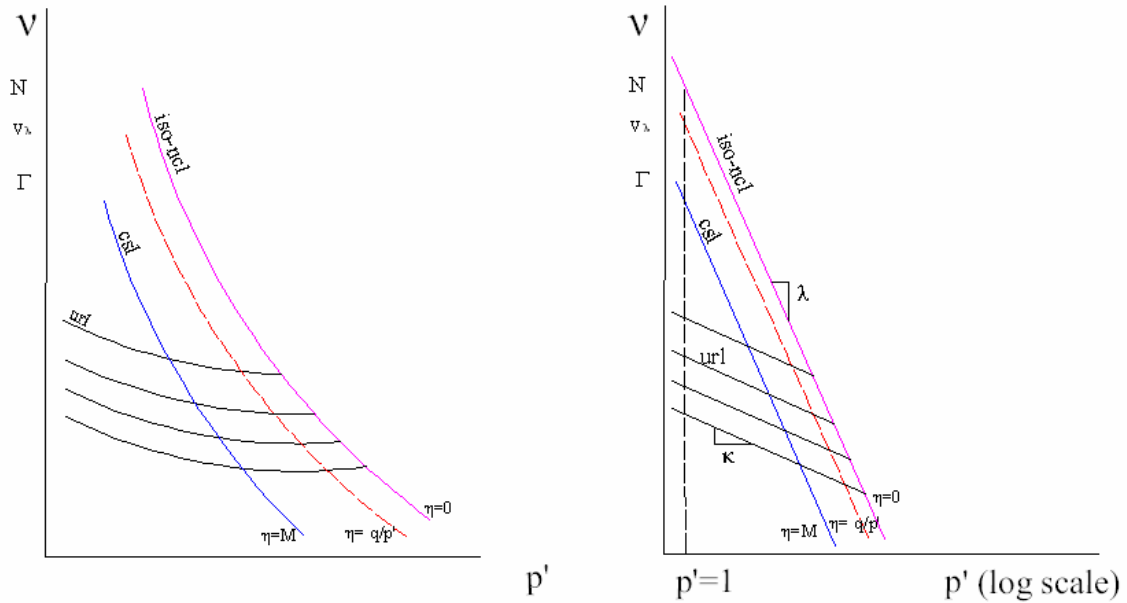


Figure 10: Normal Compression Line and Unloading-Reloading Line in Semi-logarithmic Plot (Modified from Wood, 1990)

Equation (12) is expressed in an incremental form as:

$$\delta v^e = -k \delta p' / p' \quad (13)$$

where “^e” denotes the elastic or recoverable behavior. An increment in volumetric strain is given by:

$$\delta \epsilon_p = -\delta V / V \quad (14)$$

The incremental form of this equation may be rewritten in terms of volumetric strain as:

$$\delta \epsilon_p^e = -k \delta p' / v p' \quad (15)$$

by comparing this expression with equation (9), it affirms that $K' = v p' / k$.

Any variation in deviatoric stress within the yield surface of an isotropic elastic soil will produce no changes in volume, but it will cause elastic deviatoric, or shear strains, $\delta\epsilon_q^e$. This value can be obtained from equation (10) with an appropriate value of shear modulus, G' .

Furthermore, shear modulus is also expressed in terms of the Young's modulus (E'), and the Poisson's ratio (ν') through the following expression:

$$G' = E' / 2(1 + \nu') \quad (16)$$

Plastic Volumetric Strains and Plastic Hardening

Any deformation that occurs when the yield surface is reached or further is not fully recoverable upon removal of the loading. The irrecoverable deformation is the consequence of the energy available for dissipation. For example, a soil that yields as shown in Figure 11 is trying to expand the yield surface under a change in stress state. With a stress path that goes from point "K" to point "L" (L is located on what is called yield surface No.2), one is able to obtain the shape of the new yield surface. To simplify this analysis, it is assumed that the shape of the new yield surface remains the same, irrespective of the stress path that created it. Also, from point "K" to "L", there is a change in volume (δv_p) that is shown in Figure 11.

By focusing on the region of the compression space around the points where the unloading-reloading line meets the normal compression line, point "A" and "B" of Figure 11, an alternate expression can be obtained for the change of volume.

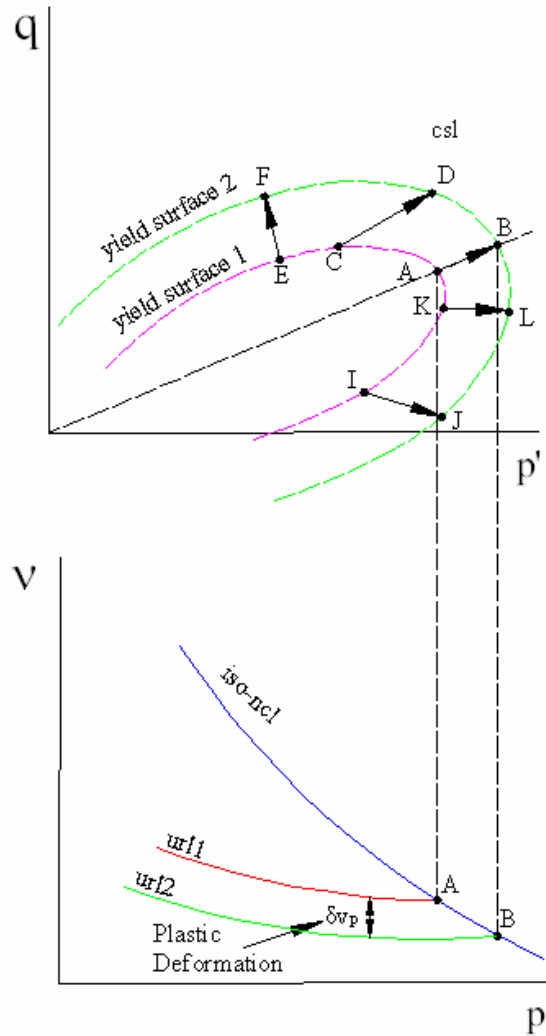


Figure 11: Expansion of Yield Locus and Change in Volume Associated (Modified from Wood 1990)

Point “A” corresponds to mean stress $p_o' = p_{o1}'$ and point “B” is $p_o' = p_{o2}'$. The change in specific volume that can be recovered between the unloading and reloading curve url_1 and url_2 which matches points “A” and “B” respectively is given by:

$$\delta v_p = -\lambda \ln(p_{o2}'/p_{o1}') + k \ln(p_{o2}'/p_{o1}') = -(\lambda - k) \ln(p_{o2}'/p_{o1}') \quad (17)$$

The first term of this expression refers to the total change in volume as the net mean stress goes from point “A” to point “B”. The second term represents the recovered volume change when the net mean stress is reduced again. In the limit value, the above equation becomes:

$$\delta v_p = -(\lambda - k) \delta p_o' / p_o' \quad (18)$$

in terms of volumetric strain:

$$\delta \varepsilon_p^p = (\lambda - k) \delta p_o' / \nu p_o' \quad (19)$$

The total volumetric strain increment and the total change in specific volume can be presented as the sum of their elastic and plastic components, respectively:

$$\delta \varepsilon_p = \delta \varepsilon_p^e + \delta \varepsilon_p^p \quad (20)$$

and

$$\delta v = \delta v^e + \delta v^p \quad (21)$$

The movement of any yield surface is strongly related to the surface definitions. Different hardening rules have been used for soils, all derived for the isotropic and kinematic hardening presented by the Von Mises' model. This model considers that this movement is assumed to be collinear to the plastic flow direction. The change of yield loci, which is also the change in p_o' , is related to the increment not only of the plastic volumetric strain but also of the plastic shear strain, according to the following plastic hardening equation:

$$\delta p_o' = (\partial p_o' / \partial \varepsilon_q^p) \delta \varepsilon_q^p + (\partial p_o' / \partial \varepsilon_p^p) \delta \varepsilon_p^p \quad (22)$$

Plastic Shear Strains

The use of plastic volumetric strain increment ($\delta\varepsilon_p^p$) is not a complete description of the plastic behavior. It is also necessary to calculate the plastic shear strains because the direction of the strain increment vectors is ruled by the characteristic combination of stresses at the point at which the yield surface was reached. To understand and simplify this important factor, considerations such as Plastic Potentials and Normality or Associated Flow will be explained next.

Plastic Potentials

Beyond the simple model described earlier in this investigation, a new element can be introduced to the plasticity analysis. In the q - p' space of Figure 12, any yielding taking place at a stress state “Y” will be linked with the occurrence of some plastic volumetric strain increment ($\delta\varepsilon_p$) and some plastic shear strain increment ($\delta\varepsilon_q$). Vector “YS” of this figure represents the magnitude of these two components with axes parallel to p' and q . Moreover, this vector can be created by drawing an orthogonal line through point “Y” with a slope given by:

$$\delta q / \delta p' = \delta v_p / \delta \varepsilon_p \quad (23)$$

A number of different combinations of stresses may occur on a soil particle at any given instant during its history, causing yielding. Also, yielding may occur under several different permutations of stresses in the history of the soil. For each one of these combinations, a vector of plastic strains through any yielding point can be drawn as more

data becomes available. These lines may be joined up to form a group of curves to which the plastic strain vectors are orthogonal. These curves are known as “the Plastic Potential Curves”, Figure 13.

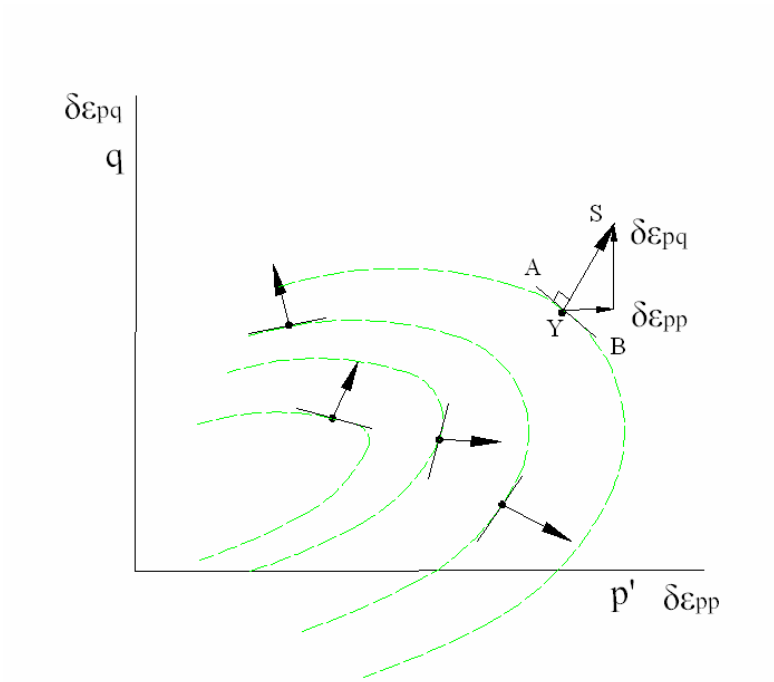


Figure 12: Plastic Strain Increment Vector Normal to Plastic Potential Curves (Modified from Wood, 1990)

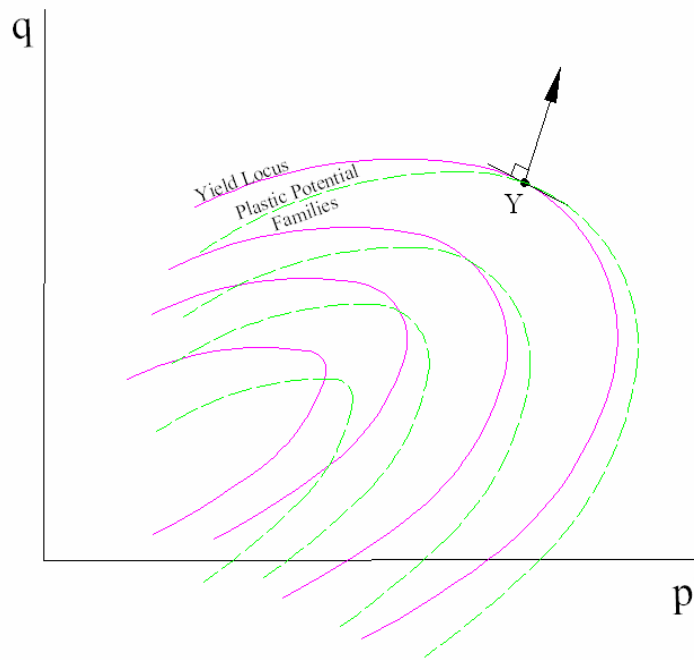


Figure 13: Families of Plastic Potential (dashed) and Yield Locus (solid) (Modified from Wood,1990)

Normality or Associated Flow

A normality condition is considered to take place when the shape of its plastic potential is almost identical to its yield surface, and the plastic strain increment vectors are in the direction outward normal to the yield surface. This condition can be seen in Figure 14. The normality trend is closely related to an associated flow rule. Therefore, the material may be defined by a law associative flow in which the nature of the plastic deformations, or flow, is associated with the yield surface of the material.

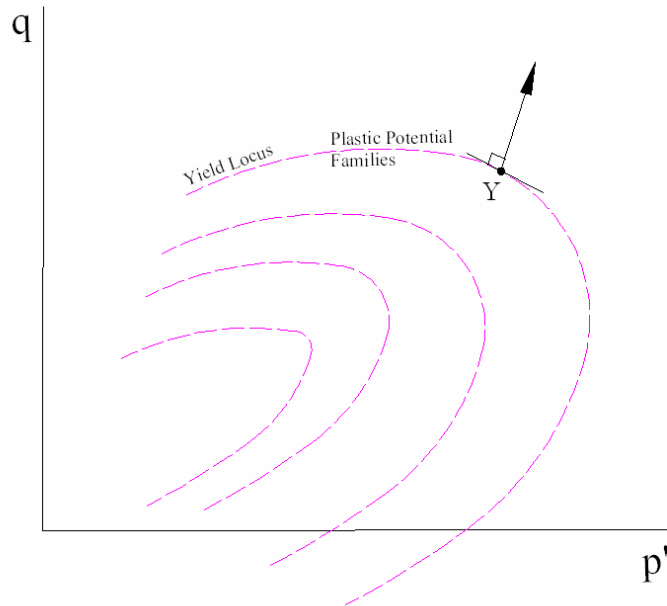


Figure 14: Normality or Associated Flow Rule (Modified from Wood 1990)

Summary

In this chapter, fundamental theoretical concepts and soil behavior assumptions were described to develop the constitutive relation used for predictive models. The critical state soil mechanics and the critical state line were discussed and expressions for the failure stress state were introduced. Also, dense sand behavior was addressed to show the effect of the peak strength.

In addition, concepts such as the Mohr-Coulomb failure criteria and the Roscoe Surface were necessary to be included due to their importance for the feasible stress-strain constitutive relations.

Following these concepts, a generalized elastic-plastic model for soil was presented. Theories such as elasticity and plasticity were related to soil as a material property, and idealizations of soil behavior were assumed in order to simplify the predictive models.

In the next chapter, the widely known model Modified Cam Clay is undertaken in details and developed for the application of this model to dense sands.

CHAPTER III
COMPUTATIONAL MODEL FOR DENSE SANDS

General

The use of the computer, and in particular computer program applications, for the analysis of the soil behavior has produced the ability to understand and simulate different complex situations. However, this advancement has not been possible without verification provided by experimental analysis and previous experiences in the field.

When a specific phenomenon is required to be studied due to its important on our society, researchers use the applicability of numerical models that allow them to simulate various situations. Therefore, many models require some idealization of the phenomenon. These are often based on previous experiences and/or scientific theories, to support and simplify the model.

Modeling in soil mechanics is related to the analysis of stress- strain- strength relationship. The present thesis is restricted to the prediction of the behavior of dense sands through the applicability of a widely known model called Modified Cam Clay Model (MCCM). This chapter presents a review of the Modified Cam Clay Model, followed by a description of the MCCM prediction in overconsolidated soils. Next, this model is adapted to a computational numerical analysis using a Matlab program. Finally, this model is modified to adapt it to the behavior of dense sands.

Modified Cam-Clay Model (MCCM)

In the previous chapter, the elastic-plastic analysis of soils was described in a general way. Yield loci and plastic potentials were sketched without any further attempt to generate possible mathematical expressions for these curves. The following is a description of a mathematical model that collects all this information into more practical applications.

The Cam Clay Model (MCCM) was originally described by Roscoe and Schofield (1963). Later, a new model called Modified Cam Clay (MCCM) was presented by Roscoe and Burland (1968). Basically, the model is described in terms of the invariant effective stresses “ p' and q ” and the invariant strains “ ϵ_p and ϵ_q ”. Also, these stress invariants were already defined and related to the conventional triaxial test in Equations (2) and (3) of Chapter 2. The strain increment values are estimated according to the conventional triaxial test as follow:

$$\delta\epsilon_p = -\delta V / V \quad (14)$$

$$\delta\epsilon_q = \delta\epsilon_a + \delta\epsilon_p/3 \quad (24)$$

$$\delta\epsilon_a = -\delta l/l \quad (25)$$

In an attempt to study the yielding behavior of NC clays, Roscoe and his coworkers conducted several tests on samples of saturated clays. They proposed a new energy dissipation relation based on the assumption that the energy can be dissipated due to both plastic volumetric and shear strain, resulting in the following equation:

$$\delta W = p \{ [(\delta\epsilon_p)^2 + M^2(\delta\epsilon_q)^2] \}^{1/2} \quad (26)$$

They found that the effective stress paths for several tests were geometrically similar, and the stress states were a straight line on the $q:p$ space. Another important feature was that the ultimate states of stresses were observed to lie on a curve, which was similar to the isotropic consolidation line on a compression space.

In the MCCM, the stress path passes through several yielding surfaces, also called hardening caps, causing plastic deformations. The yielding will continue to occur until the material reaches a *critical void ratio* (e_{cr}), after which the void ratio remains constant during subsequent deformations. In other words, this critical void ratio can be considered as the ultimate state of the material. It has been observed that a soil with void ratio lower than the critical value will deform in such a manner as to increase its volume, while at a void ratio higher than the critical value, deformations will decrease in volume.

Yield criterion and post yield behavior are two important factors of the plastic behavior of a material. The yield criterion defines the limit of purely elastic behavior. When the state of stresses comes in contact with the current yield surface, the material undergoes elastic-plastic deformations. During this process, the material hardens and the yield surface expands to a new position. In order to describe the elastic-plastic response of the soil, it is essential that we develop explicit relations in an incremental (flow) fashion. The formulations will then be used to predict the response of a soil as the stresses or strains are incrementally increased or decreased, depending on the purpose of the investigation.

The MCCM is represented by an ellipse in the $q:p$ 'space, as shown in Figure 15. This ellipse is centered to the p' axis, and it can be plotted by using the following expression:

$$p'/p_o' = M^2 / (M^2 + h^2) \quad (27)$$

where h is the relation of q/p' . In summary, this equation represents a set of ellipses that pass through the origin of the $q:p'$ space and whose size and shape is controlled by p_o' and M respectively. If this equation is presented in terms of the general considerations discussed in the elastic-plastic concepts for soil, Equation 27 of the ellipse can be expressed as:

$$f = p'^2 + p'p_o' + q^2/M^2 = 0 \quad (28)$$

Considering the assumption of the plastic potential and normality conditions for the soil (Figures 12, 13 and 14) as discussed in Chapter 2, it is possible to establish Equation 28 as the representation of a family of plastic potential curves given by:

$$g = f = p'^2 + p'p_o' + q^2/M^2 = 0 \quad (29)$$

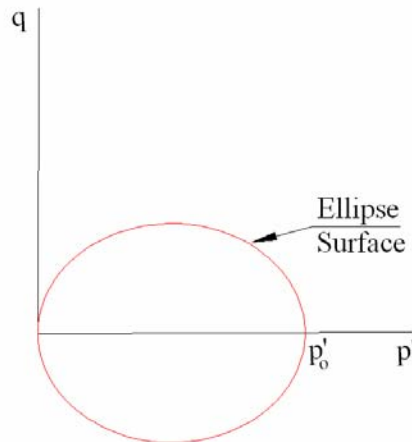


Figure 15: Modified Cam Clay Model (after Wood, 2000)

Moreover, because the normality condition proposes that the plastic strain increment vectors, $\delta\epsilon_p^p$ and $\delta\epsilon_q^p$, in Figure 12, flow in the direction of the outward normal

to the yield locus, and it may be mathematically represented by the following flow rule equation:

$$\delta\varepsilon_p^p / \delta\varepsilon_q^p = (\partial g / \partial p') / (\partial g / \partial q) = M^2(2p' - p_o') / 2q = M^2 - h^2 / 2h \quad (30)$$

In addition, it is assumed that the shape of the yield loci remains constant while expanding. This yield loci expansion effect is also called the hardening of the soil, which is linked to the normal compression line presented in previous chapters. Now, following the idea of the hardening rule, Equation 11 may be expressed as a linear relationship between specific volume (v) and the logarithm scale of the mean effective stress (p_o') during isotropic normal compression of the soil as follows:

$$v = N - \lambda \ln p_o' \quad (31)$$

where N represents a soil constant specifying the position of the isotropic compression line in the compression plane $v: p'$. To estimate the magnitude of plastic volumetric strains, Equation 19 results in:

$$\delta\varepsilon_p^p = [(\lambda - k) / v] \delta p_o' / p_o' \quad (19)$$

Now, due to the recognition of the plastic volumetric strain and the assumption of the normality condition, the elements of the yield loci expansion defined by the hardening relationship expressed in Equation 22 are:

$$\partial p_o' / \partial \varepsilon_p^p = v p_o' / (\lambda - k) \quad (32)$$

$$\partial p_o' / \partial \varepsilon_q^p = 0 \quad (33)$$

Now, by combining Equations 9 and 10, the elastic stress-strain response in soil is presented in the following matrix equation:

$$\begin{bmatrix} \delta \varepsilon_p^e \\ \delta \varepsilon_q^e \end{bmatrix} = \begin{bmatrix} 1/K' & 0 \\ 0 & 1/G \end{bmatrix} \begin{bmatrix} \delta p' \\ \delta q \end{bmatrix} \quad (34)$$

Also, the plastic stress-strain response can be represented by the expression:

$$\begin{bmatrix} \delta \varepsilon_p^p \\ \delta \varepsilon_q^p \end{bmatrix} = \frac{(\lambda - \kappa)}{v_p'(M^2 - \eta^2)} \begin{bmatrix} (M^2 - \eta^2) & 2\eta \\ 2\eta & (M^2 - \eta^2) \end{bmatrix} \begin{bmatrix} \delta p' \\ \delta q \end{bmatrix} \quad (35)$$

The Modified Cam Clay Predictions for Conventional Triaxial Tests

This section explains the use of this constitutive model to predict the soil behavior patterns. This model can be applied to conventional drained and undrained triaxial test. The MCCM prediction is also based on the overconsolidation ratio soil classification.

Moreover, pre-consolidation stress applied to a soil will define the level of elastic-plastic deformations. This pre-consolidation stress is related to the past maximum effective pressure ($p_o' = \sigma'_{max}$) and expressed as overconsolidation ratio (OCR):

$$OCR = p_o' / p_i' \quad (36)$$

where $p_i' = \sigma'_{3o}$ represents the initial pre-consolidation pressure applied to a soil.

According to the overconsolidation ratio (OCR) classification, the MCCM prediction establishes three types of soil behavior. When $OCR=1$, the soil is classified as Normally Consolidated, and the predictive behavior must be considered for this type of soil. On the other hand, when OCR ranges between 2 and 1, a Lightly Overconsolidated soil classification will define the predictive soil behavior. If OCR is considered greater than 2, the soil is called Highly Overconsolidated Soil.

A group of conventional triaxial tests will be used to acquire the necessary data for the analysis and verify the numerical modeling of the soil behavior. The tests were applied under drained and strain-controlled compression conditions. Because these tests were applied to principally sand materials by FDOT and were compacted to an average of 95% of the maximum unit weight at the optimum moisture content, the predictive behavior of these samples were considered as Highly Overconsolidated soils which is similar to the response of dense sands. The following sub-sections show the MCCM prediction under conventional drained triaxial tests in highly overconsolidated soils.

Predictions for Conventional Triaxial Compression Test under Drained Condition

Depending on the ability of the water inside the soil structure to drain, the soil can be considered a drained medium. The drain option of the conventional triaxial test is provided when the drain valves are kept open during the triaxial test. Moreover, because of the test drain condition, pore pressure is neglected and considered equal to zero.

If the water pressure is neglected, the total invariant stress (p) is considered equal to the effective stress (p') according to the stress principle of Terzaghi , expressed as:

$$p' = p - u \quad (6)$$

where u represents the water pore pressure. Considering the drainage condition,

$$u = 0$$

$$p' = p$$

It is important to recall that the stress invariant “q” is independent to the water pressure. In addition, Figure 16 shows the total stress path (q-p) and the effective stress path (q-p’) where the slope can be represented by:

$$\delta q = 3 \delta p' \quad (37)$$

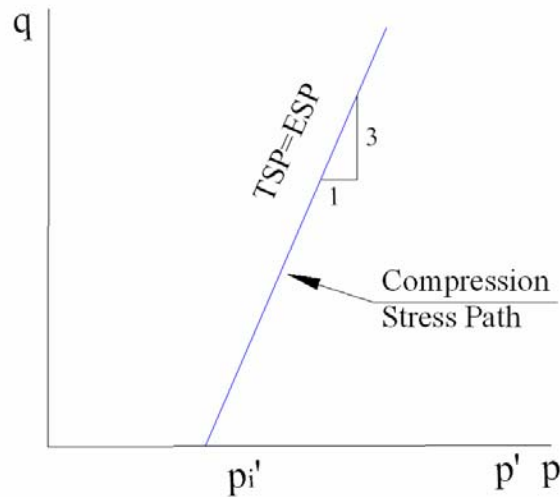


Figure 16: Stress Path “q – p” Space for Drained Conditions (after Wood, 1990)

Predictions on Highly Over Consolidated Soils

Modified Cam Clay Model also estimates the behavior of soils according to the soil overconsolidation ratio (OCR). Highly overconsolidated soil is the classification used for those soils whose existing isotropic pressure is less than half of the past maximum effective pressure ($p_o' = \sigma'_{max}$).

On conventional compression triaxial test under drained condition, the behavior from the initial state until the yield locus is considered to be elastic. However, when the stress path reaches and passes the yield surface, elastic-plastic pattern behavior defines the stress-strain relationship.

In addition, it is important to mark that at the yield point, point “Q” Figure 17 (a), the plastic strain increment vector points to the left. Any further increment of the plastic shear strain has the same direction as the preceding elastic shear strains, and negative plastic volumetric strains must be observed, Figure 17 (d).

In other words, a plastic volumetric expansion defines the soil deformation pattern after the yield surface is reached. Also, due to the soil volumetric expansion, any increment of the effective invariant p' must be considered negative, $\delta p' < 0$. Therefore, a contraction of the yield locus should be expected.

To define the invariants stress path, it is important to consider that any increment or reduction of p' and q maintain the relation expressed in Equation 37. Figure 17 shows the typical plots of the Highly Overconsolidated soils under drained conditions.

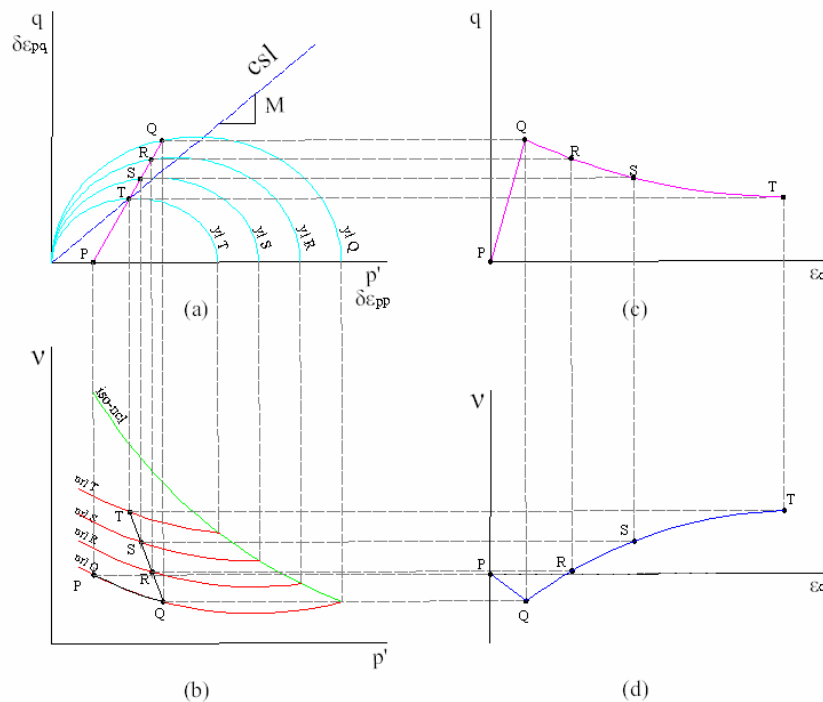


Figure 17: Typical Plots under Drained Conditions in Highly Overconsolidated Soils (after Wood, 1990)

The Modified Cam Clay Model in Matlab

Since the computer has been applied for the advancement of the science, the human knowledge has increased to levels that never before were anticipated. The applications of software to the study of many phenomena in our life have improved the solutions to these situations. For example, a problem that lasted days, months or even years to be analyzed, is today solved in micro-seconds.

Matlab, a programming software produced by Matlab, Inc., is used as a very practical environment for the numerical implementation of the Modified Cam-Clay Model in this investigation. The behavior prediction of dense granular material based on the MCCM is the focus of this thesis. A comparison between triaxial test data applied on dense sand and the use of this model in Matlab is conducted.

Jefferies and Shuttle (1992) established in their paper that this model is a idealized soil model which is based on few postulates giving the models a “predictive power,”. These few postulates depend basically on nine parameters which represent the input data necessary of the MCCM. This input data is conformed by the initial void ratio (e_0), angle of friction (ϕ), swelling and compression index (κ, λ), Poisson’s modulus (ν'), Young’s modulus (E'), the initial isotropic consolidation ($p_i' = \sigma'_{30}$), and the past maximum effective pressure ($\sigma'_{\max} = p_o'$). Next chapter will explain and show the evaluation and calculation of these parameters.

Prediction of highly overconsolidated soils under drained condition is basically defined in two phases according to the MCCM. The first phase corresponds to the increments of deviator stress from the initial isotropic stress state, point “P” in Figure 17,

to a point where the stress path reaches the yielding surfaces, point “Q”. Some rules define the behavior prediction in this phase, which are presented as follows:

1. The shape and size of the yield surface is defined by the ellipse Equation 28, which depends on “M” and “ p_o' ”.
2. Due to drained condition, total stress and effective stress path are equivalent.
3. The stress path is defined by Equation 37, and any stress increment follows the same relation.
4. The yield point, which corresponds to the peak stress in highly overconsolidated soils, is obtained at the intersection of the stress path and the yield surface. This point is represented as “ q_y and p_y' ”.
5. Because the stress path of highly overconsolidated during this phase is within the yield surface, elastic behavior defines any soil deformation. Therefore, Matrix-equation 34 defines the specific calculation for the increment of the volumetric strains (ϵ_p) and shear strains (ϵ_q) during this phase.

The second phase is characterized by a softening pattern behavior which goes from the yield point “P” to a failure or better-called ultimate point “T”, Figure 17(a). This ultimate point is identified as “ q_f and p_f' ”. Similar to the initial phase considerations, this phase must consider the following:

1. Total stress and effective stress path maintain the same slope and increment relationship.
2. Because of the softening behavior, increments of the effective invariant p' must be considered negative, $\delta p' < 0$.

3. The failure, or ultimate, point value is obtained at the intersection of the stress path, Equation 37, and the critical state line, Equation 4. This point is identified as “ q_f and p_f ”.
4. When the stress path reaches the yield surface, MCCM assumes that further deformations are defined by the elastic-plastic theory. Therefore, Matrix-equation 35 or Equations 30 and 19 estimate the elastic-plastic increments of the shear strain (ε_q) and volumetric strain (ε_p).

The application of the previous rules into the Matlab computational program allows for the prediction of the stress-strain responses for highly overconsolidated soils. Flow Chart 1 illustrates this computational prediction algorithm. Typical plots such as the “ q versus p ” and “ q versus ε_q ” are generated to graphically display the predicted calculations for each soil sample. Appendix “C” exhibits the Matlab program using the MCCM prediction in highly overconsolidated soils, and Appendix “B” shows the predicted calculations for each soil sample.

Flow Chart 1

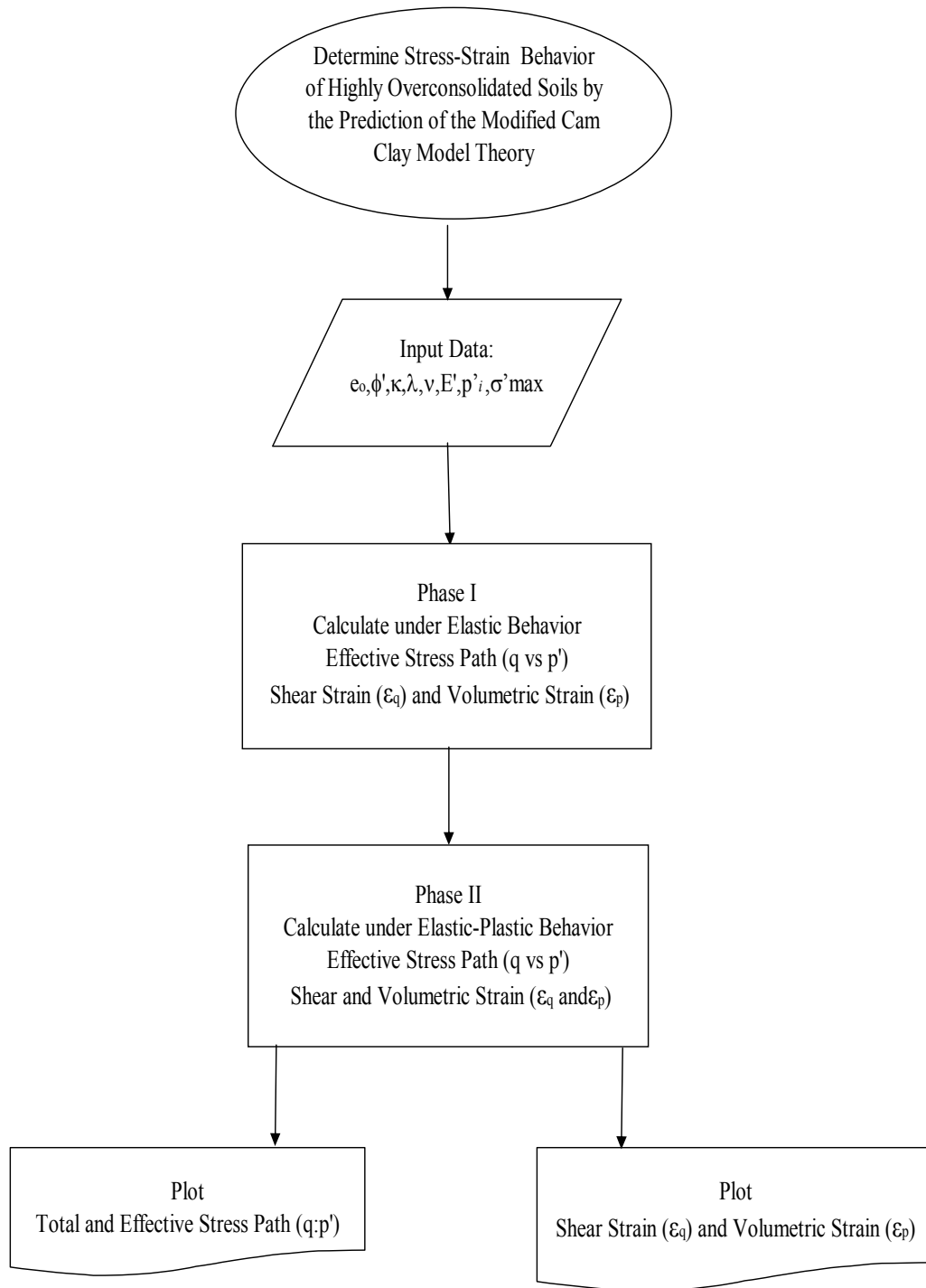


Figure 18: Flow Chart 1

Adapting MCCM to Prediction of dense granular soil behavior

According to the analysis of the test data used in this research, it is important to point out that the MCCM prediction on highly overconsolidated soils has some inconsistency with respect to the behavior observed on the triaxial tests in dense sands. The raw data of each sample test were transformed and plotted in harmony with the model invariant parameters. This analysis was also made to obtain some soil properties which will be presented in the following chapter.

To make more accurate the behavior prediction of dense sands, some observations are made and the used to revise the MCCM to accommodate dense sand. These are presented as follows:

1. The elastic behavior expected from the MCCM prediction does not match with the tendency observed in the triaxial tests. Figures 19 and 20 show typical plots of the “ e vs. q ” and “ q vs. ε_q ”. Furthermore, by observing the change of void ratio in relation to the deviator stress in Figure 19, it is important to note that the range of the linear elastic deformation does not continue linearly until the peak stress value of “ q_y ”.

In addition, volumetric deformation is related to this linear elastic deformation corresponds to an initial soil compaction phase (Figure 21). The stress point at which this linear effect is over is approximately the intersection of the critical state line (CSL) and the stress path ($q:p'$), point “T” in Figure 17(a).

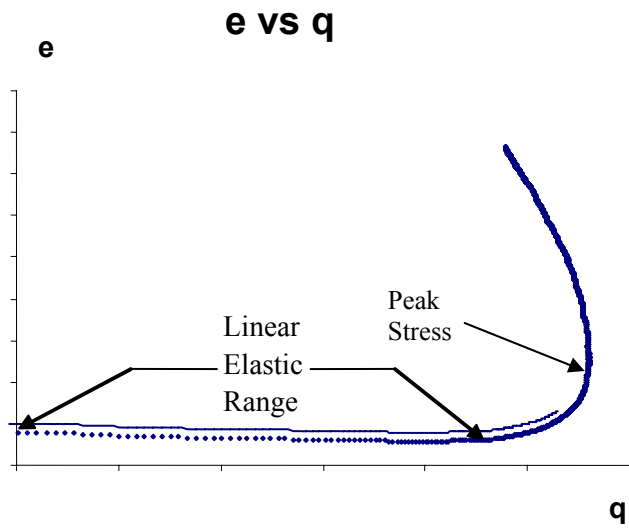


Figure 19: Typical "e vs. q" Plot in Dense Sand

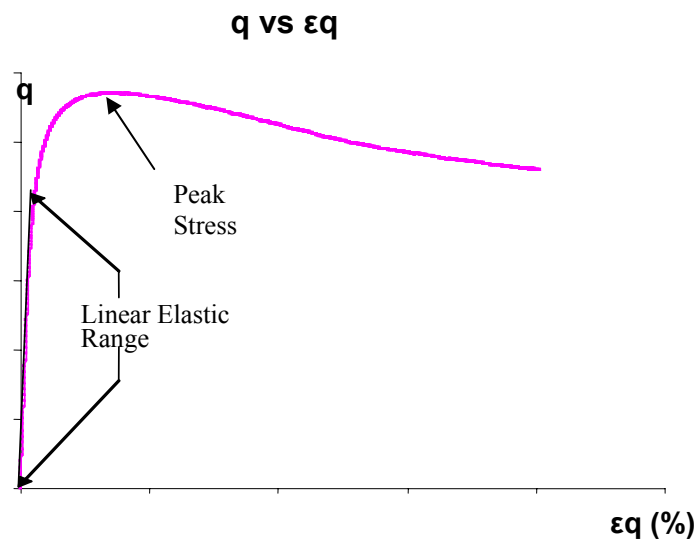


Figure 20: Typical "e vs. ϵ_q " Plot in Dense Sand

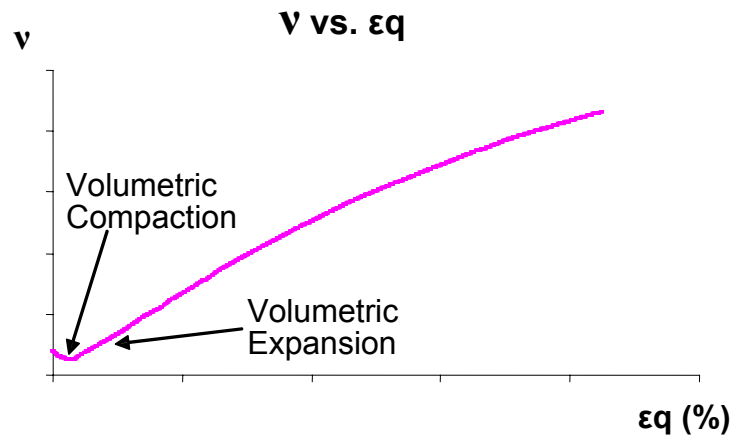


Figure 21: Typical “v vs. ϵ_q ” Plot in Dense Sand

2. Volumetric strain, ϵ_p , after point “T” of Figure 17 (a) is defined by a volumetric expansion. However, it is worth noting that the stress path and the deviator stress increment maintain the configuration of the MCCM prediction.

Therefore, phase I, described in the previous section, must be subdivided into two sub-phases. The first sub-phase is defined by the linear elastic deformation, and the second sub-phase continues until the peak stress, and it is considered to follow plastic deformation.

Phase II, as presented in MCCM, is also defined by a softening of the yield surface. Thus, a reduction of deviator stress is noticed after the peak stress point. In MCCM, the plastic shear strain is related to the plastic volumetric strain, (Equation 19) and the flow rule assumption (Equation 30). This relation gives a characteristic sag curvilinear deformation of the “q: ϵ_q ” plot, Figure 17 (c).

However, this pattern is not similar to the same plot from the triaxial tests whose shear strain deformation tendency is slightly curvilinear.

3. The inaccurate estimation not only of the total shear strain but also of the total volumetric strain, encourages a re-evaluation of Equations 9, 10, 19 and 30, specifically in relation to the parameters used in these equations.

Important elements were observed and summarized as follows:

- The volumetric strain values for the triaxial tests at the peak stress point are greater than the predicted volumetric strain, according to the elastic volumetric strain increment expressed in Equation 34. This effect was explained in observation “1”.
- For the softening effect of the yield surface, if the axial strain calculated for the triaxial test data, using Equation 25, is plotted against the volumetric strain (Equation 14) a slight curvilinear relationship is noticed, as shown in Figure 22. This observation is repetitive with a slope range between 4 and 10 for a linear trend relationship. Appendix “A” shows the “ ε_a and ε_v ” plot and the linear trend for each soil sample.

It is important to mention that the axial strain “ ε_a ” is characterized by a continuous reduction of the soil height along the triaxial test, and the softening behavior does not affect this deformation pattern. Therefore, the soil volumetric expansion occurs in the radial direction orthogonal to the axial compression load.

- By using the triaxial test data and considering the softening phase of this data, if “ p_o' ” based on Equation 27 is calculated and then plotted against

the void ratio (e) in a semi-logarithmic scale, similar to Figure 17 (b), a linear relationship is obtained, as in Figure 23.

Besides, the slope of this linear relationship represents the compression index “ λ ” according to the plastic theory. If this index is related to the swelling index “ κ ”, calculated for the elastic range, a rate of 40 times the plastic index is greater than the elastic index. In his book, Wood (1990) states that compression index is about five times the swelling index value.

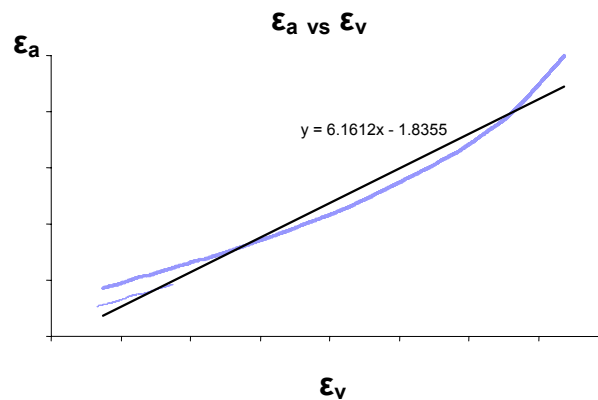


Figure 22: Typical “ ϵ_a vs. ϵ_v ” Plot for Dense Sands During Softening

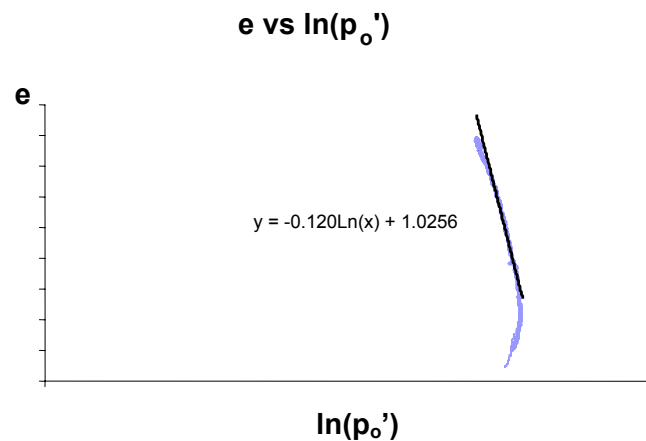


Figure 23: Typical “ e vs. $\ln(p_o')$ ” Plot for Dense Sands During Softening

Considering the previous observations and the use of the Modified Cam Clay model for the prediction of highly overconsolidated soil under drained conditions, the following adaptations to the MCCM are proposed:

1. The elastic behavior is going to be considered from the beginning of the test until the critical state line has been reached. Then, plastic deformation is defined between the CSL and the yielding point. The strain increments are determined by using Equations 19 and 30 for volumetric strain increments and shear strain increments respectively.

$$\delta\varepsilon_p^p = (\lambda - k)\delta p_o' / \nu p_o' \quad (19)$$

$$\delta\varepsilon_p^p / \delta\varepsilon = M^2 - h^2 / 2h \quad (30)$$

2. For the softening phase, plastic deformation is considered. Also, the plastic index, estimated according to the previous consideration of Figure 23, is used as input data for the calculation of the plastic volumetric strain increment in Equation 19.

$$\delta\varepsilon_p^p = (\lambda - k)\delta p_o' / \nu p_o' \quad (19)$$

3. Assuming the linear relationship between the axial strain and the volumetric strain explained previously, and considering Equation 24 based on the axial and

volumetric strain, ε_a and ε_v , it is possible to relate the shear strain with respect to the volumetric strain as a linear factor. In other words, the flow rule defined in Equation 30 is proposed to be a constant value.

$$\delta\varepsilon_q = \delta\varepsilon_a + \delta\varepsilon_p/3 \quad (24)$$

4. Finally, peak stress and ultimate stress points maintain the same definition as the MCCM.

The Matlab program is changed to incorporate these adaptations. It is then used for the prediction of the stress-strain response of dense granular materials. Flow Chart 2 shows the computer program configuration after these proposed adaptations. Plots of the stress path “q versus p” and “q versus ε_q ” are published in Appendix “B” to show the program calculations graphically. Appendix “C” exhibits details of the Matlab program.

Flow Chart 2

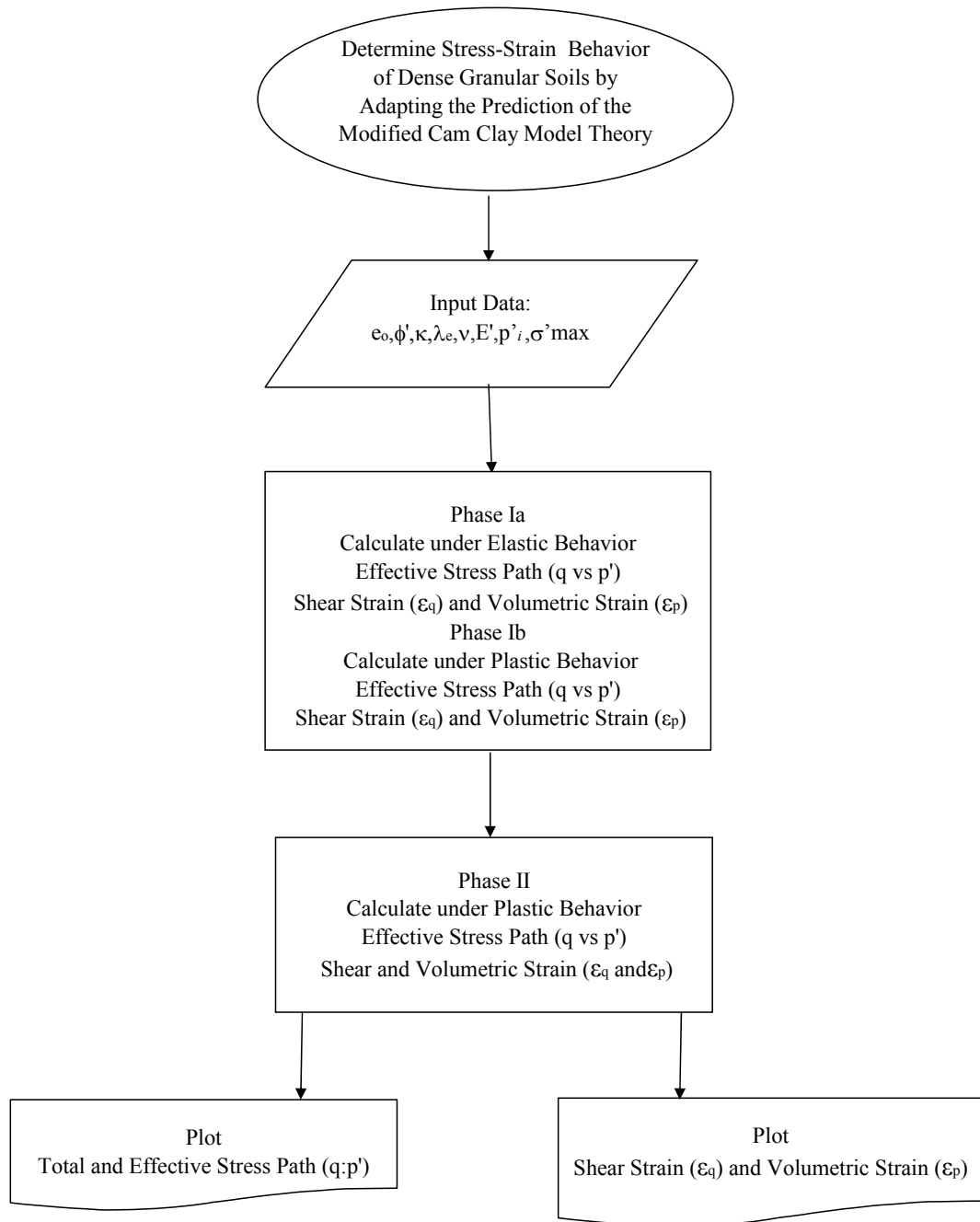


Figure 24: Flow Chart 2

CHAPTER IV

TEST RESULTS

General

This chapter presents the results of the modeling study for analysis of dense granular materials. Comparison are made with results of triaxial test done by the FDOT. These granular materials were classified as “A-3” according to the ASHTO soil classification system and tested by isotropically conventional triaxial test under drained condition. The raw data from these tests were evaluated in order to obtain some material properties and to calculate the MCCM stress –strain invariant states. Furthermore, these material properties obtained were used as input data for the computational model.

Calculations of the stress-strain invariants were made based on the MCCM invariants in order to compare the test data results and the numerical simulations. This chapter displays the material properties evaluation and the calculation of the stress-strain invariants according to the MCCM. Computational calculations based on the MCCM and the newly proposed adapted model will be shown.

Material Properties

Because the intention of this research is to evaluate the behavior of dense granular materials by using the MCCM, it is necessary to obtain the input data parameters. These

parameters are the internal angle of friction (ϕ'), the initial void ratio (e_o), the past maximum effective pressure (σ'_{max}), the compression index (λ) and the swelling index (κ), the Poisson's modulus (ν'), and the Young's modulus (E'). These parameters are calculated based on not only the triaxial test raw data analysis but also from different experimental information available from reference literature.

Internal Angle of Friction (ϕ')

The Mohr-Coulomb criterion is the most popular method to estimate the internal angle of friction of a soil, and it is calculated by using the famous Mohr-Coulomb Envelope Equation, presented as follows:

$$\tau_f = c' + \sigma'_f \tan \phi' \quad (7)$$

where “ τ_f and σ'_f ” are the effective shear and normal stresses respectively at failure, c' represents the cohesion, and ϕ' symbolizes the internal angle of friction. If this equation is considered in terms of the triaxial test principal and effective stresses at failure, and assuming the cohesionless characteristic of granular soils, Equation (7) becomes as:

$$\sin \phi' = (\sigma'_{1f} - \sigma'_{3f}) / (\sigma'_{1f} + \sigma'_{3f}) \quad (38)$$

Massachusetts Institute of Technology (MIT) theory relates the “ q and p' ” invariants in terms of the principal stress “ σ'_{1f} and σ'_{3f} ” as follows:

$$p' = (\sigma'_{1f} + \sigma'_{3f}) / 2 \quad (39)$$

$$q = (\sigma'_{1f} - \sigma'_{3f}) / 2 \quad (40)$$

Figure 25 shows the failure envelope in terms of the MIT's p' and q stress-path, known as K_f line. For cohesionless soils, the K_f equation line is represented as:

$$q = p' \tan(\alpha') \quad (41)$$

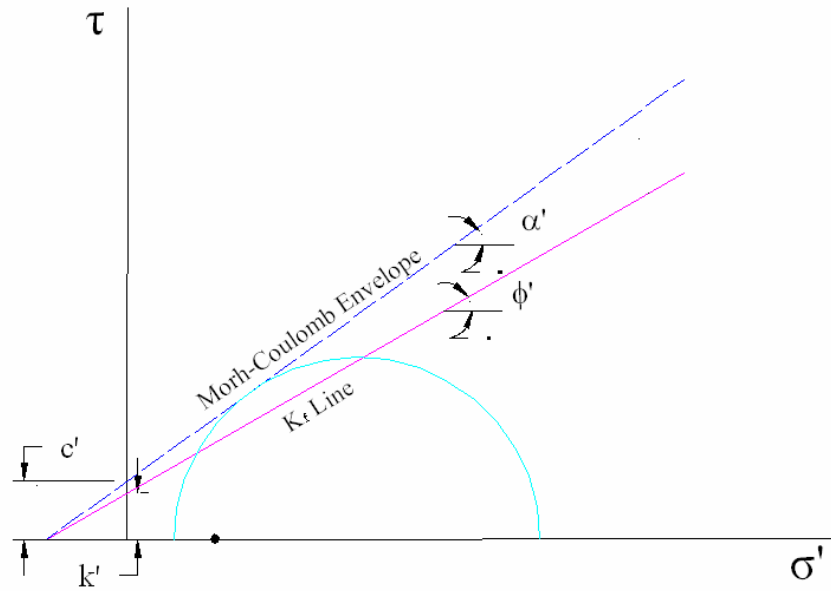


Figure 25: Mohr-Coulomb Envelope and K_f Failure Envelope

If Equations 38, 39, 40 and 41 are combined, it is possible to calculate the internal angle of friction in terms of “ α' ”, as follows:

$$\phi' = \text{ArcSin}(\tan(\alpha')) \quad (42)$$

Because each soil sample was tested at different stress states, calculation of the trend line slope gives the value of “ $\tan(\alpha')$ ” which is applied in Equation 42. Table 1 shows the estimated effective internal friction angle for each soil sample from the triaxial tests used in this research.

Table 1

Internal Friction Angles (ϕ')

Soil Test #	ϕ' (ult)
21398	33.24
21399	31.65
21401	32.66
21434	36.64
21481	33.90
21482	33.05
21483	33.31
21515	34.51
21516	31.29
21548	34.96

Initial Void Ratio (e_o)

Initial void ratio is the parameter required by MCCM to estimate the soil volumetric strain deformations. This void ratio is measured according to Equation 43 below. Moreover, when the soil is considered in saturated condition, the relation of the previous equation is calculated in terms of the moisture content “w (%)” and the specific gravity of soil solids “ G_s ”, as presented in Equation 44.

$$e = V_v/V_s \quad (43)$$

$$e = w * G_s \quad (44)$$

The specific gravity of dense sands is considered to be a value ranging between 2.60 and 2.75. This thesis assumes an average value of $G_s = 2.7$ to estimate the initial void ratio. The initial moisture content of each sample was measured in the laboratory before each test. Table 2 presents the estimated initial void ratio used in this research.

Table 2

Initial Void Ratio (e_o)

Test #	Cell Pressure (σ_r)	w (%)	Initial Void Ratio (e_o)
21398	14.00	10.50	0.28
	21.00	10.94	0.30
21399	14.00	11.22	0.30
	21.00	10.93	0.30
21401	7.00	11.93	0.32
	14.00	11.69	0.32
	21.00	11.96	0.32
21434	7.00	12.06	0.33
	14.00	12.12	0.33
	21.00	11.86	0.32
21481	7.00	12.68	0.34
	14.00	12.35	0.33
	21.00	12.31	0.33
21482	7.00	12.96	0.35
	14.00	12.62	0.34
	21.00	12.52	0.34
21483	7.00	13.10	0.35
	14.00	12.92	0.35
21515	14.00	15.75	0.43
	17.00	15.36	0.41
	21.00	15.11	0.41
21516	14.00	15.95	0.43
21548	7.00	10.20	0.28
	14.00	10.19	0.28
	21.00	10.22	0.28

Past Maximum Effective Pressure (σ'_{max})

This parameter represents the maximum effective overburden stress that a soil has supported in the past. This parameter is important because it defines the size of the yield surface which limits the elastic and plastic deformations of a soil.

The real estimation of this parameter may be difficult due to the historical evaluation of the possible maximum effective overburden. However, by simulating the elliptical surface defined by MCCM at the peak strength of each test, it is possible to estimate the equivalent past maximum effective overburden pressure for each soil sample. Figure 26 shows an example of the MCCM ellipse surface represented in the $q:p'$ space that intersects the peak strength “ q_y and p_y ”, obtained from the triaxial test.

Table 3 shows the estimated past maximum effective overburden pressure and the overconsolidation ratio (OCR) for each soil sample.

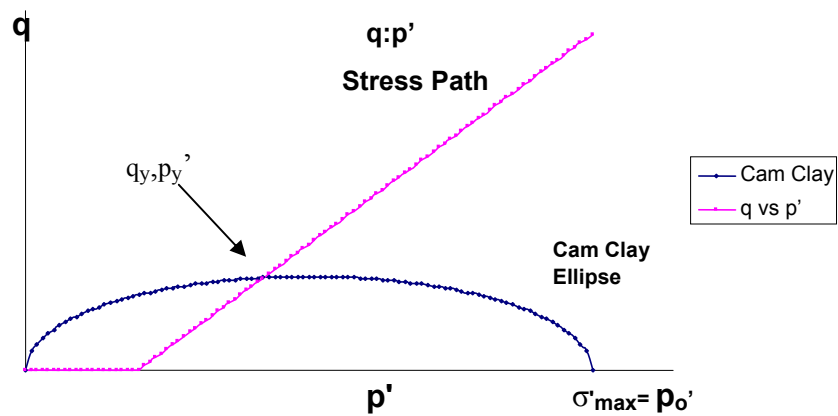


Figure 26: Cam Clay Ellipse and “ q vs. p ” Stress Path

Table 3

Past Maximum Effective Pressure (σ'_{max})

Test #	Cell Pressure (σ_r) (psi)	p_o' (psi)	OCR
21398	14.00	70.00	5.00
	21.00	90.00	4.29
21399	14.00	55.00	3.93
	21.00	91.00	4.33
21401	7.00	30.00	4.29
	14.00	59.00	4.21
	21.00	83.00	3.95
21434	7.00	36.00	5.14
	14.00	72.00	5.14
	21.00	100.00	4.76
21481	7.00	34.00	4.86
	14.00	63.00	4.50
	21.00	90.00	4.29
21482	7.00	33.00	4.71
	14.00	67.00	4.79
	21.00	87.00	4.14
21483	7.00	33.00	4.71
	14.00	62.00	4.43
21515	14.00	62.00	4.43
	17.00	70.00	4.12
	21.00	81.00	3.86
21516	14.00	77.00	5.50
21548	7.00	35.00	5.00
	14.00	65.00	4.64
	21.00	93.00	4.43

Swelling Index (κ)

The volume recovery capacity which is associated to the elastic behavior of a soil is estimated by this factor. This index is represented by the slope of the unload-reload portion of the “ $e-\ln(p')$ ” line as shown in Figure 27.

It is important to point out that Figure 27 is a typical plot for soils with a medium or loose density in which the soil compaction is possible to occur along the test. However, dense granular material behavior is generally ruled by an initial compression phase, which is considered under elastic behavior, followed by a continued volume expansion of the soil sample. According to the change of volume data obtained from the triaxial test, Figure 28 shows typical “e versus $\ln(p')$ ” plot for dense sands.

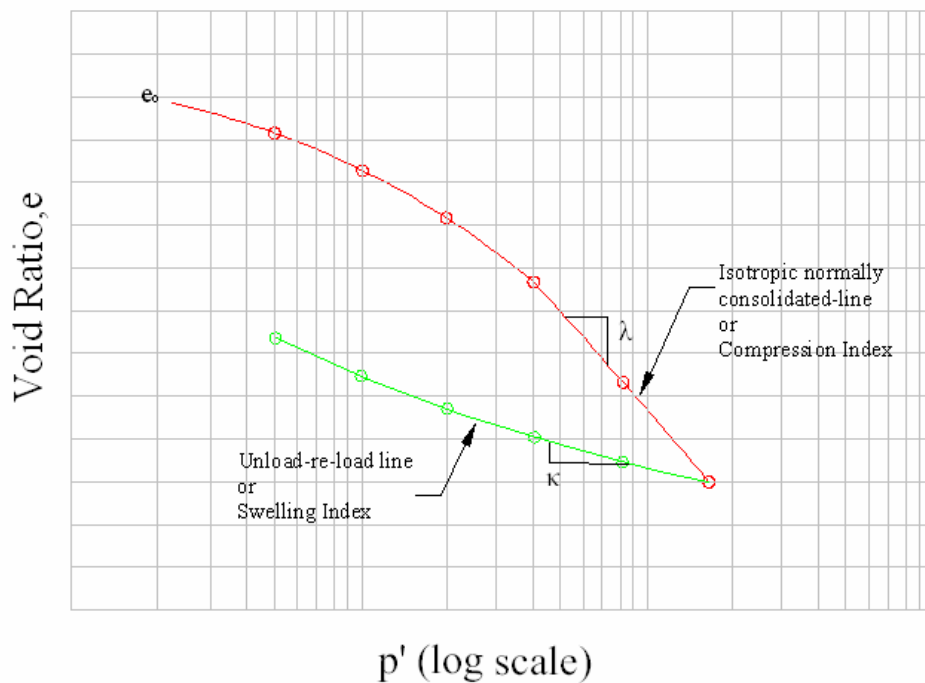


Figure 27: Typical “e- $\ln(p')$ ” Plot

In addition, because the initial compression phase is related to elastic behavior, the swelling indexes (κ) used in this research are estimated by the “e- $\ln p'$ ” trend line slope of each soil sample.

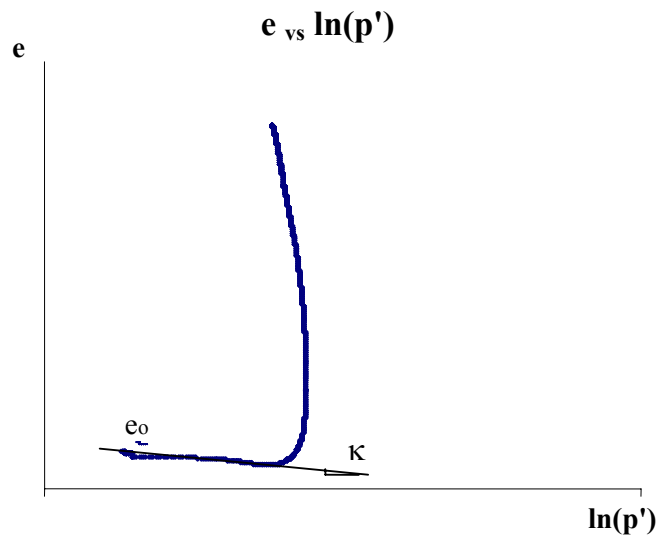


Figure 28: Typical “e-lnp” Plot for Dense Sands

Compression Index (λ)

The effect of the compression index is measured when the stress increments applied to a soil make unrecoverable volumetric soil deformation. According to the behavior of dense granular materials, as explained before, it is not possible to obtain this compression index number. Nevertheless, a relation presented in Wood (1990) states that the compression index (λ) is equivalent to 5 or 6 times the swelling index (κ).

Figure 29 depicts the relation between the void ratio “e” and the tip stress value “ p_o ” of the ellipse surface, in a semi-logarithm scale. If a trend line is projected along the softening process, it is possible to estimate the plastic index which is proposed to be called “Expansion Index (λ_e)” due to the volumetric expansion of the soil.

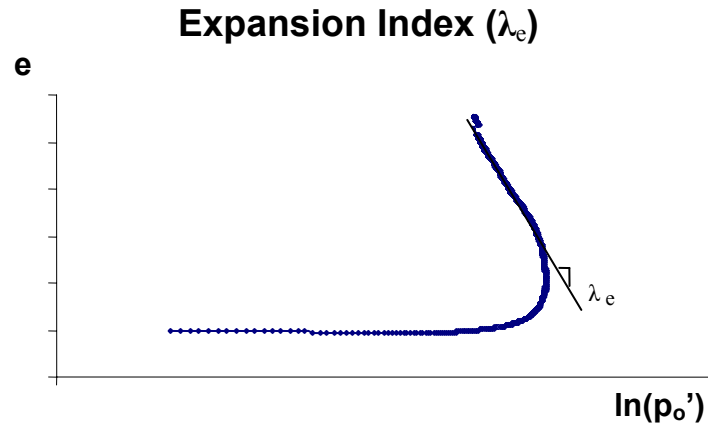


Figure 29: Typical “e-lnp_o” Plot for Dense Sands

Table 4 shows the swelling index (κ), the compression index (λ), and the expansion index (λ_e) estimated for each soil sample.

Poisson's Ratio (ν)

Poisson's ratio is the relation of the induced transverse strain to the imposed longitudinal strain. Each material has a specific range of Poisson's ratio, and because dense sands Poisson's ratio range from 0.30 to 0.45, a value equal to 0.35 is considered in this research.

Table 4

Compression and Swelling Indexes

Test #	Cell Pressure (σ)	λ_e	λ	κ
21398	14.00	0.1250	0.0216	0.0036
	21.00	0.1460	0.0192	0.0032
21399	14.00	0.1210	0.0102	0.0017
	21.00	0.1070	0.0150	0.0025
21401	7.00	0.1039	0.0126	0.0021
	14.00	0.0999	0.0174	0.0029
	21.00	0.0959	0.0138	0.0023
21434	7.00	0.0979	0.0270	0.0045
	14.00	0.1393	0.0228	0.0038
	21.00	0.1435	0.0204	0.0034
21481	7.00	0.0920	0.0108	0.0018
	14.00	0.0859	0.0222	0.0037
	21.00	0.1397	0.0240	0.0040
21482	7.00	0.1184	0.0222	0.0037
	14.00	0.0827	0.0162	0.0027
	21.00	0.1228	0.0246	0.0041
21483	7.00	0.1116	0.0150	0.0025
	14.00	0.1345	0.0138	0.0023
21515	14.00	0.2240	0.0198	0.0033
	17.00	0.0883	0.0228	0.0038
	21.00	0.1828	0.0192	0.0032
21516	14.00	0.2484	0.0084	0.0014
21548	7.00	0.0867	0.0180	0.0030
	14.00	0.1422	0.0132	0.0022
	21.00	0.1399	0.0126	0.0021

Young's Modulus (E')

This material property describes the slope of the axial stress in relationship with the axial strain. For a conventional triaxial compression test, it is measured as the slope of the deviator stress against the axial strain. Figure 30 depicts a typical plot of the “ q vs ϵ_a ” and the trend line which define the Young's Modulus. Table 5 presents the estimated Young's Modulus for each soil sample. Appendix “A” depicts the graphical calculations of the material properties that were shown in previous tables for all the soil samples.

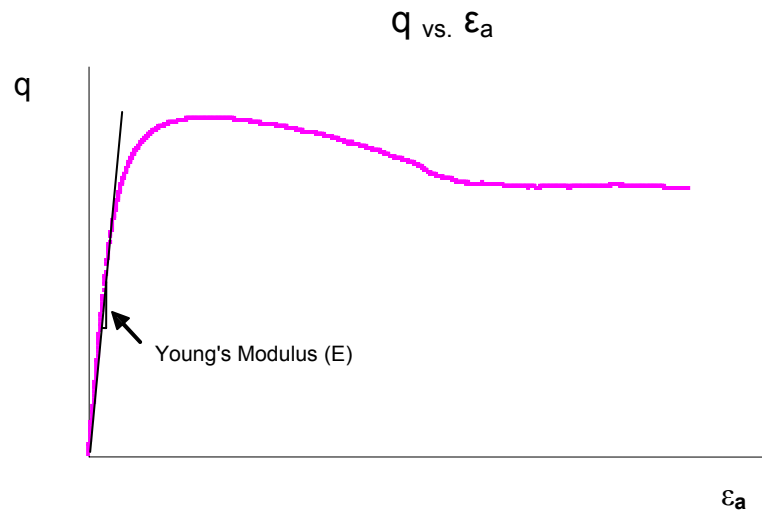


Figure 30: Typical “ q - ϵ_a ” Plot for Dense Sands

Table 5
Young's Modulus (E')

Test #	Cell Pressure (σ)	E' (lb/in ²)
21398	14.00	3973.00
	21.00	6152.00
21399	14.00	5435.00
	21.00	6841.00
21401	7.00	2908.00
	14.00	4980.00
	21.00	6796.00
21434	7.00	2988.00
	14.00	3793.00
	21.00	6672.00
21481	7.00	3465.00
	14.00	3972.00
	21.00	6040.00
21482	7.00	2668.00
	14.00	5176.00
	21.00	4496.00
21483	7.00	3327.00
	14.00	5126.00
21515	14.00	4367.00
	17.00	4831.00
	21.00	5873.00
21516	14.00	5975.00
21548	7.00	3789.00
	14.00	5239.00
	21.00	6954.00

Triaxial Test Results

First, processing the triaxial test data in terms of the MCCM stress-strain invariants is required. This section provides the stress invariants (q and p'), and the shear strain invariant (ϵ_q) at the peak and ultimate points observed in the experimental data. Appendix “B” provides the MCCM typical plots similar to Figure 17, made for each soil sample, which will then be used for graphical verification.

Stress invariants (q and p') are calculated and plotted as Figure 31 (a) to show the stress paths of each sample during the triaxial test. Because the axial displacement and the change of volume of the soil samples are measured during the triaxial test, the “ q versus ϵ_q ” relationship can be plotted similar to Figure 31 (b).

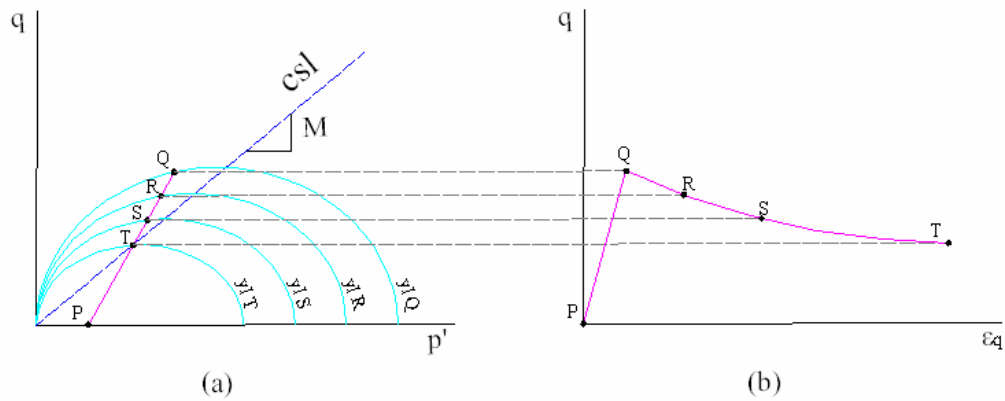


Figure 31: MCCM Typical Plots under Drained Conditions in Highly Overconsolidated Soils (after Wood, 1990)

To estimate the “ q and p' ” stress and the strain increments “ $\delta\epsilon_p$ and $\delta\epsilon_q$ ”, the following equations are applied based on the triaxial test data:

$$q = (\sigma_1' - \sigma_3') \quad (2)$$

$$p' = (2\sigma_3' + \sigma_1')/3 \quad (3)$$

$$\delta\varepsilon_p = -\delta V/V \quad (14)$$

$$\delta\varepsilon_q = -\delta l/l + (\delta V/V)/3 \quad (24)$$

Table 6 provides final results of the stress- strain invariant calculations for each soil sample. This table shows the stress-strain calculations for the peak point “Q” and “T” of Figure 31(a) and (b), which represent the yielding point (q_y, p_y' , and ε_{qy}) and the ultimate or failure point (q_f, p_f' , and ε_{qf}) respectively.

It is important to note that the shear strain at the failure point “T” is presented as ε_{qf} and ε_{qfmax} . ε_{qf} represents the approximate shear strain value whose deviator stress “q” matches the failure point, while the ε_{qfmax} is the maximum shear strain value of the triaxial test data. Figure 32 shows the typical location of the shear strains the peak and failure points. Finally, it is important to recall that each soil sample was tested at different initial isotropic consolidation pressures.

Table 6

Stress Invariants

Test #	Cell Pressure ($\sigma_r=p_i'$)	Peak Point			Ultimate Point			
		p_y	q_y	ϵ_{q_y} (%)	p_r	q_r	ϵ_{q_r} (%)	$\epsilon_{q_r \max}$ (%)
21398	14.00	29.00	44.99	2.30	25.56	34.69	15.90	29.10
	21.00	41.12	60.35	2.76	37.98	50.95	10.16	18.48
21399	14.00	25.67	35.02	2.84	23.46	28.39	10.69	19.91
	21.00	40.02	57.06	2.65	37.26	48.79	17.50	18.83
21401	7.00	13.47	19.41	2.65	12.18	15.53	10.05	16.67
	14.00	26.86	38.59	2.81	25.41	34.24	14.65	18.00
	21.00	39.34	55.03	2.90	37.19	48.56	12.36	22.13
21434	7.00	15.89	26.66	1.70	13.45	19.36	10.61	14.41
	14.00	31.98	53.93	3.60	29.33	45.99	13.90	16.55
	21.00	45.63	73.88	2.64	40.77	59.30	6.52	19.94
21481	7.00	15.15	24.44	2.44	13.61	19.84	16.92	18.59
	14.00	28.25	42.76	2.89	26.04	36.13	11.08	13.79
	21.00	41.17	60.50	3.04	38.21	51.63	11.29	19.05
21482	7.00	14.15	21.44	2.90	13.16	18.48	19.21	19.21
	14.00	28.85	44.56	3.04	25.86	35.59	15.30	19.19
	21.00	40.17	57.51	2.89	37.13	48.38	10.48	13.88
21483	7.00	14.17	21.51	2.03	12.80	17.41	13.52	15.05
	14.00	27.72	41.16	2.48	25.64	34.92	13.20	16.06
21515	14.00	28.12	42.35	3.78	27.12	39.36	21.00	22.40
	17.00	33.13	48.38	3.08	31.96	44.88	13.80	18.09
	21.00	40.00	56.99	3.45	38.51	52.54	10.37	18.96
21516	14.00	25.16	33.49	1.46	24.40	31.19	16.10	18.61
21548	7.00	15.31	24.94	2.11	13.30	18.91	13.90	13.90
	14.00	29.44	46.32	2.73	27.11	39.32	16.25	16.25
	21.00	42.85	65.54	2.70	39.37	55.10	13.32	15.98

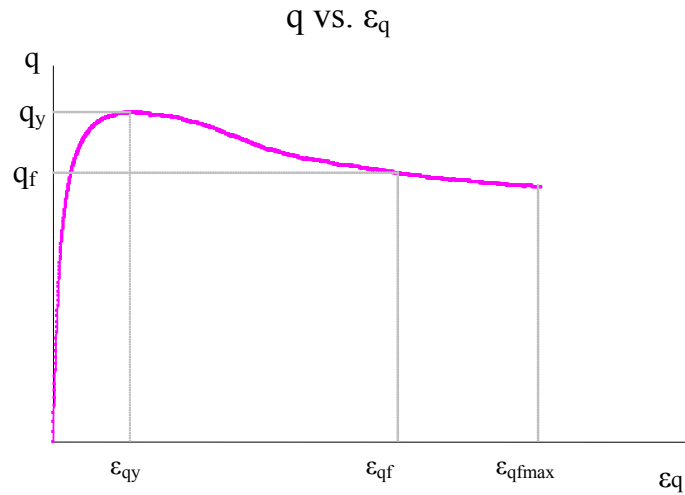


Figure 32: “q-εq” Values at Peak and Failure Points

Data Analysis and Computation

Previous chapter explained the applicability of the MCCM and implementation of the adapted model into a Matlab program. According to the flow charts presented for both prediction programs, the input data represents the initial step. Then, it is followed by the stress-strain invariants calculation process for each model. Finally, the results are tabulated for the stress-strain invariants at the peak and failure points and plotted according to Figure 31 (a) and (b).

Appendix “B” also contains the plots of the MCCM and adapted model predictions, which can be compared with the graphical representation of the triaxial test data processed in terms of the same stress-strain invariants.

In the following section, it is presented the computational stress- strain results for the analysis and comparison to the test data.

Analysis of the Test Results

The experimental data, which have been summarized in terms of the general stress-strain tables, are compared with the numerical models based on Critical States Soil Mechanics concepts. Even though these model concepts were originally developed for cohesive soils, they may be applicable for other types of soils such as dense sands. Moreover, MCCM was created due to the consistent interpretation of experimental data which basically were obtained from triaxial test experiments.

These interpretations have been transformed into idealized and numerical equations that predict the pattern of behavior of soils. This research has been supported by the experimental data of 25 conventional triaxial tests under drained condition applied in dense sands and performed by the Florida Department of Transportation.

The intention of the analyses presented in this section is to offer additional information that may improve the prediction of the behavior of dense granular soils. Such analysis is principally shown in terms of the MCCM stress-strain invariants as shown in Figure 31 (a) and (b). Initially, the results are presented in term of the stress invariants “ q and p' ” based on the stress path pattern, as depicted in Figure 31 (a). Then, the shear strain prediction, ϵ_q , is analyzed based on the “ q versus ϵ_q ” plot, similar to Figure 31 (b).

Stress Invariants “ q and p' ”

This section explains the stress path predictability of the model. Stress invariants “ q and p' ” have been evaluated at the peak and ultimate or failure points.

Figure 32 depicts the typical behavior of the dense sands, and Appendix “B” shows the same plot configurations for each soil sample. It is important to recall that Figure 32 and Appendix “B” are presented in term of the same invariant parameters used for the prediction models, as shown is Figure 31.

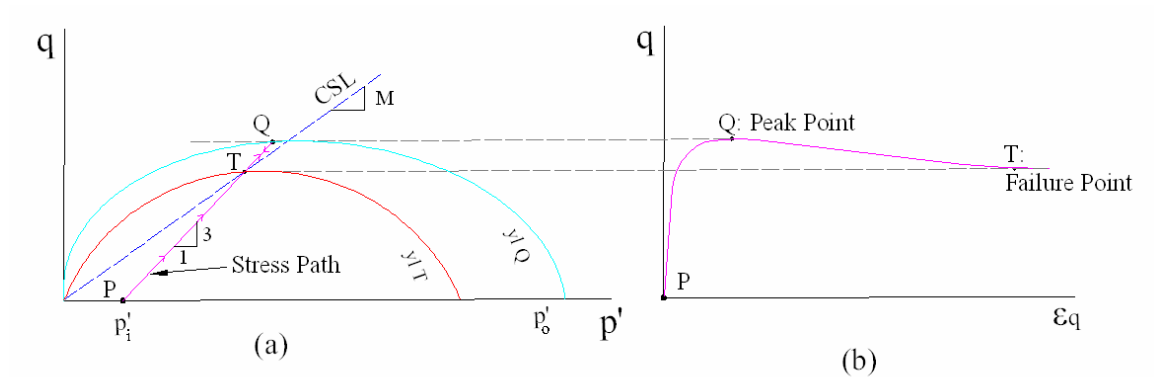


Figure 33: Typical Plots for Dense Sands

For the analysis of the predictive stress path and the peak and failure states, it is important to recognize that the peak points for the test data were matched to the MCCM ellipse equation earlier to estimate the past maximum effective pressure for each soil sample. However, it is worth noting that except for past maximum effective pressure, no other parameters were assumed. There is good comparison between the model predictions and the experimental observations.

For example, the experimental stress path maintains the stress relationship expressed in Equation 37 even though the strain control option had been used for the triaxial tests. Moreover, this relation is also applicable for the softening behavior when the stress states return from point “Q” to point “T” of Figure 33.

$$\delta q = 3\delta p' \quad (37)$$

Another similarity corresponds to the softening pattern observed after the yield surface is reached. This softening process is addressed by the MCCM assuming the contraction of the yield loci from “yIQ” to “yIT”, as shown in Figure 33.

This softening effect marks the intensity of the peak shape observed in the “q vs. ϵ_q ” plot of Figure 33. The shape of the peak observed in the “q vs. ϵ_q ” plot depends principally on the size of the yield surface, which is defined by the factor “M” and the past maximum effective pressure, and the location of the initial isotropic pre-consolidation pressure.

An example of this peak shape effect can be observed on Figure 34. In this case, the past maximum effective pressure (p_o') is changed, but the initial isotropic pre-consolidation pressure (p_i') and internal friction angle (ϕ') are kept unchanged.

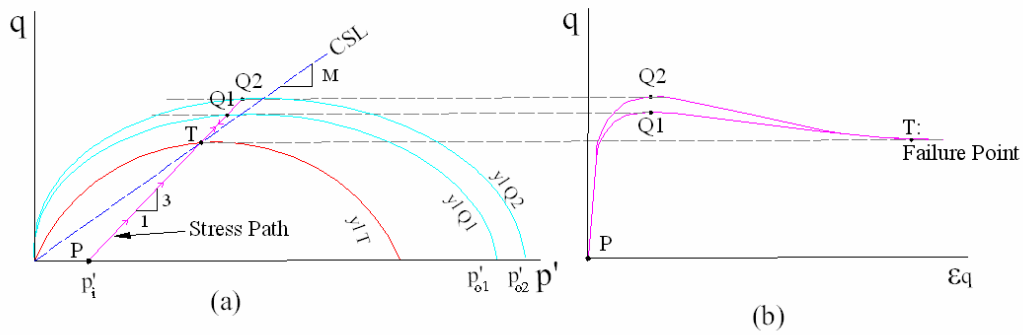


Figure 34: Peak Shape Effect

The peak and failure stresses predicted by the MCCM and the adapted model do not consider any difference in their calculation. Therefore, analysis for these stresses values are compared between the test data and MCCM model.

In reference to the test ultimate or failure stress points, the model prediction agree well with the FDOT triaxial test results. Therefore, the ultimate stress values for each soil sample were estimated at the average value of deviator stress where continuous deformations occur without significant deviator stress increments.

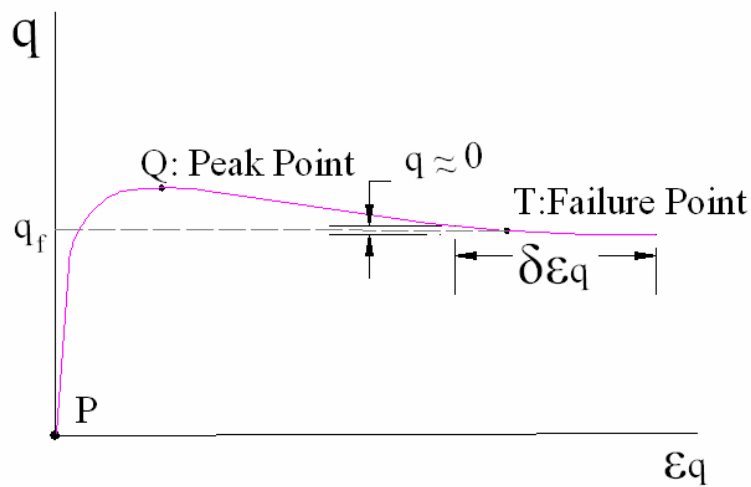


Figure 35: Ultimate or Failure Deviator Stress

The test ultimate stress values are compared to the predicted values giving a maximum difference of $\pm 10\%$. This difference shows that the Critical State Line which is defined by the Mohr-Coulomb theory in terms of the angle of friction also works for the prediction of the ultimate or failure stress point for dense sands, Point “T” of Figure 31 and 33 (a).

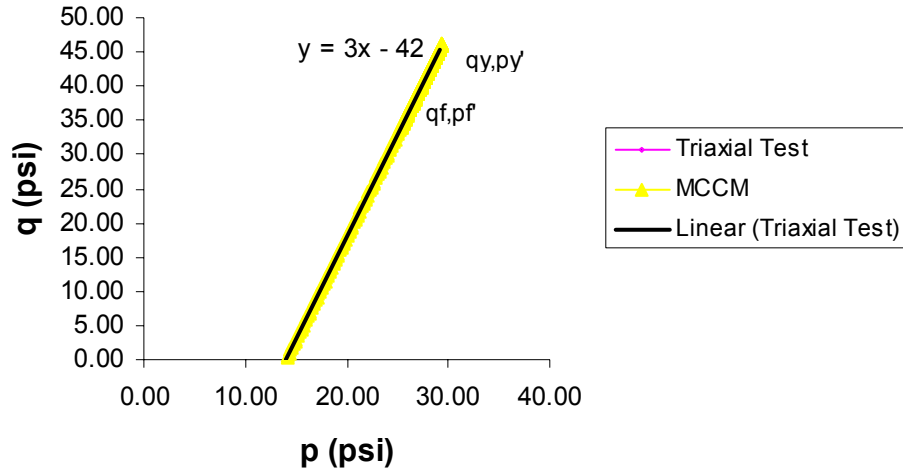
Table 7 summarizes the peak and failure stresses for the test data and the prediction of the MCCM. In summary, the predictability of the models in relation to the stress path and the peak and failure states were appropriate for the stresses observed in the experimental data. Figures 36 through 45 show the stress path plots for each soil sample used in this research. In addition, Appendix “B” presents the details of the test data and prediction models plots according to the MCCM plots similarly to that shown in Figure 17.

Table 7
Peak and Failure Stresses

Test #	Cell Pressure ($\sigma_r = p_r$)	Peak Point						Failure or Ultimate Stress Point					
		Triaxial Test		Model		Diference in percent at Peak Stress	Triaxial Test		Model		Diference in percent at Ultimate Stress		
		p_y	q_y	p_y	q_y		p_r	q_r	p_r	q_r			
21398	14.00	29.00	44.99	29.45	46.35	-1.53%	-2.93%	25.56	34.69	25.32	33.97	0.95%	2.12%
	21.00	41.12	60.35	41.04	60.13	0.27%	0.37%	37.98	50.95	37.96	50.89	0.05%	0.12%
21399	14.00	25.67	35.02	25.63	34.89	0.14%	0.37%	23.46	28.39	24.30	30.91	-3.45%	-8.17%
	21.00	40.02	57.06	40.16	57.47	-0.47%	-0.71%	37.26	48.79	36.46	46.37	2.20%	5.21%
21401	7.00	13.47	19.41	13.55	19.65	-0.28%	-1.24%	12.18	15.53	12.47	16.41	-2.34%	-5.34%
	14.00	26.86	38.59	26.89	38.67	-0.09%	-0.21%	25.41	34.24	24.94	32.82	1.90%	4.33%
	21.00	39.34	55.03	39.18	54.53	0.56%	0.92%	37.19	48.56	37.41	49.24	-0.59%	-1.37%
21434	7.00	15.89	26.66	15.88	26.63	0.02%	0.11%	13.45	19.36	13.91	20.72	-3.27%	-6.55%
	14.00	31.98	53.93	31.75	53.26	0.77%	1.26%	29.33	45.99	27.81	41.44	5.47%	10.99%
	21.00	45.63	73.88	45.74	74.23	-0.39%	-0.48%	40.77	59.30	41.72	62.16	-2.29%	-4.60%
21481	7.00	15.15	24.44	14.69	23.08	1.55%	5.87%	13.61	19.84	12.88	17.66	5.69%	12.34%
	14.00	28.25	42.76	28.31	42.94	-0.20%	-0.43%	26.04	36.13	25.77	35.31	1.06%	2.33%
	21.00	41.17	60.50	41.49	61.47	-1.10%	-1.58%	38.21	51.63	38.66	52.97	-1.17%	-2.54%
21482	7.00	14.15	21.44	14.26	21.79	-0.39%	-1.61%	13.16	18.48	12.59	16.79	4.52%	10.05%
	14.00	28.85	44.56	28.73	44.20	0.42%	0.82%	25.86	35.59	25.19	33.59	2.67%	5.95%
	21.00	40.17	57.51	40.28	57.83	-0.38%	-0.56%	37.13	48.38	37.79	50.38	-1.76%	-3.97%
21483	7.00	14.17	21.51	14.33	21.99	-0.55%	-2.20%	12.80	17.41	12.68	17.05	0.96%	2.09%
	14.00	27.72	41.16	27.82	41.46	-0.34%	-0.72%	25.64	34.92	25.37	34.11	1.06%	2.36%
21515	14.00	28.12	42.35	28.38	43.15	-0.89%	-1.85%	27.12	39.36	26.19	36.59	3.56%	7.58%
	17.00	33.13	48.38	33.28	48.83	-0.53%	-0.93%	31.96	44.88	31.81	44.44	0.47%	0.98%
	21.00	40.00	56.99	39.86	56.57	0.46%	0.74%	38.51	52.54	39.29	54.89	-1.98%	-4.28%
21516	14.00	25.16	33.49	25.28	33.85	-0.41%	-1.06%	24.40	31.19	24.09	30.26	1.29%	3.07%
21548	7.00	15.31	24.94	15.19	24.57	0.42%	1.52%	13.30	18.91	13.26	18.79	0.33%	0.65%
	14.00	29.44	46.32	29.27	45.81	0.58%	1.12%	27.11	39.32	26.52	37.57	2.21%	4.66%
	21.00	42.85	65.54	42.89	65.67	-0.15%	-0.20%	39.37	55.10	39.79	56.36	-1.06%	-2.23%

Test # 21398

Stress Path (q:p')



Stress Path (q:p')

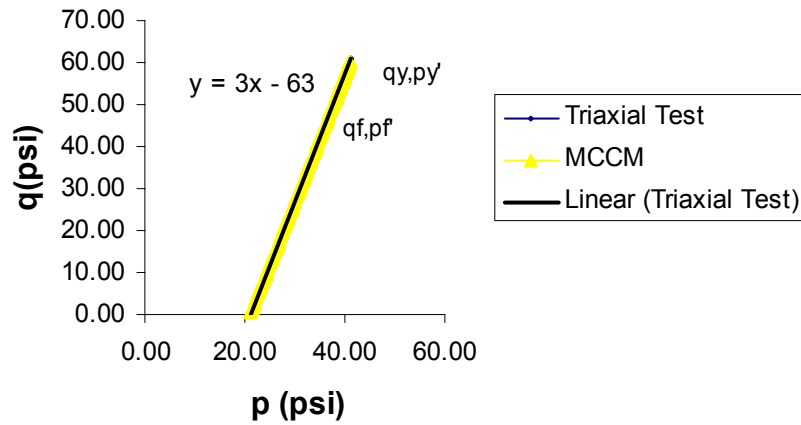
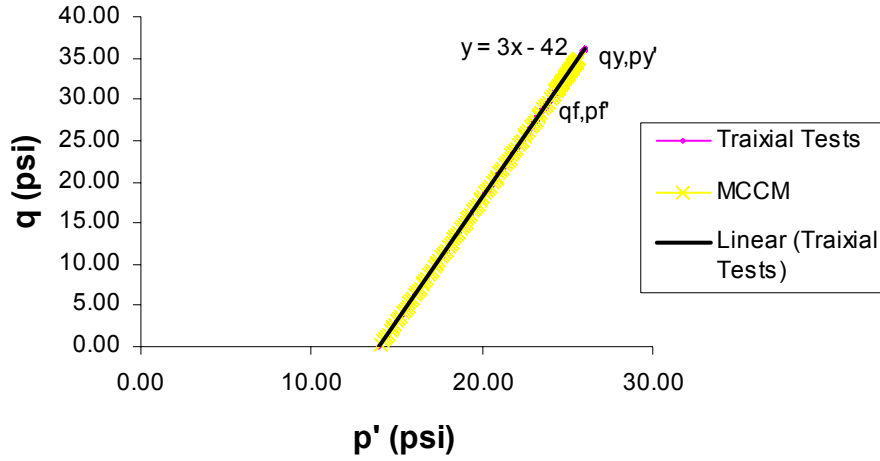


Figure 36: Stress Path, Peak and Ultimate or Failure Stresses

Test # 21399

Stress Path (q:p')



Stress Path (q:p')

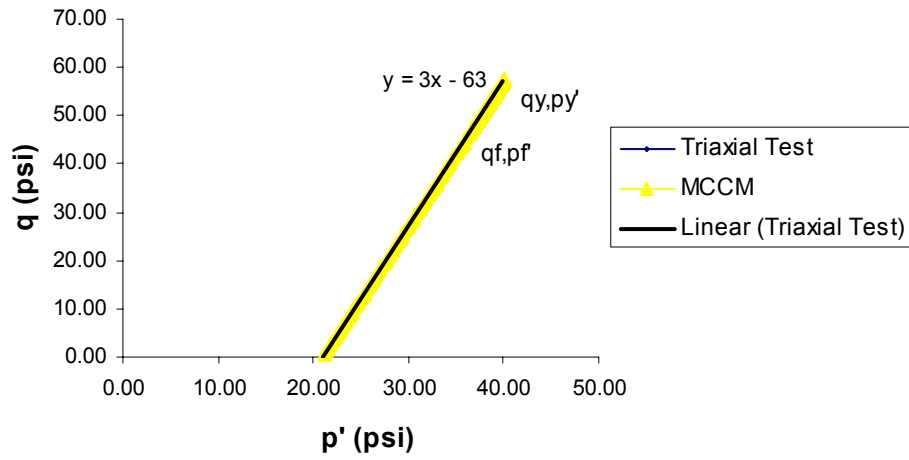
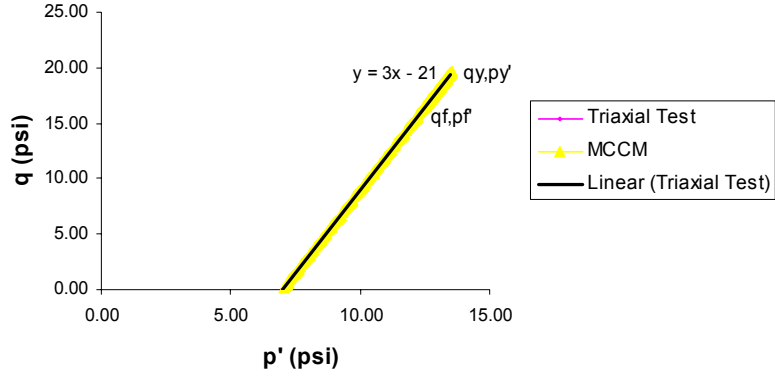


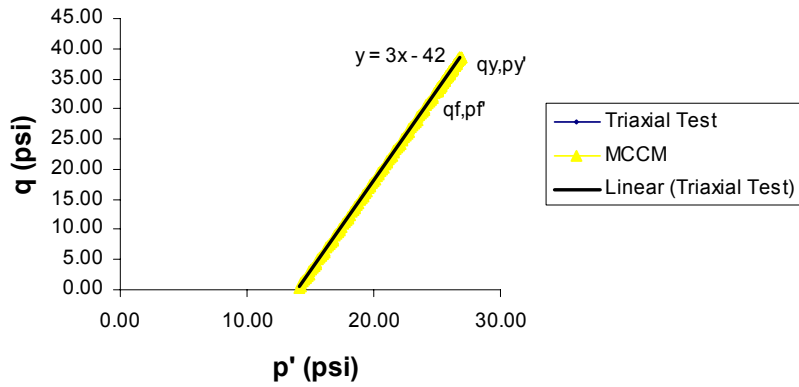
Figure 37: Stress Path, Peak and Ultimate or Failure Stresses

Test # 21401

Stress Path (q:p')



Stress Path (q:p')



Stress Path (q:p')

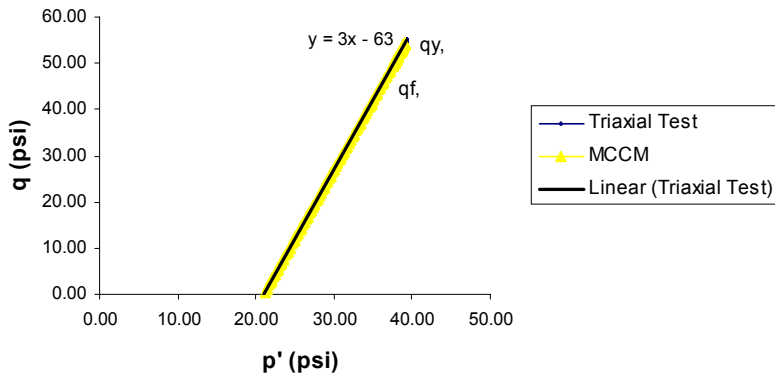
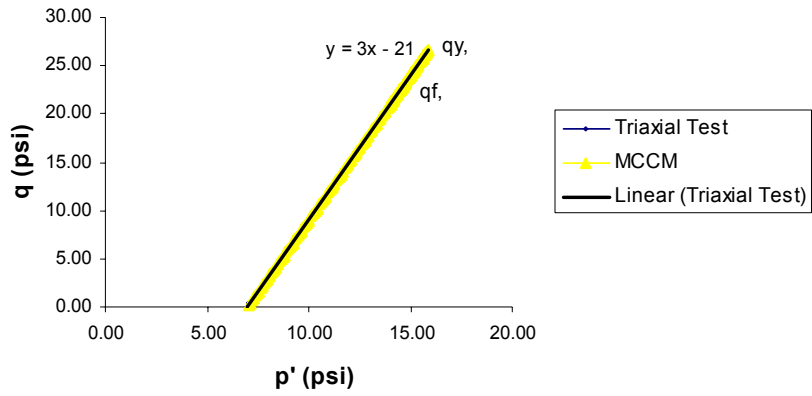


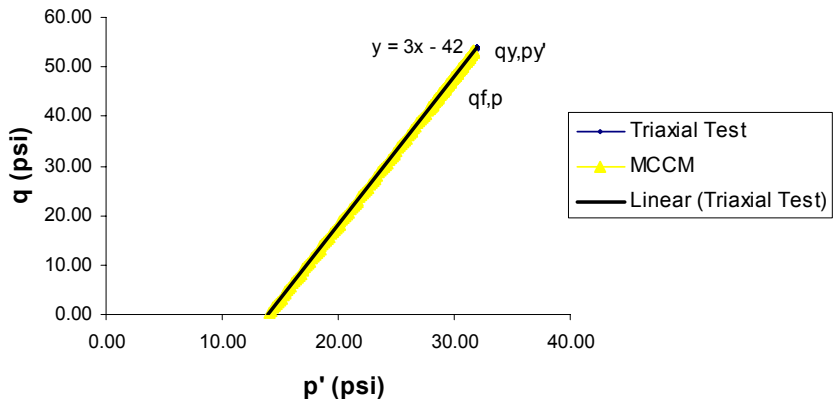
Figure 38: Stress Path, Peak and Ultimate or Failure Stresses

Test # 21434

Stress Path (q:p')



Stress Path (q:p')



Stress Path (q:p')

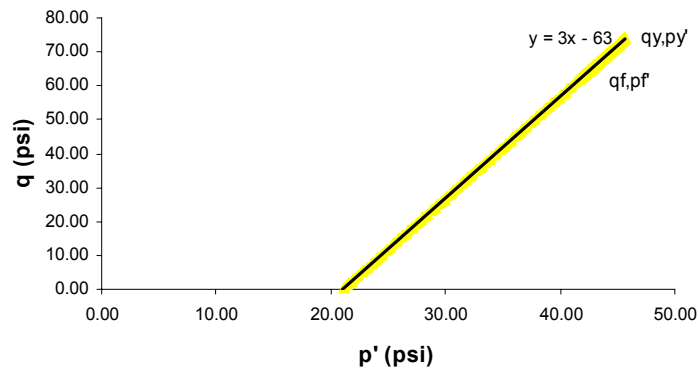
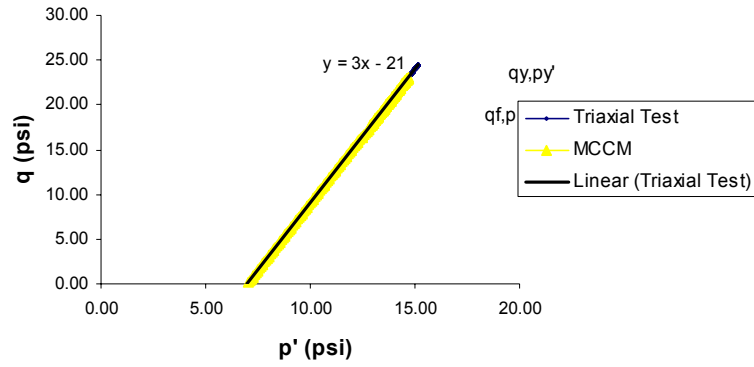


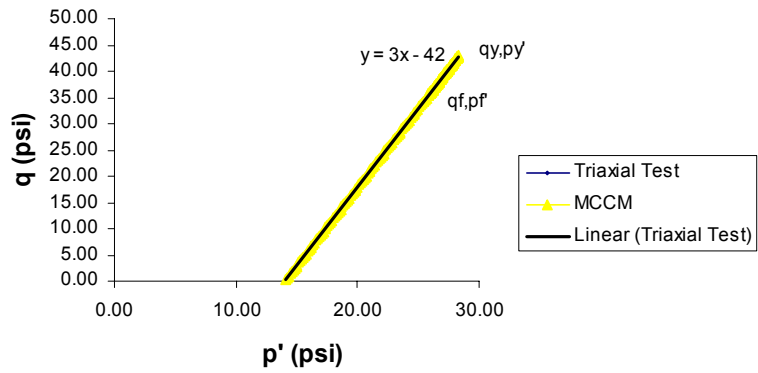
Figure 39: Stress Path, Peak and Ultimate or Failure Stresses

Test # 21481

Stress Path (q:p')



Stress Path (q:p')



Stress Path (q:p')

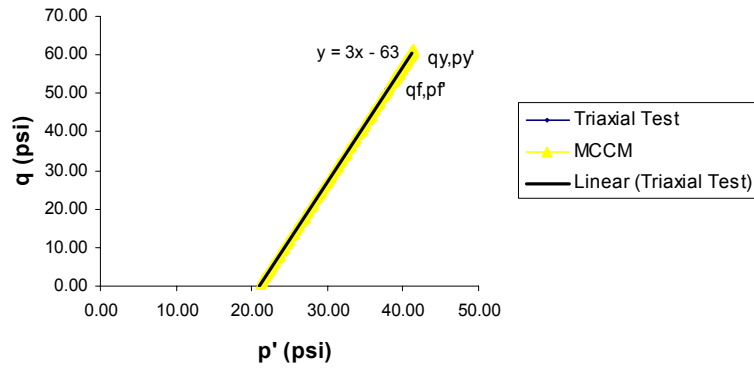
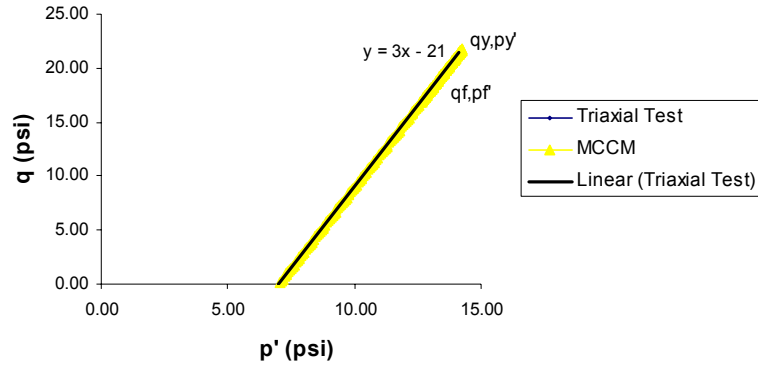


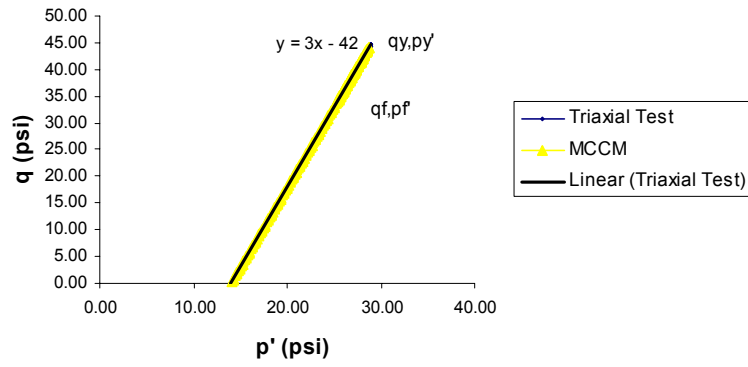
Figure 40: Stress Path, Peak and Ultimate or Failure Stresses

Test # 21482

Stress Path (q:p')



Stress Path (q:p')



Stress Path (q:p')

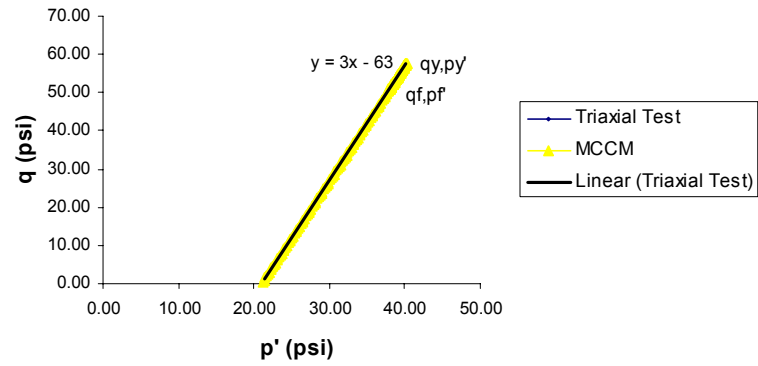
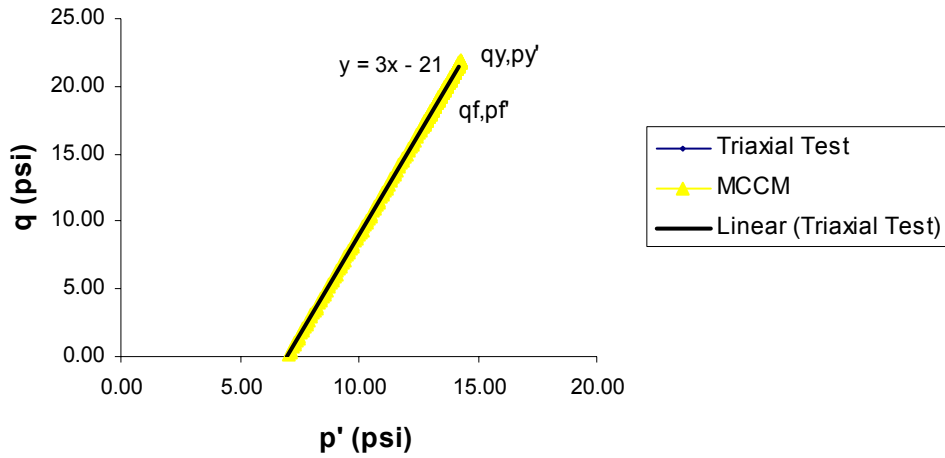


Figure 41: Stress Path, Peak and Ultimate or Failure Stresses

Test # 21483

Stress Path (q:p')



Stress Path (q:p')

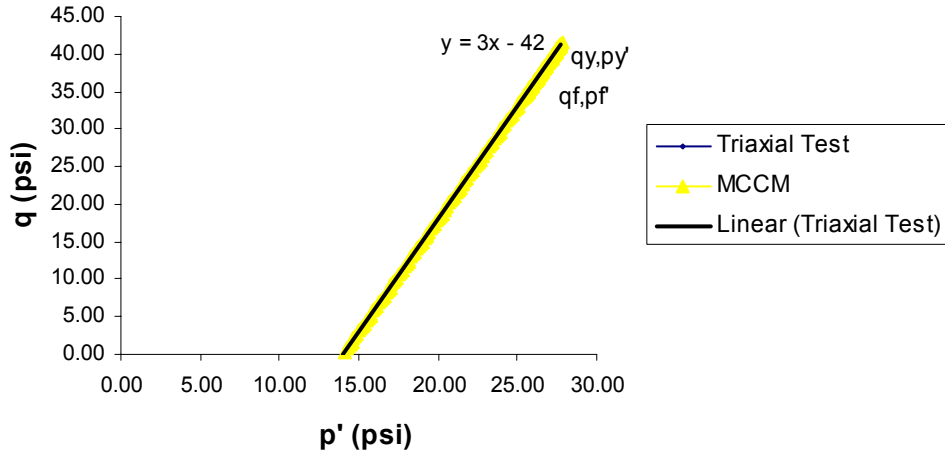
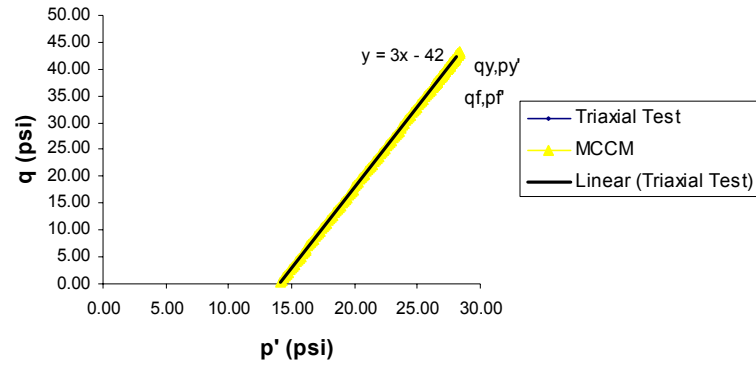


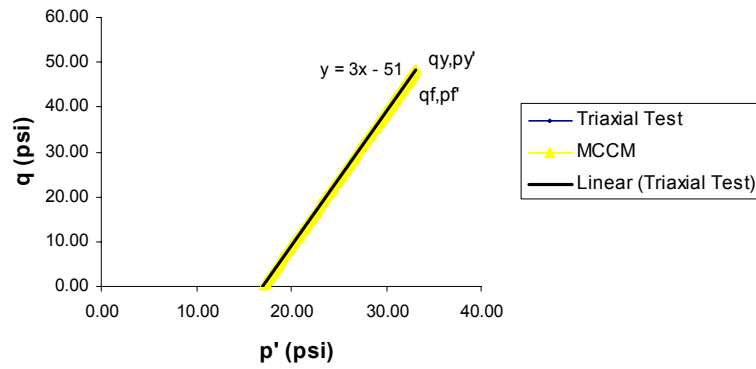
Figure 42: Stress Path, Peak and Ultimate or Failure Stresses

Test # 21515

Stress Path (q:p')



Stress Path (q:p')



Stress Path (q:p')

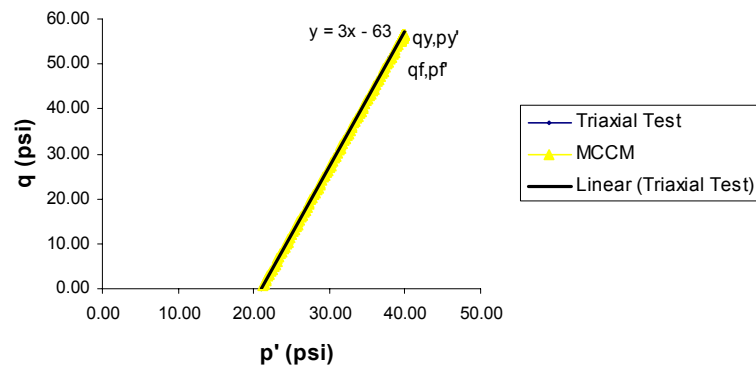


Figure 43: Stress Path, Peak and Ultimate or Failure Stresses

Test # 21516

Stress Path (q:p')

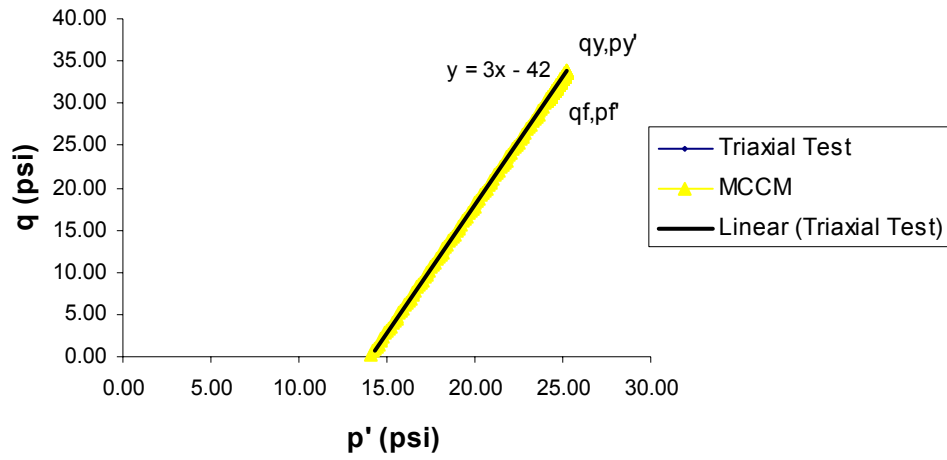
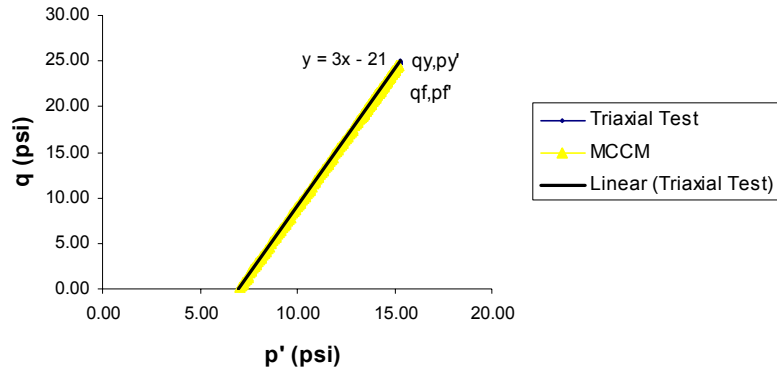


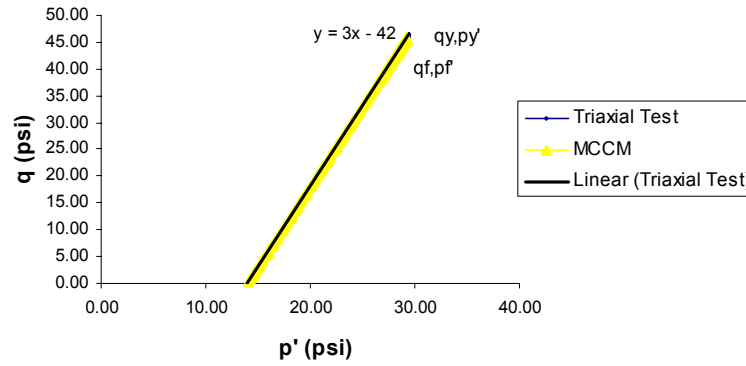
Figure 44: Stress Path, Peak and Ultimate or Failure Stresses

Test # 21548

Stress Path (q:p')



Stress Path (q:p')



Stress Path (q:p')

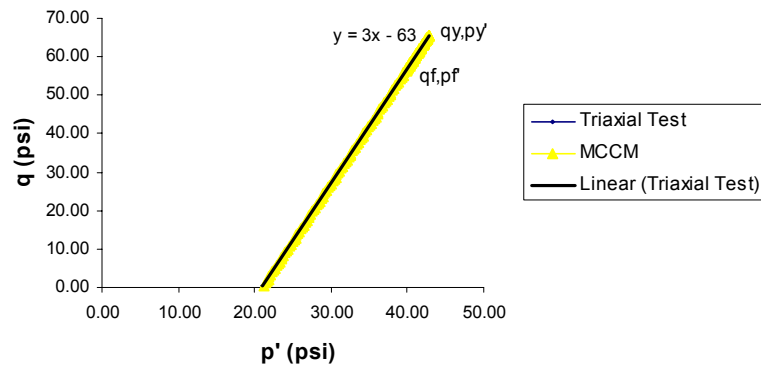


Figure 45: Stress Path, Peak and Ultimate or Failure Stresses

Shear Strain (ε_q) Prediction

The second part of the test results analysis corresponds to prediction of the shear strain invariant. First of all, it is important to recall how the strain invariants are calculated based on the test data and the proposed models. Equation 24 and 25 states the calculation of the shear strain increment for triaxial test data, which is basically related to the increments of axial strain and one-third of the volumetric strain, while Equation 14 shows the volumetric strain increment calculation.

$$\delta\varepsilon_p = -\delta V / V \quad (14)$$

$$\delta\varepsilon_q = \delta\varepsilon_a + \delta\varepsilon_p/3 \quad (24)$$

$$\delta\varepsilon_a = -\delta l/l \quad (25)$$

On the other hand, matrix equations 34 and 35 were proposed by MCCM to estimate the volumetric and shear strain increments for the elastic and elastic-plastic behavior. Also, equation 30 establishes the flow rule equation which relates the plastic shear strain and the plastic volumetric strain increment. This equation was derived from the assumption of the Plastic Potentials and the Normality considerations. Moreover, elastic and elastic-plastic volumetric strain increments are derived from the triaxial test consolidation analysis, which are previously represented in Equations 15 and 19 respectively.

$$\delta\varepsilon_p^p / \delta\varepsilon_q^p = M^2 - h^2 / 2h \quad (30)$$

$$\begin{bmatrix} \delta \varepsilon_p^e \\ \delta \varepsilon_q^e \end{bmatrix} = \begin{bmatrix} 1/K' & 0 \\ 0 & 1/G \end{bmatrix} \begin{bmatrix} \delta p' \\ \delta q \end{bmatrix} \quad (34)$$

$$\begin{bmatrix} \delta \varepsilon_p^e \\ \delta \varepsilon_q^e \end{bmatrix} = \frac{(\lambda - \kappa)}{\nu p' (M^2 - \eta^2)} \begin{bmatrix} (M^2 - \eta^2) & 2\eta \\ 2\eta & (M^2 - \eta^2) \end{bmatrix} \begin{bmatrix} \delta p' \\ \delta q \end{bmatrix} \quad (35)$$

$$\delta \varepsilon_p^e = -k \delta p' / \nu p' \quad (15)$$

$$\delta \varepsilon_p^p = (\lambda - k) \delta p_o' / \nu p_o' \quad (19)$$

The strain invariants results analysis must be focused on the comparison of the not only shear strain values but also the deformation pattern. The estimation of the shear strain using the MCCM prediction for highly overconsolidated soils is found to be not accurate in comparison to the experimental data. Table 8 tabulates the predicted and the experimental calculations of the shear strain at the peak and ultimate points, as point “Q” and “T” of Figure 33. As is evident, there is significant differences between MCCM and experimental results for shear strains both at yield and failure.

Table 8

Shear Strain (MCCM Prediction)

Test #	Cell Pressure (σ_r)	Peak Point		Ultimate Point		
		Test Data	MCCM	Test Data		MCCM
		ϵ_{qy} (%)	ϵ_{qy} (%)	ϵ_{qf} (%)	$\epsilon_{qf \max}$ (%)	ϵ_{qf} (%)
21398	14	2.3	1.05	15.9	29.1	9.65
	21	2.76	0.87	10.16	18.48	7.98
21399	14	2.84	0.58	10.69	19.91	4.16
	21	2.65	0.75	17.5	18.83	7.37
21401	7	2.65	0.61	10.05	16.67	5.93
	14	2.81	0.69	14.65	18	6.65
	21	2.9	0.72	12.36	22.13	5.56
21434	7	1.7	0.79	10.61	14.41	10.33
	14	3.6	1.25	13.9	16.55	9.35
	21	2.64	0.99	6.52	19.94	7.93
21481	7	2.44	0.59	16.92	18.59	5.42
	14	2.89	0.97	11.08	13.79	9.96
	21	3.04	0.91	11.29	19.05	9.24
21482	7	2.9	0.73	19.21	19.21	11.07
	14	3.04	0.77	15.3	19.19	8.5
	21	2.89	1.16	10.48	13.88	9.6
21483	7	2.03	0.59	13.52	15.05	5.9
	14	2.48	0.72	13.2	16.06	5.9
21515	14	3.78	0.88	21	22.4	8.24
	17	3.08	0.9	13.8	18.09	7.74
	21	3.45	0.86	10.37	18.96	4.39
21516	14	1.46	0.52	16.1	18.61	3.47
21548	7	2.11	0.63	13.9	13.9	8.56
	14	2.73	0.78	16.25	16.25	5.63
	21	2.7	0.85	13.32	15.98	4.95

This model inaccuracy is addressed by comparing the test data deformation to the predictive deformation based on the elastic and elasto-plastic theories.

According to MCCM, soil behavior within the yield surface is defined by elastic deformations. Points “P” and “Q” of Figure 46 show the elastic deformation under volumetric compression. However, the experimental data depicts that this compression process occurs initially between points “P” and “E”. Then, it turns into a volumetric expansion before the peak point “Q” has been reached, as shown in Figure 47.

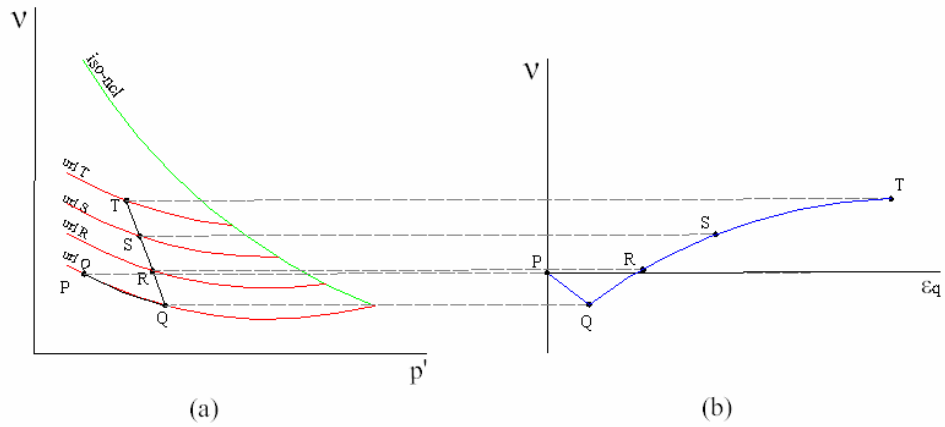


Figure 46: MCCM Volumetric Deformation on Highly Overconsolidated Soils

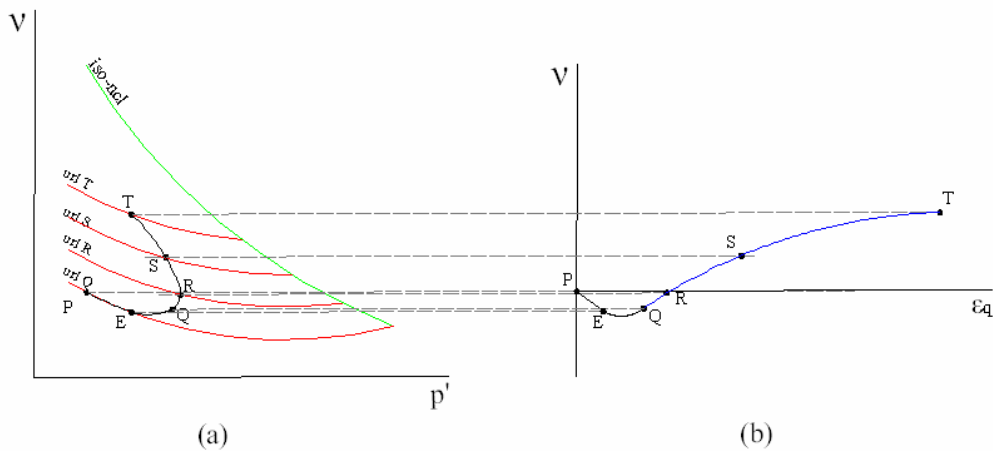


Figure 47: Typical Volumetric Deformation on Dense Sands

This expansion effect occurs when the overburden pressure acting over the soil structure, which lacks of void spaces, forces the soil particles to move to different directions producing the soil volumetric increment.

MCCM associates the volumetric expansion to the softening of the yield surface, and it is thought that the volumetric expansion reduces the deviator strength capacity of the soil. However, by observing Figure 48, the phase between the final point of the linear elastic deformation “E” and the peak stress point “Q” is defined by a volumetric expansion and a continuous increment of deviator stress. This increment stress effect is associated to frictional displacement between the soil particles, dilatancy, the particle crushing and particles rearranging effect. Appendix “B” presents similar plots for each soil sample.

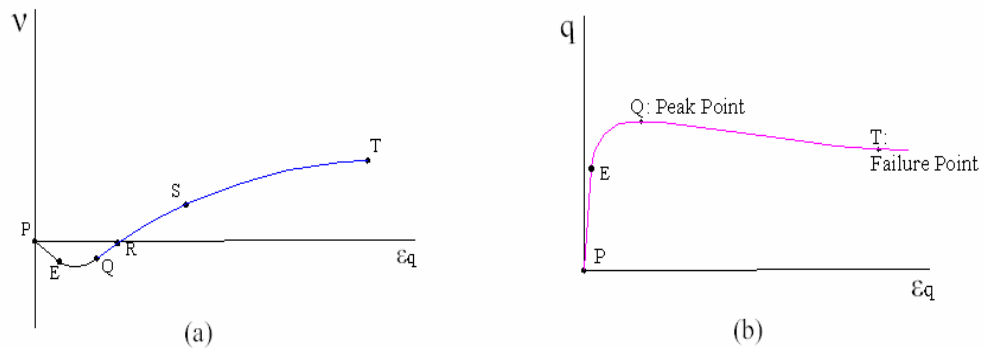
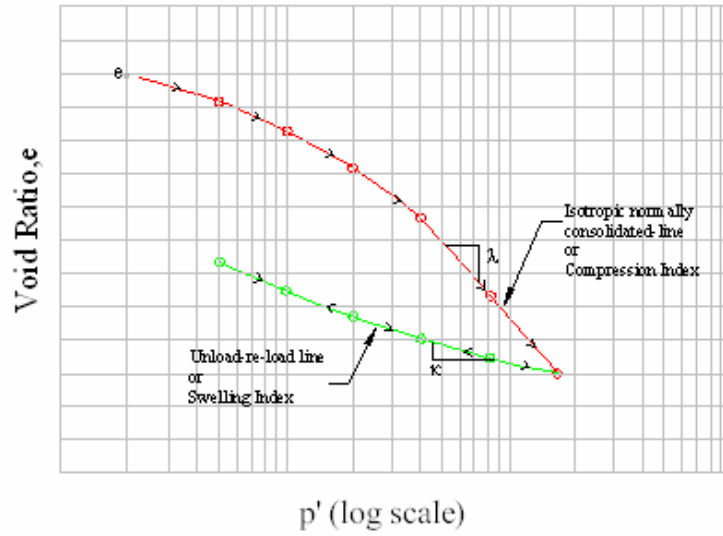


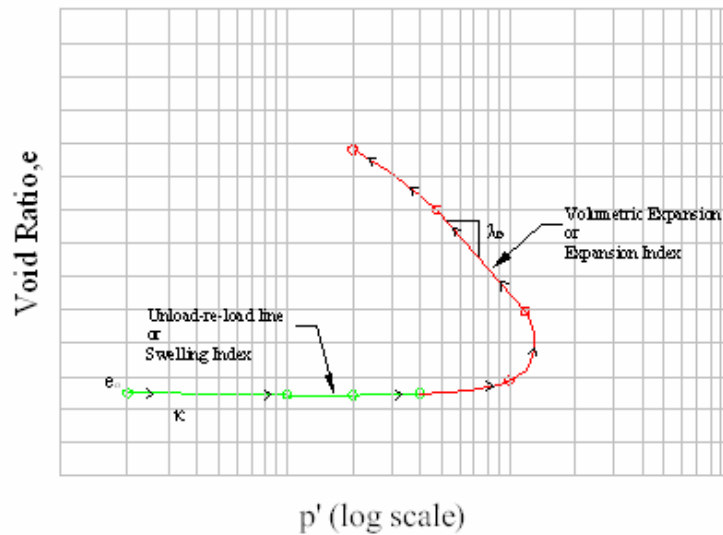
Figure 48: Expansion Volumetric and Deviator Stress on Dense Sands

Another dissimilarity of the MCCM is related to the compression index, λ . Figure 49 (a) reflects typical plot of a soil consolidation under axial compression and volumetric compaction where it is possible to note the compression index and swelling index

parameters. This compression index, λ , represents the slope of the isotropic-normally consolidated line, which is used to estimate the plastic volumetric compaction.



(a)



(b)

Figure 49: Compression Index and Expansion Index Comparison

However, this parameter differs for a volumetric expansion effect. Figure 49 (b) depicts the typical triaxial test consolidation plot for dense sands, Appendix B shows this “e-lnp’” plot configuration for each soil sample, and Table 4 tabulates these index factors.

By comparing the compression index, λ , and the expansion index, λ_e , it is possible to note that the expansion index is approximately 40 times bigger than the compression index if it is consider equivalent to 5-6 times the swelling index. Therefore, this typical equivalence can not be applied for volumetric expansion in dense granular soils.

In reference to the relation between the plastic volumetric strain and the plastic shear strain, known as Flow Rule, analysis of the test data reflects that the shear strain is highly influenced by the axial strain. This axial strain “ ϵ_a ” is characterized by a continuous reduction of the soil height along the triaxial test, and the softening behavior does not affect this deformation pattern. Therefore, the soil volumetric expansion occurs in the radial direction and orthogonal to the axial compression load. The plastic deformation of the soil is defined by the volumetric expansion which begins before the yield surface is reached, as shown in Figure 48 (a).

Also, a plot of the relationship between the axial strain and the volumetric strain was generated for each soil sample in order to evaluate an experimental relationship, as shown in Figure 22. Appendix “A” presents similar plots for all soil samples. These plots display a slight curvilinear relationship which can approximately be represented by a trend line whose average slope is about 6.5.

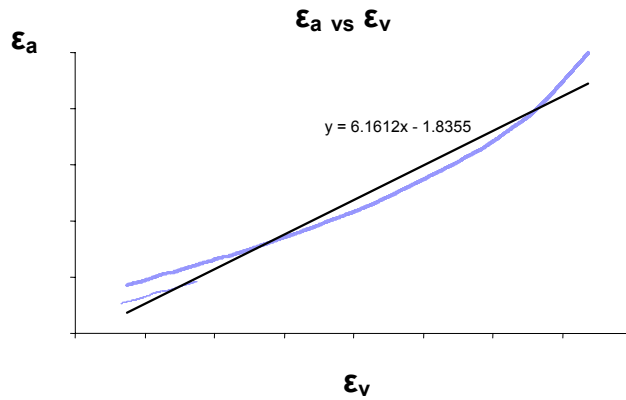


Figure 22: Typical “ ϵ_a vs. ϵ_v ” Plot for Dense Sands During Softening

All these observations have been possible due to the analysis of the test data and the model equations. An adjustment of the soil parameters and equations relationship is now proposed, in order to adapt the behavior of dense sands into the Modified Cam Clay Model framework. This adaptation is presented and implemented for the computational prediction of dense granular soils discussed in Chapter III. Table 9 shows similar calculations made in Table 8, but in this case, it is applied to the adapted model.

The shear strain prediction for the adapted model is significantly more accurate than the predicted by the MCCM. It is important to note that the intention of this adapted model is not to diminish the reliability of the Modified Cam Clay Model, but to improve its applicability based on observed behavior and related phenomena.

Table 9

Shear Strain (Adapted Model)

Test #	Cell Pressure (σ_r)	Peak Point		Ultimate Point		
		Test Data	Adapted Model	Test Data		Adapted Model
		ϵ_{qy} (%)	ϵ_{qy} (%)	ϵ_{qf} (%)	$\epsilon_{qf \max}$ (%)	ϵ_{qf} (%)
21398	14	2.3	2.56	15.9	29.1	22.04
	21	2.76	2.27	10.16	18.48	15.13
21399	14	2.84	1.27	10.69	19.91	9.32
	21	2.65	1.95	17.5	18.83	14.24
21401	7	2.65	1.42	10.05	16.67	11.51
	14	2.81	2.12	14.65	18	12.28
	21	2.9	1.99	12.36	22.13	6.1
21434	7	1.7	1.92	10.61	14.41	14.79
	14	3.6	2.8	13.9	16.55	16.04
	21	2.64	2.33	6.52	19.94	15.59
21481	7	2.44	0.9	16.92	18.59	13.92
	14	2.89	2.59	11.08	13.79	11.49
	21	3.04	2.59	11.29	19.05	13.71
21482	7	2.9	2.26	19.21	19.21	17.99
	14	3.04	1.78	15.3	19.19	13.59
	21	2.89	2.16	10.48	13.88	11.84
21483	7	2.03	1.63	13.52	15.05	16.33
	14	2.48	1.72	13.2	16.06	15.59
21515	14	3.78	2.53	21	22.4	21.57
	17	3.08	2.53	13.8	18.09	7.06
	21	3.45	2.5	10.37	18.9	5.74
21516	14	1.46	1.12	16.1	18.61	16.03
21548	7	2.11	2.07	13.9	13.9	14.26
	14	2.73	1.83	16.25	16.25	16.79
	21	2.7	1.65	13.32	15.98	13.07

Another consideration to point out is the shape difference of the “ q vs. ϵ_q ” plot for dense sands. Figure 50 (a) depicts the typical deformation pattern of highly overconsolidated clayey soils according to MCCM, while Figure 50 (b) shows the typical “ q - ϵ_q ” plot for the experimental test data of dense sands. Figure 50 (b) reflects an initial linear-elastic deformation followed by a plastic curvilinear deformation up to the peak point. Then, a softening phase is characterized by a smooth convex curvilinear deformation.

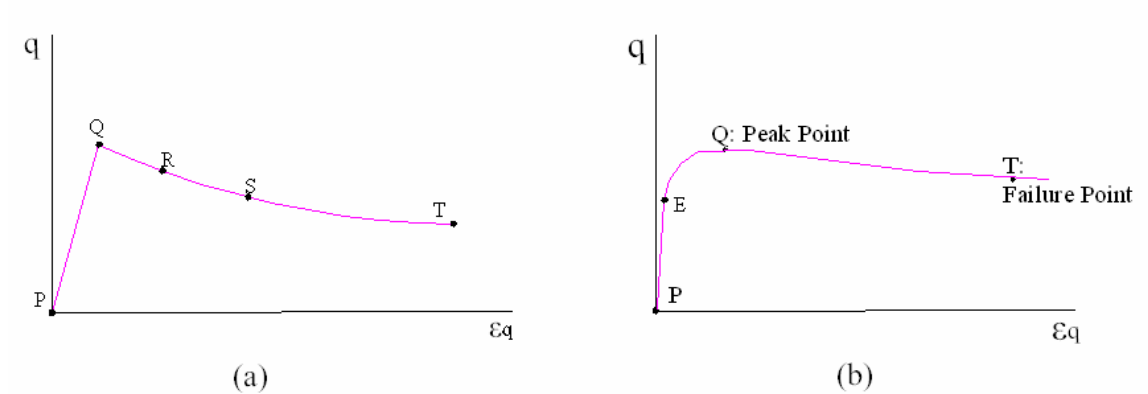
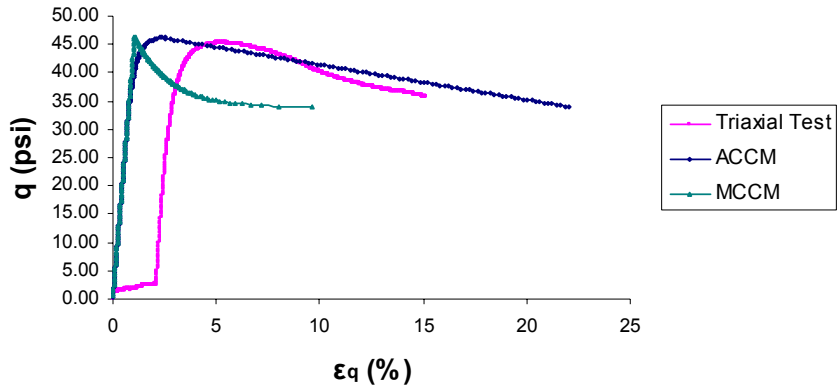


Figure 50: Typical “ q - ϵ_q ” for Highly Overconsolidated Soils (MCCM) and Dense Sands Plots

Figures 51 through 66 show the “ q - ϵ_q ” plot for each soil sample studied in this research. These figures include the results obtained by the prediction of the MCCM as well as the adapted model. On these figures, it is possible to notice the quality approach for the adapted model to predict the “ q versus ϵ_q ” relation. Finally, Appendix “B” presents the plots based on the MCCM for highly overconsolidated soils, similar to Figure 17.

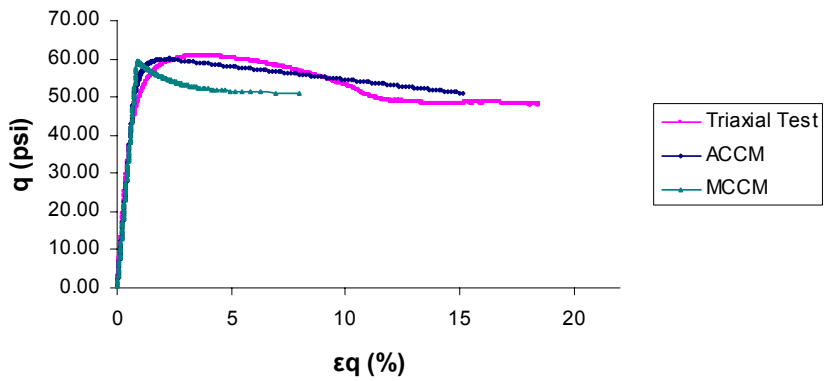
Test # 21398

q VS ϵ_q



Initial Isotropic Pre-consolidation Pressure: 14 psi

q VS ϵ_q

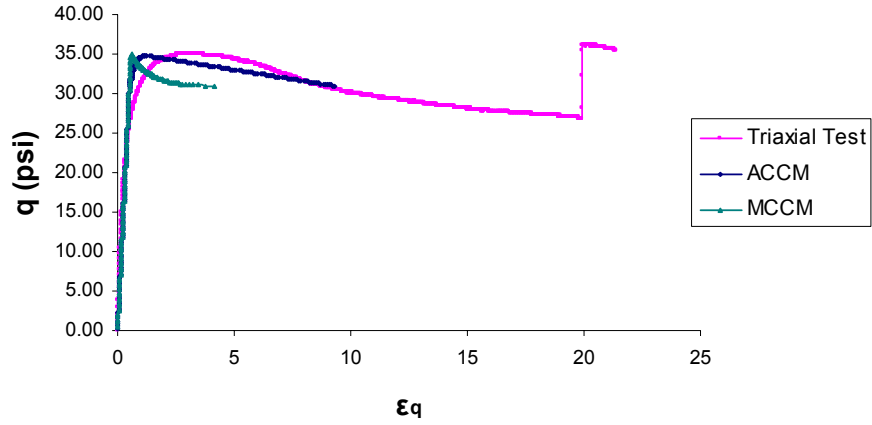


Initial Isotropic Pre-consolidation Pressure: 21 psi

Figure 51: “q- ϵ_q ” Plot

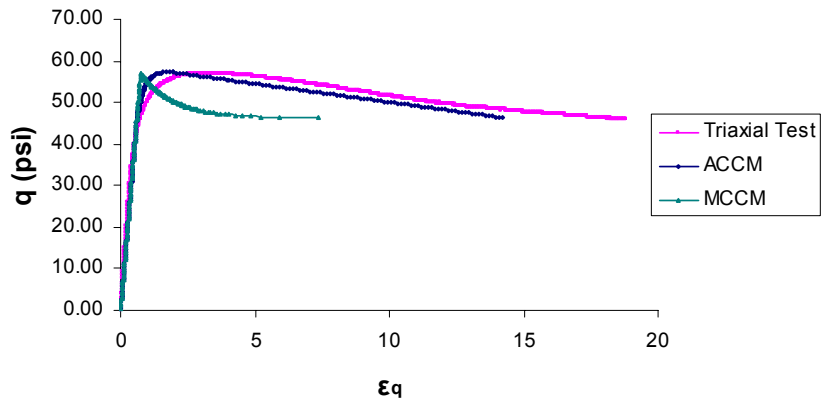
Test # 21399

q vs ϵ_q



Initial Isotropic Pre-consolidation Pressure: 14 psi

q vs ϵ_q

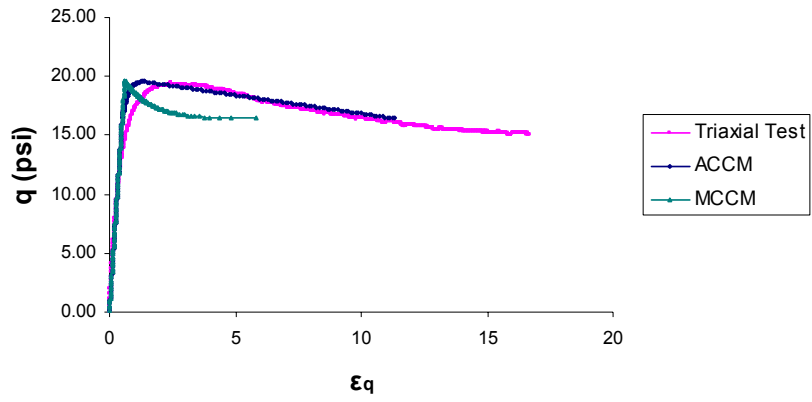


Initial Isotropic Pre-consolidation Pressure: 21 psi

Figure 52: “q- ϵ_q ” Plot

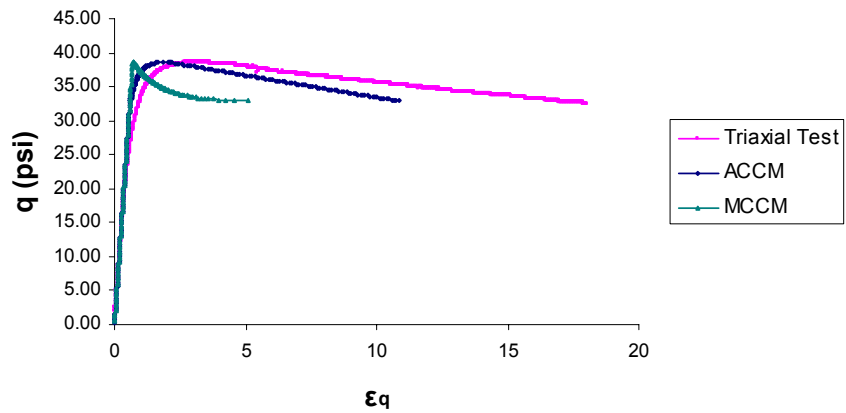
Test # 21401

q vs ϵ_q



Initial Isotropic Pre-consolidation Pressure: 7 psi

q vs ϵ_q

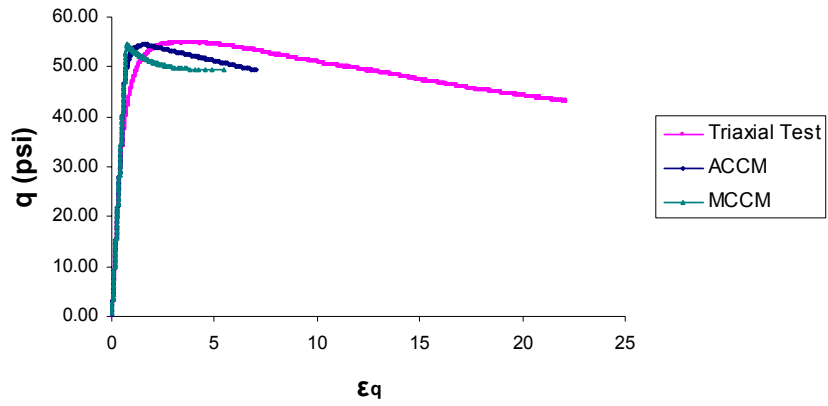


Initial Isotropic Pre-consolidation Pressure: 14 psi

Figure 53: “q- ϵ_q ” Plot

Test # 21401

q vs ϵ_q

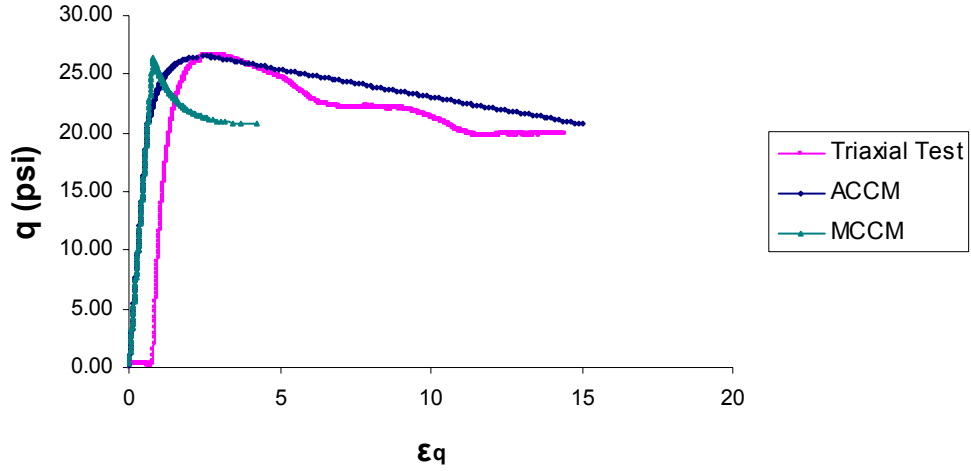


Initial Isotropic Pre-consolidation Pressure: 21 psi

Figure 54: “q- ϵ_q ” Plot

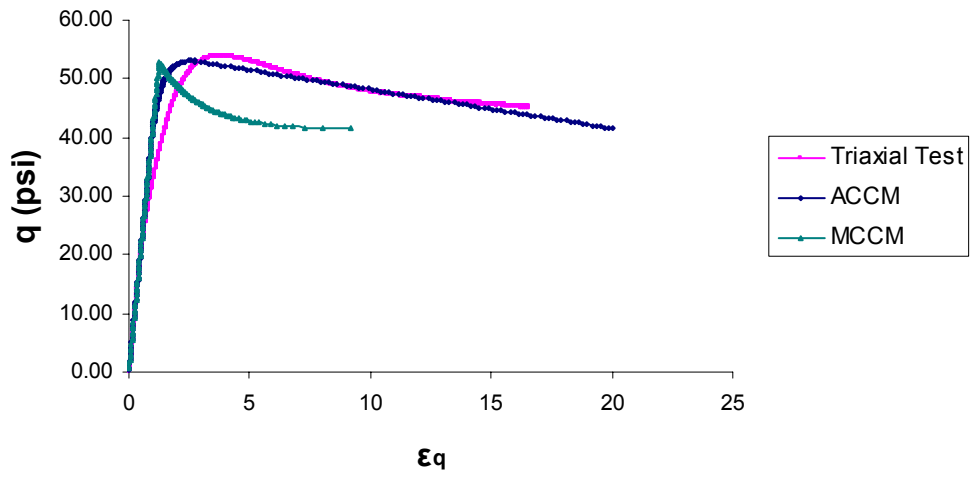
Test # 21434

q vs ϵ_q



Initial Isotropic Pre-consolidation Pressure: 7 psi

q vs ϵ_q

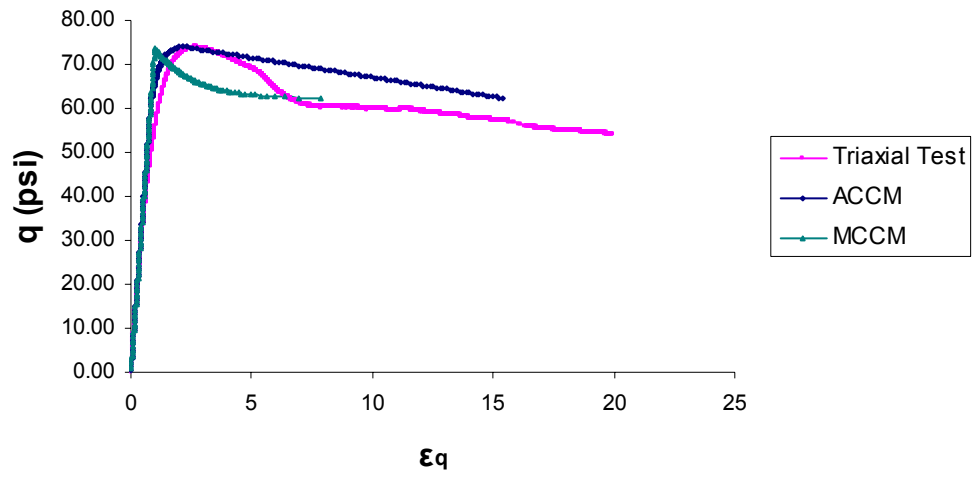


Initial Isotropic Pre-consolidation Pressure: 14 psi

Figure 55: “q- ϵ_q ” Plot

Test # 21434

q vs ϵ_q

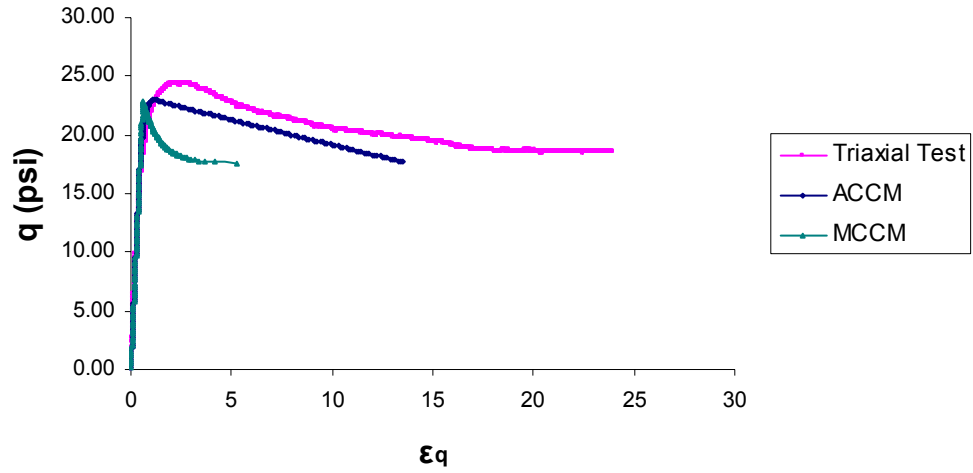


Initial Isotropic Pre-consolidation Pressure: 21 psi

Figure 56: “q- ϵ_q ” Plot

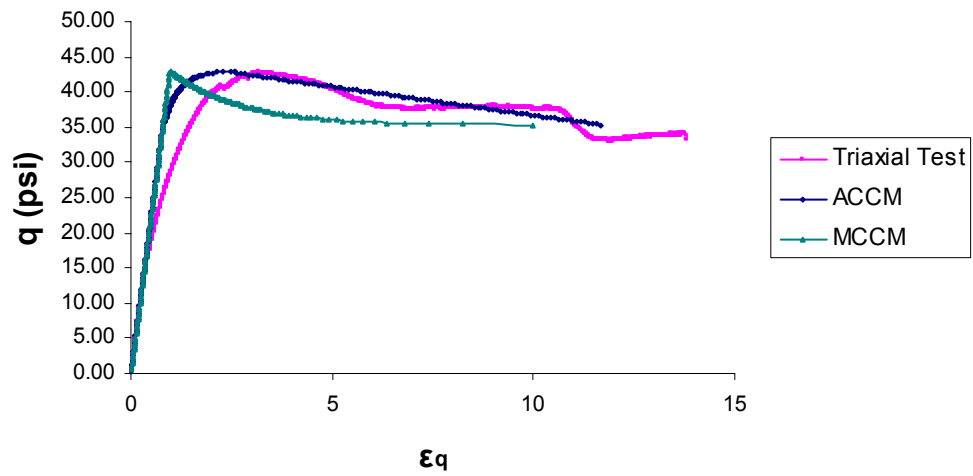
Test # 21481

q vs ϵ_q



Initial Isotropic Pre-consolidation Pressure: 7 psi

q vs ϵ_q

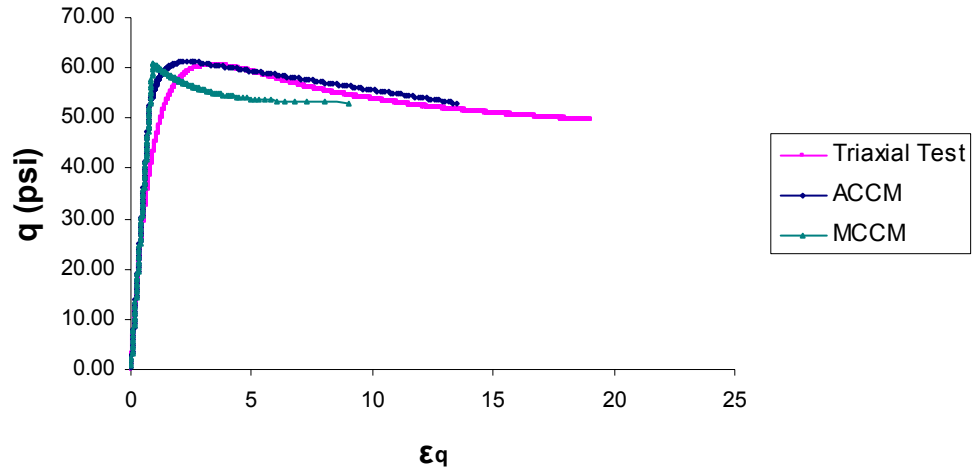


Initial Isotropic Pre-consolidation Pressure: 14 psi

Figure 57: "q- ϵ_q " Plot

Test # 21481

q vs ϵ_q

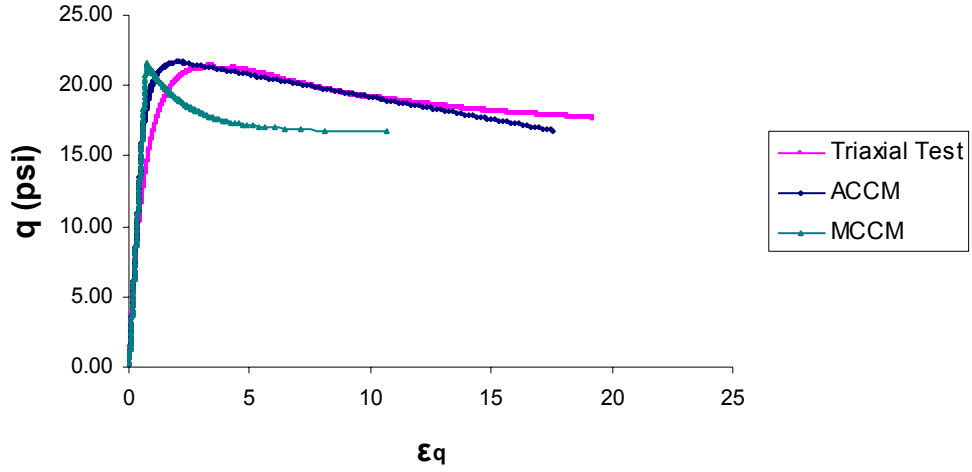


Initial Isotropic Pre-consolidation Pressure: 21 psi

Figure 58: “q- ϵ_q ” Plot

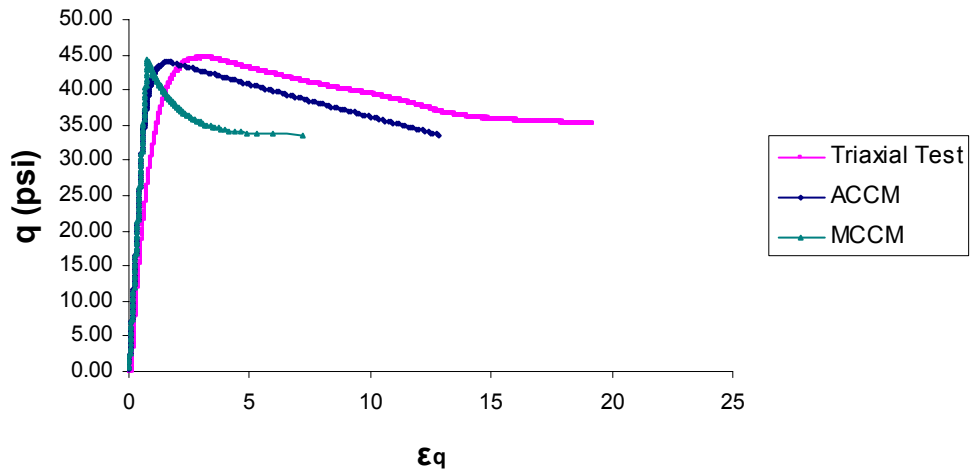
Test # 21482

q vs ϵ_q



Initial Isotropic Pre-consolidation Pressure: 7 psi

q vs ϵ_q

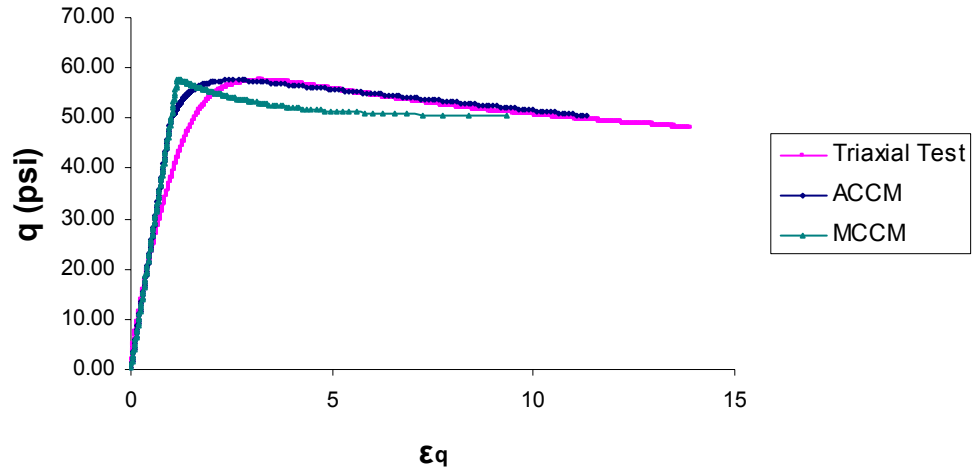


Initial Isotropic Pre-consolidation Pressure: 14 psi

Figure 59: “q- ϵ_q ” Plot

Test # 21482

q vs ϵ_q

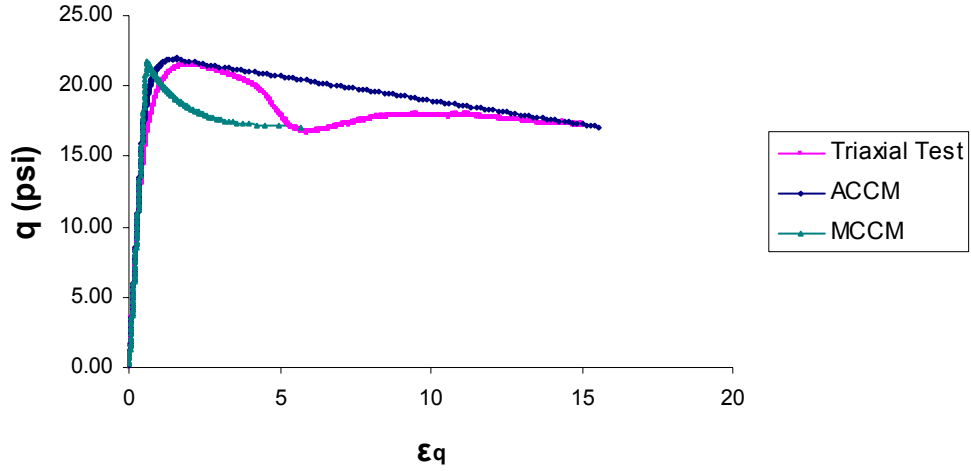


Initial Isotropic Pre-consolidation Pressure: 21 psi

Figure 60: “q- ϵ_q ” Plot

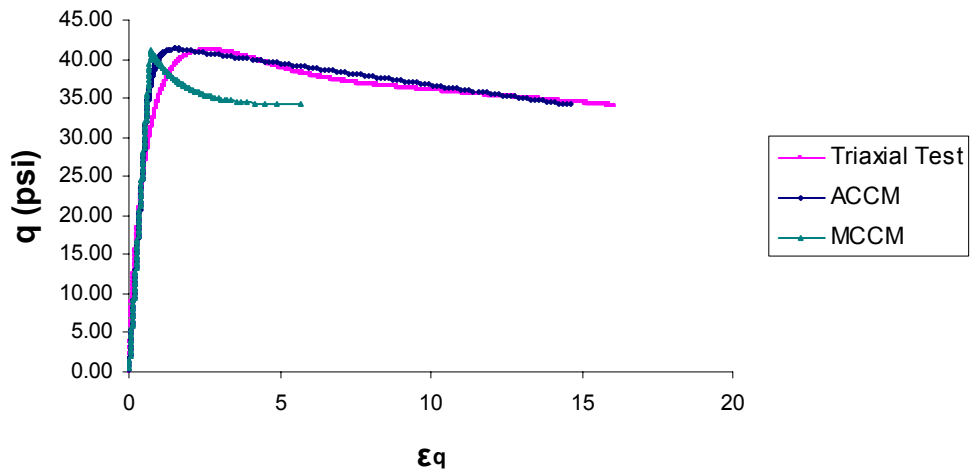
Test # 21483

q vs ϵ_q



Initial Isotropic Pre-consolidation Pressure: 7 psi

q vs ϵ_q

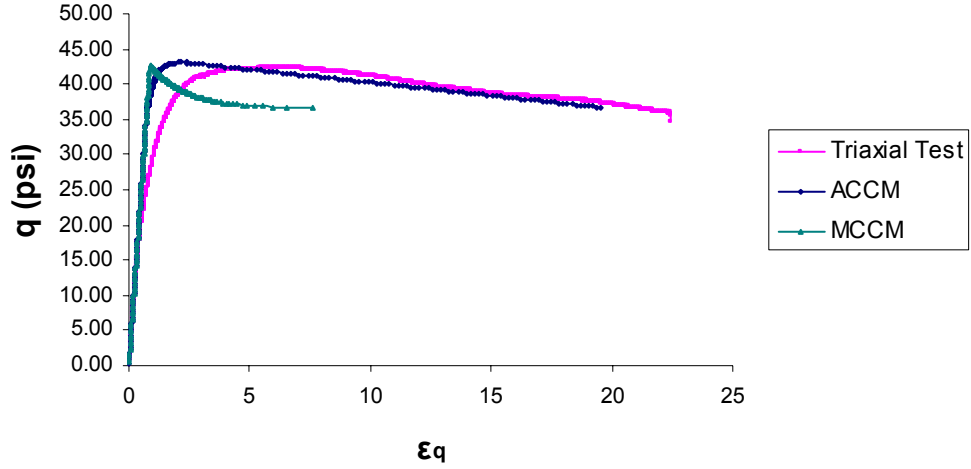


Initial Isotropic Pre-consolidation Pressure: 14 psi

Figure 61: “q- ϵ_q ” Plot

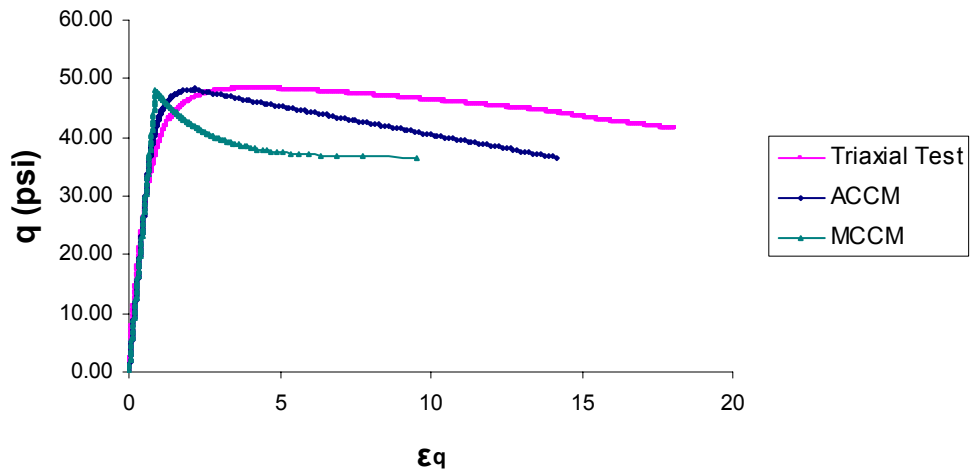
Test # 21515

q vs ϵ_q



Initial Isotropic Pre-consolidation Pressure: 14 psi

q vs ϵ_q

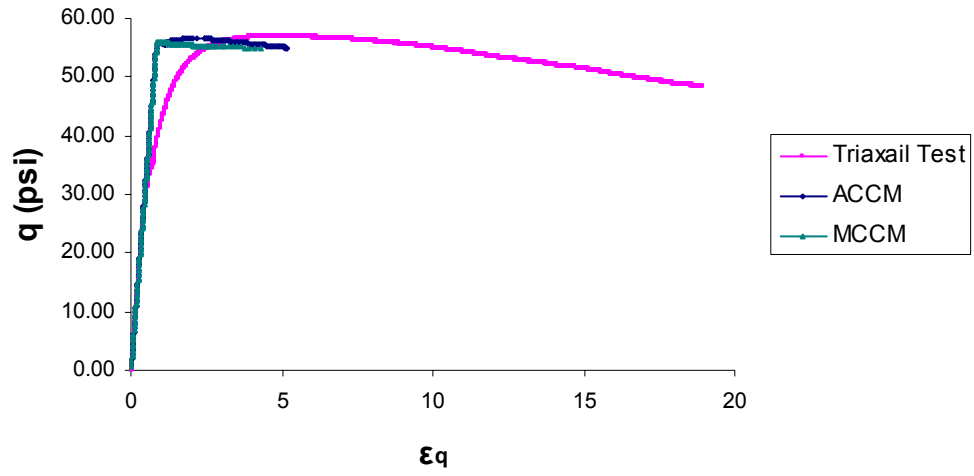


Initial Isotropic Pre-consolidation Pressure: 17 psi

Figure 62: “q- ϵ_q ” Plot

Test # 21515

q vs ϵ_q

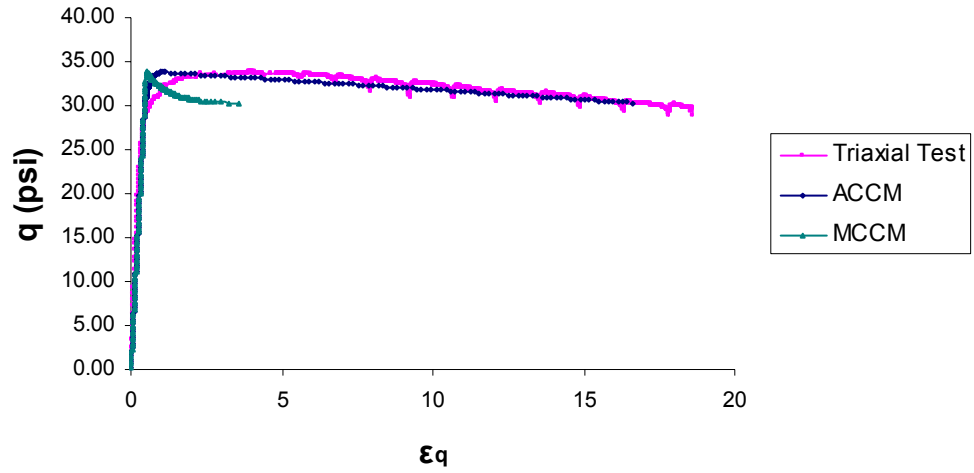


Initial Isotropic Pre-consolidation Pressure: 21 psi

Figure 63: “ q - ϵ_q ” Plot

Test # 21516

q vs ϵ_q

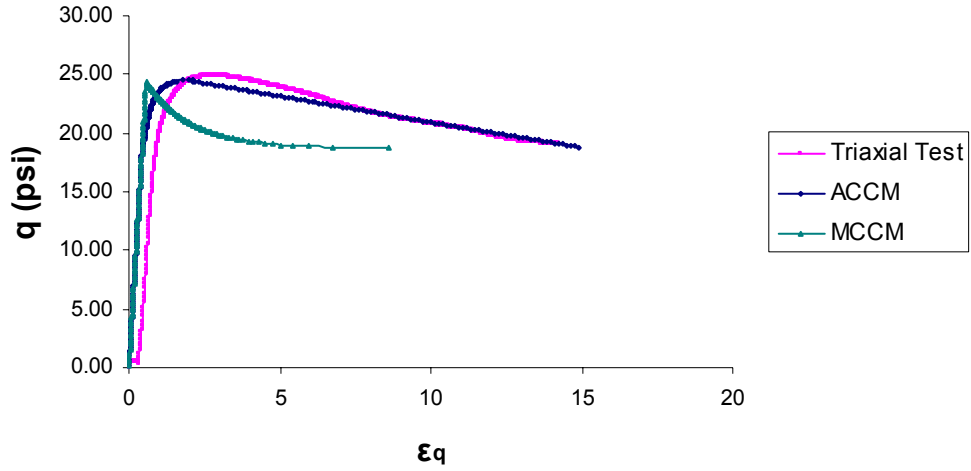


Initial Isotropic Pre-consolidation Pressure: 14 psi

Figure 64: “ q - ϵ_q ” Plot

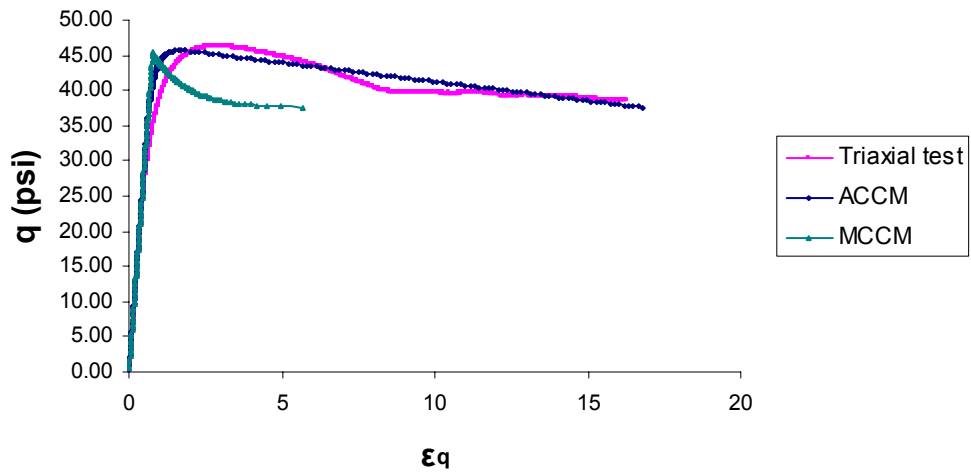
Test # 21548

q vs ϵ_q



Initial Isotropic Pre-consolidation Pressure: 7 psi

q vs ϵ_q

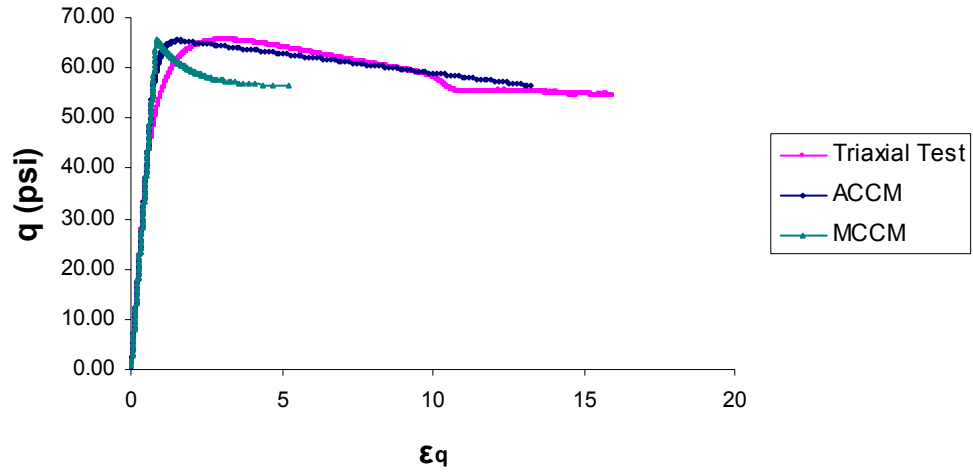


Initial Isotropic Pre-consolidation Pressure: 14 psi

Figure 65: “q- ϵ_q ” Plot

Test # 21548

q vs ϵ_q



Initial Isotropic Pre-consolidation Pressure: 21 psi

Figure 66: “q- ϵ_q ” Plot

CHAPTER V

CONCLUSIONS AND RECOMMENDATIONS

SUMMARY AND CONCLUSIONS

This thesis has presented the applicability and reliability of the elastic-plastic model “Modified Cam Clay” for the prediction of the soil behavior in dense sands. Initial work by Roscoe and Burland (1968) in developing this model was done to analyze the behavior of clay soil. This model was described in terms of the stress-strain invariants, which relate the stresses and deformations of soil under the application of conventional triaxial tests. The applicability of mathematical and physical principles used in this model can also be projected to different types of soils. For example, this thesis uses the elastic and plastic theories as the basic principle in dense sands to estimate the occurrence of elastic and plastic deformations in dense sands.

A computational implementation of this model was developed in a Matlab environment to illustrate and calculate the stress-strain relationship of highly overconsolidated soils. This model was then adapted to the behavior of dense sands. The results of the adapted model were compared to the results obtained from triaxial tests on dense sands.

The laboratory triaxial tests were conducted by FDOT. The database was composed of molded sands classified as “A3” according to the AASHTO soil classification system. These samples were compacted up to 95% of maximum unit weight at the optimum moisture content.

These test data were plotted in terms of the stress-strain invariants defined by the MCCM. From the analysis and comparison of the numerical and experimental test data, several observations were made with reference to the soil properties and behavior. It was noted that the MCCM did not adequately predict the shear strain response based on the shear strain versus deviatoric stress plots. An adapted model based on the lesson learnt from these observations was then implemented in the computational program to better estimate the stress-strain behavior in dense sands. It was demonstrated that the adapted Modified Cam Clay was able to improve the general characteristic response of dense sands under triaxial tests. Overall, the elastic and elastic-plastic deformation theories are also found to be applicable to the prediction of the behavior of dense sands.

There was some difference in regards to the specific location and deformation pattern observed in both elastic and plastic deformations. It is important to mention that the model was initially less effective in simulating the behavior of the plastic deformation because of the volumetric expansion parameters observed in dense sand.

MCCM considers some assumptions and idealizations to simplify the predictive model applicability. For example, the yield surface, kinematic hardening or softening, and the anisotropic soil condition were simplified by this model. A flow rule defined by the normality condition, a yield surface hardening or softening calculation based on the equivalence of the plastic potential curve equation to the yield surface equation, and the yield surfaces consistency principles are examples of the sophistication of this model.

Finally, it is important to recognize that the prediction of soil behavior requires the implementation of mechanisms and models. Even though these idealizations do not

reproduce the real situation analysis, it is possible to estimate ranges or boundaries that approximate the real solution space.

RECOMMENDATIONS FOR FUTURE WORK

Some modifications should be implemented for the prediction of highly overconsolidated soils, also applicable to dense sands. Because dense soils are characterized by a volumetric expansion, this effect requires more analysis and experimental investigation. For example, it is important to evaluate the volume recover capacity for soils under volumetric expansion. This consideration may determine the applicability of pure plastic or the elasto-plastic deformations during the expansion phase.

Because of the dense condition of the soil and the consolidation pressure, the tendency of soil particles to crush and rearrange is an important element to consider in the energy available for dissipation. Particles crushing and re-arranging produce variation of the soil shear strength as well as the volumetric and shear strain.

Considering dilatancy effect in granular materials, the increment of the internal friction angle influences the steep slope of the failure envelope on dense sand. It is recommended that this issue be addressed due to the variation of the angle of friction values between the peak and failure points.

It is also important to evaluate the behavior of dense sands by the application of different models. For example, the option of using a non-associated flow rule model is necessary to be researched in order to compare the predictability of dense sands. Dense sands must also be tested under conventional undrained condition to evaluate the shear

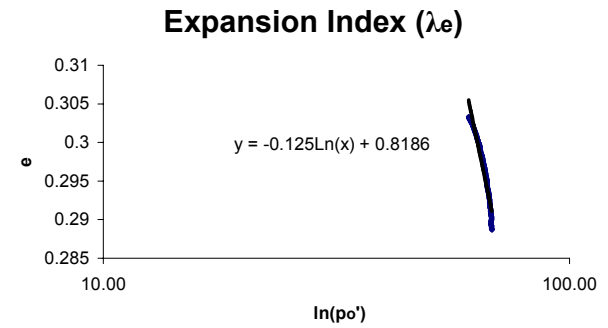
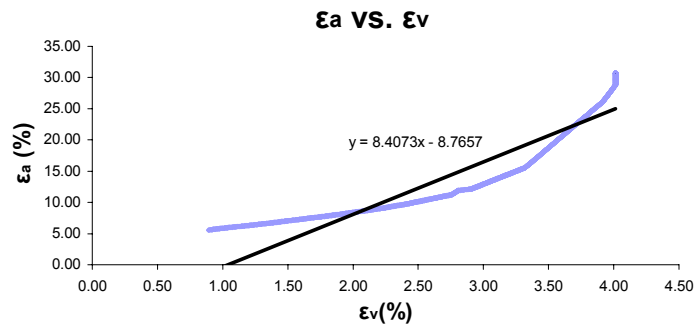
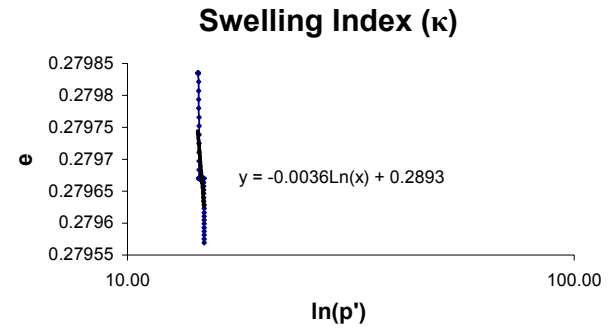
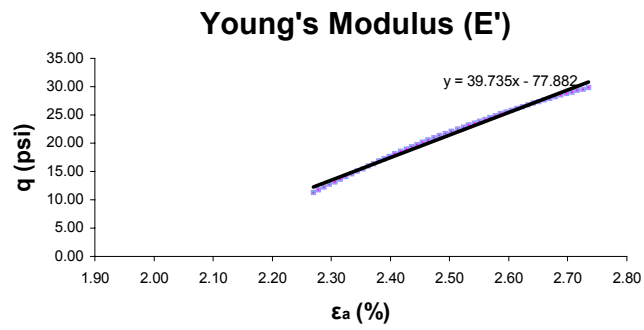
strain deformation and the effective stress paths. This consideration is important due to the neglected volumetric strain.

Normally consolidated and lightly consolidated soils that behaves like loose sands in the drained study are recommended for a more complete evaluation of the adapted MCCM. For these soils conditions, there are no volumetric expansion considerations. Finally, anisotropic triaxial test conditions and predictive models should be considered for the analysis of dense sands because soils structure is formed under anisotropic stress conditions either at normal or loaded conditions. Anisotropic constitutive equations should be incorporated into the adapted MCCM for a more realistic and generalized treatment.

APPENDIX A

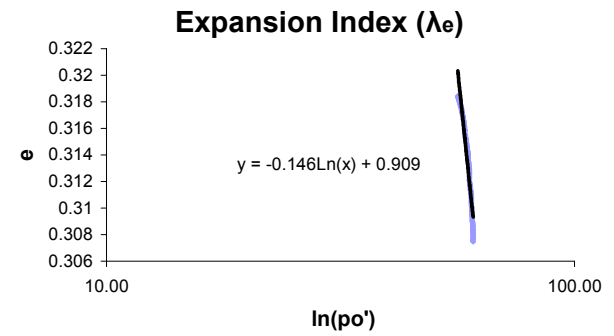
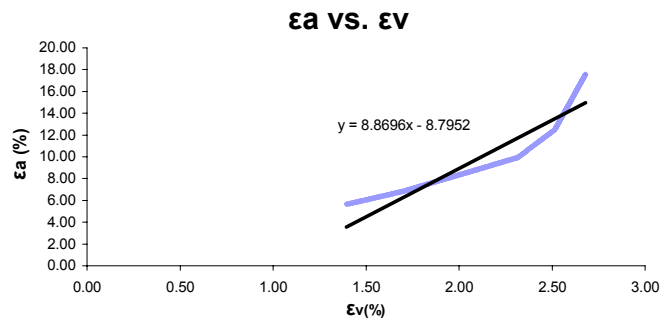
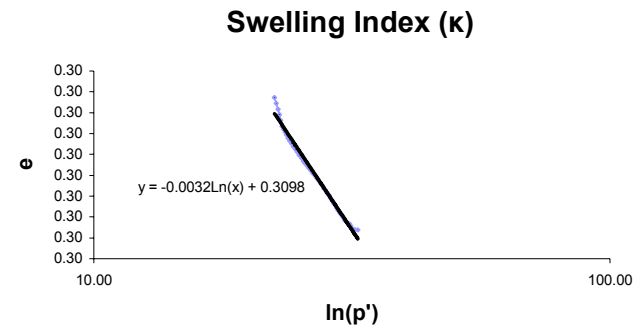
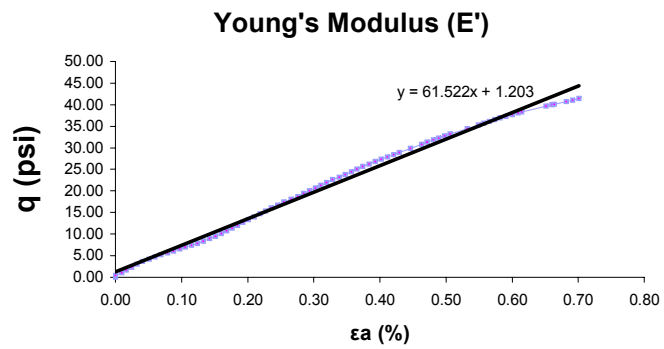
Test # : 21398
 Initial p' (psi): 14

Soil Properties



Test # : 21398
 Initial p' (psi): 21

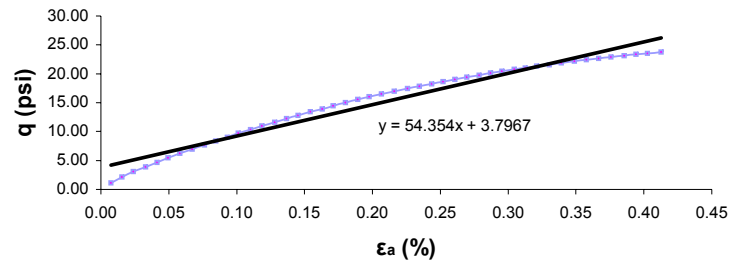
Soil Properties



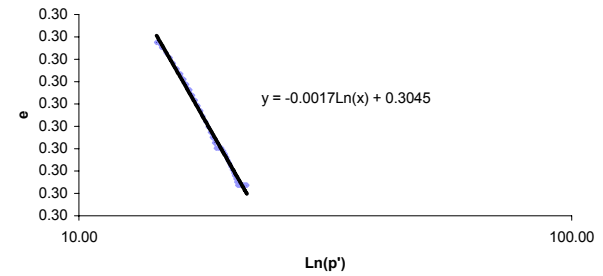
Test # : 21399
 Initial p' (psi): 14

Soil Properties

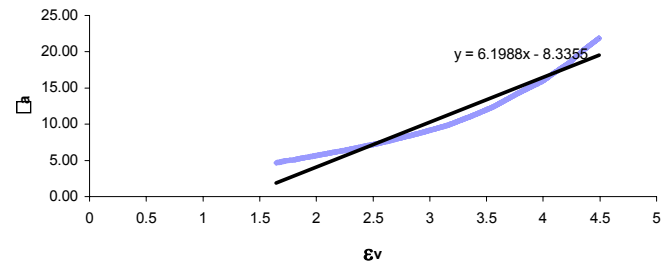
Young's Modulus (E')



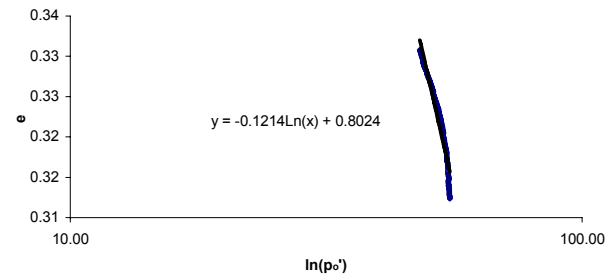
Swelling Index (κ)



ϵ_a vs ϵ_v



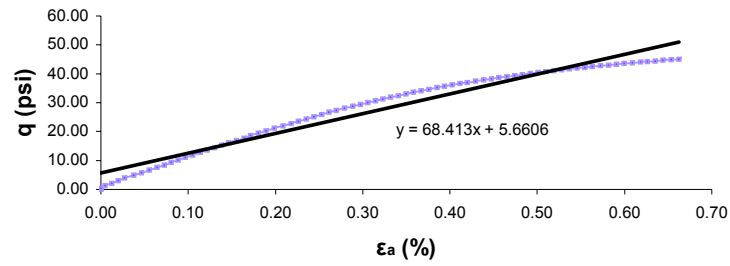
Expansion Index (λ_e)



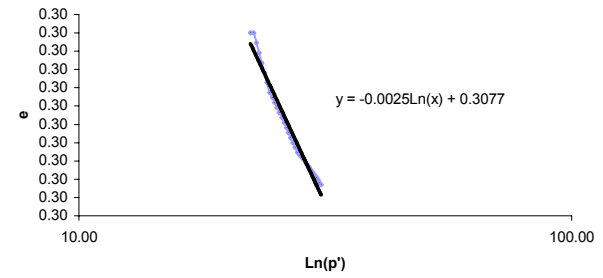
Test # : 21399
 Initial p' (psi): 21

Soil Properties

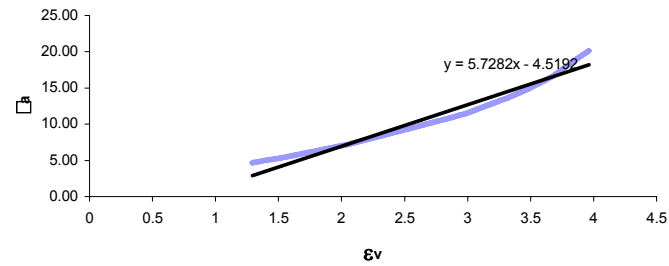
Young's Modulus (E')



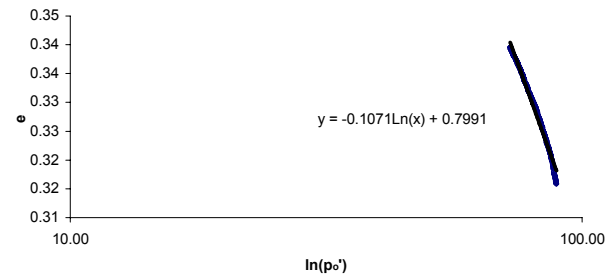
Swelling Index (κ)



ϵ_a vs ϵ_v



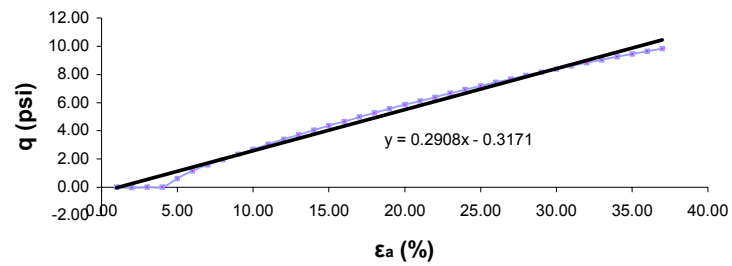
Expansion Index (λ_e)



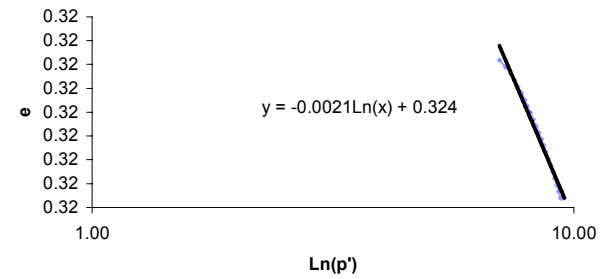
Test # : 21401
Initial p' (psi): 7

Soil Properties

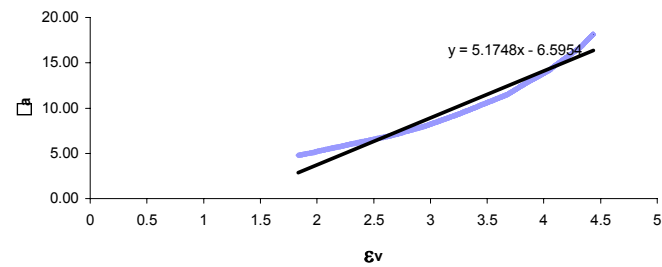
Young's Modulus (E')



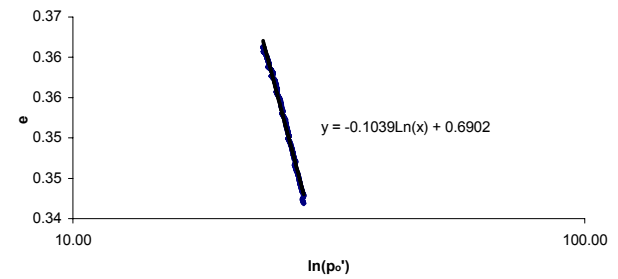
Swelling Index (κ)



ϵ_a vs ϵ_v



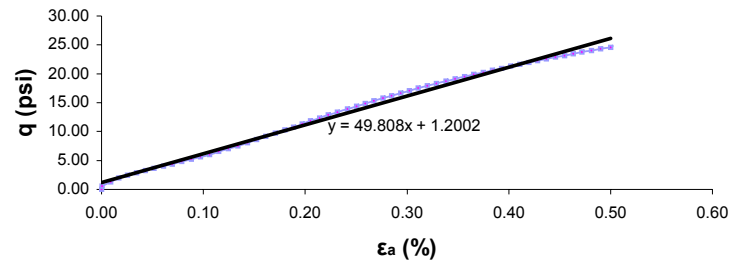
Expansion Index (λ_e)



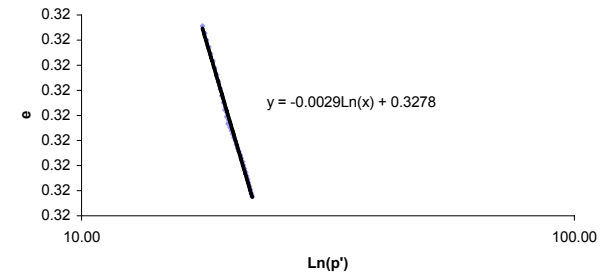
Test # : 21401
 Initial p' (psi): 14

Soil Properties

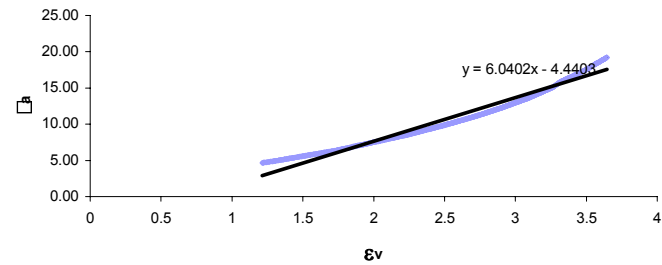
Young's Modulus (E')



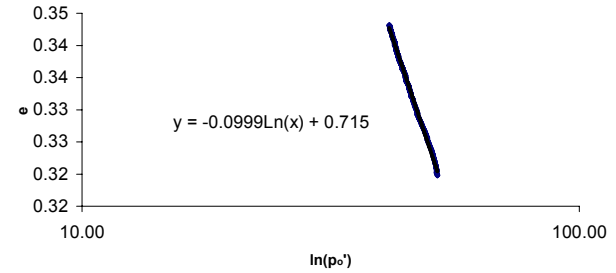
Swelling Index (κ)



ϵ_a vs ϵ_v



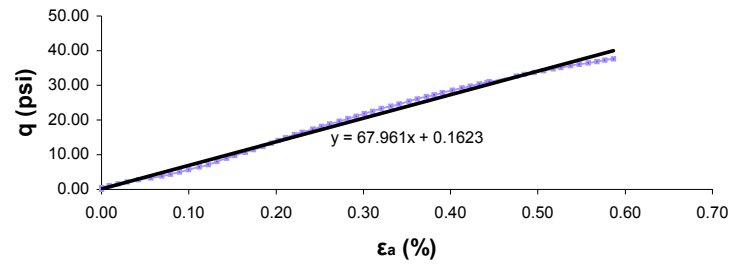
Expansion Index (λ_e)



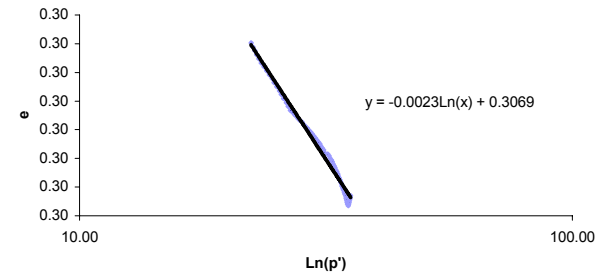
Test # : 21401
 Initial p' (psi): 21

Soil Properties

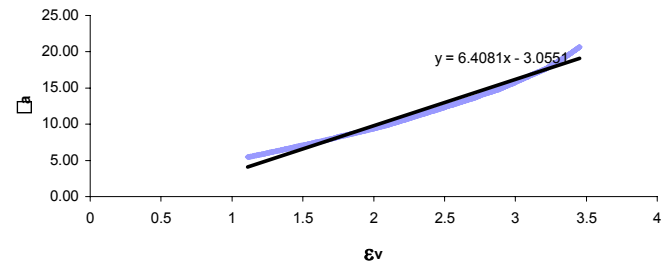
Young's Modulus (E')



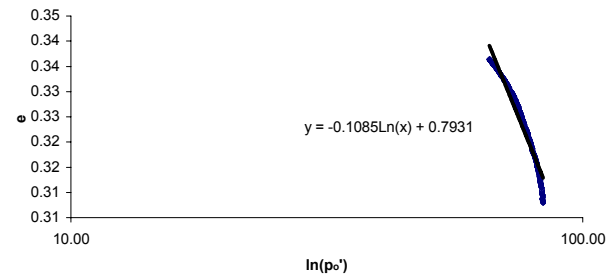
Swelling Index (κ)



ϵ_a vs ϵ_v



Expansion Index (λ_e)

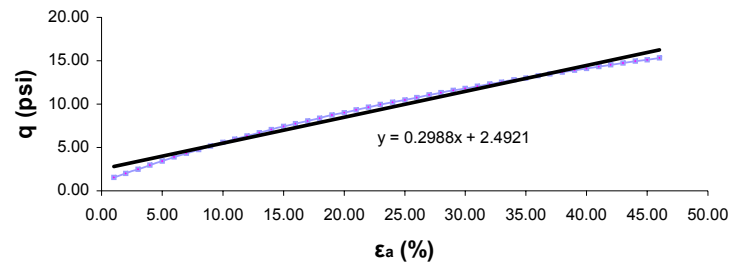


Test # : 21434

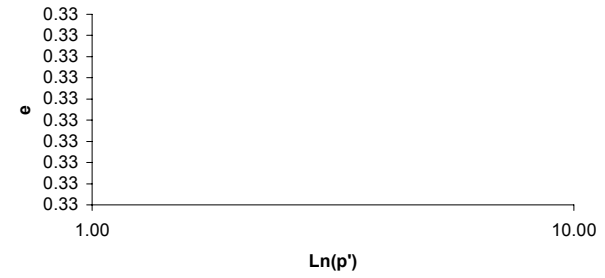
Initial p' (psi): 7

Soil Properties

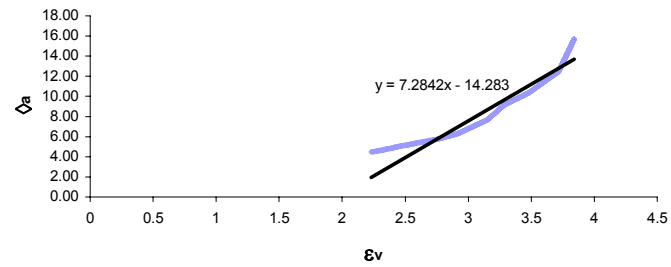
Young's Modulus (E')



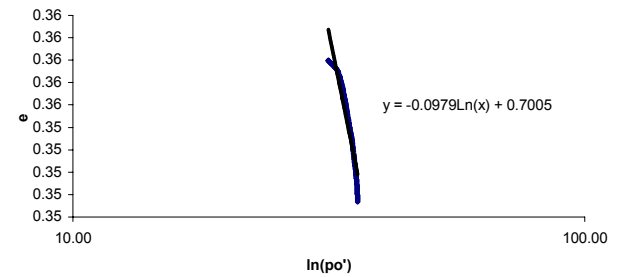
Swelling Index (κ)



ϵ_a vs ϵ_v



Expansion Index (λ_e)

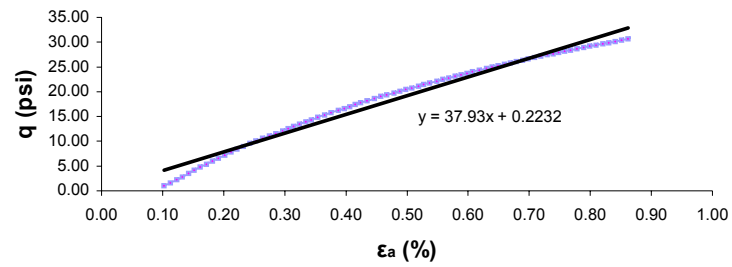


Test # : 21434

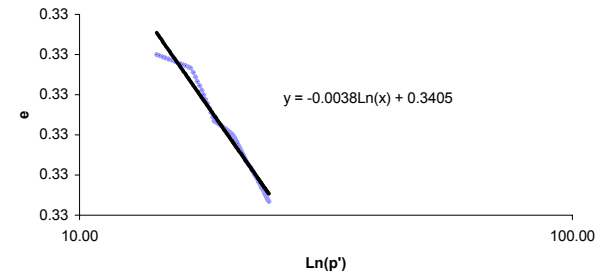
Initial p' (psi): 14

Soil Properties

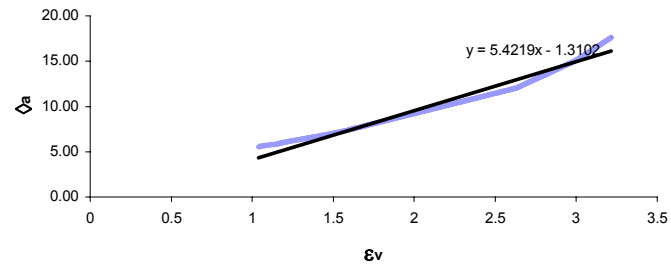
Young's Modulus (E')



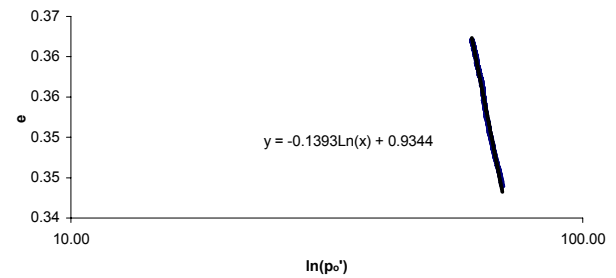
Swelling Index (κ)



ϵ_a vs ϵ_v



Expansion Index (λ_e)

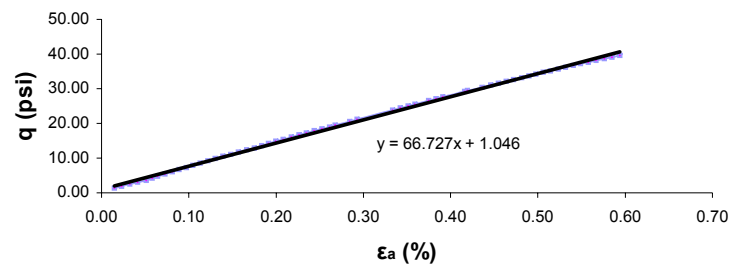


Test # : 21434

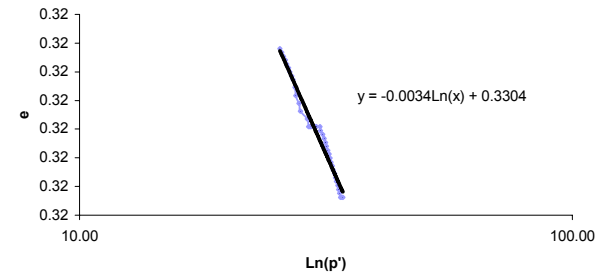
Initial p' (psi): 21

Soil Properties

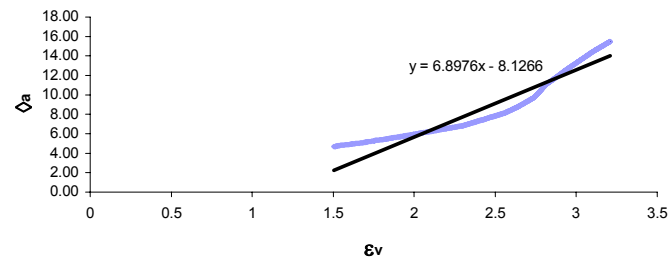
Young's Modulus (E')



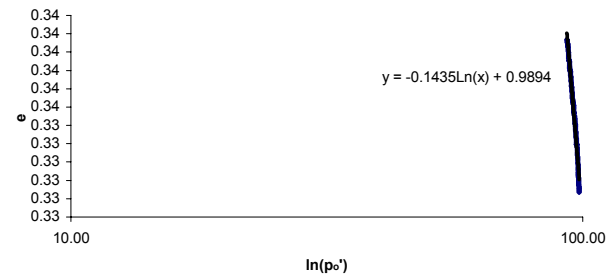
Swelling Index (κ)



ϵ_a vs ϵ_v



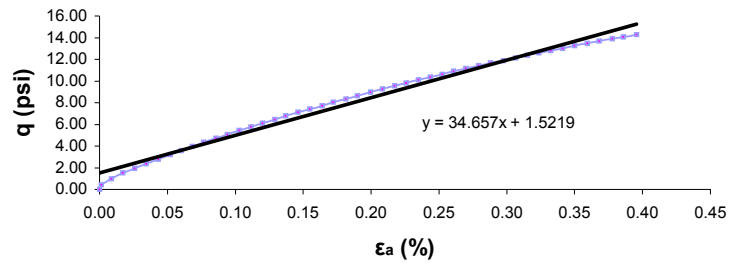
Expansion Index (λ_e)



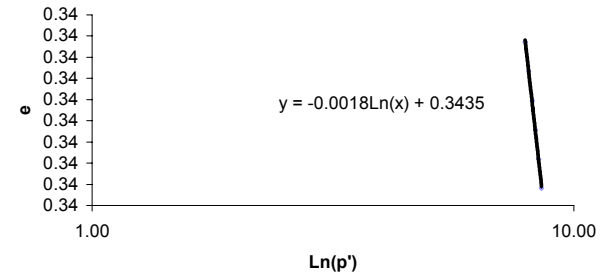
Test # : 21481
 Initial p' (psi): 7

Soil Properties

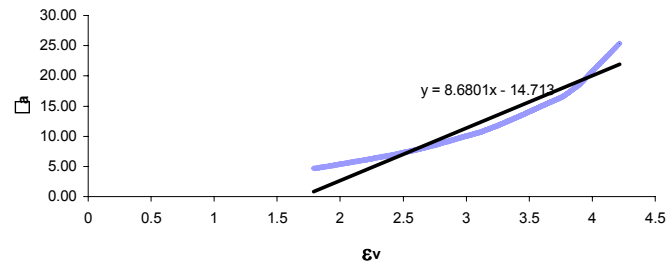
Young's Modulus (E')



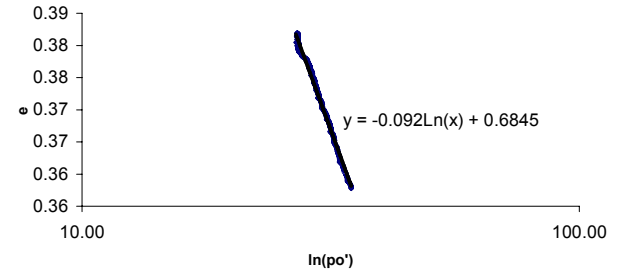
Swelling Index (κ)



ϵ_a vs ϵ_v



Expansion Index (λ_e)

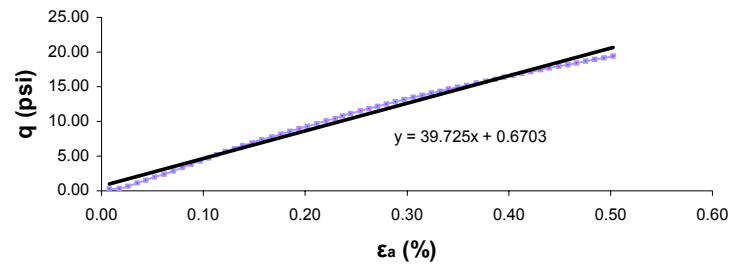


Test # : 21481

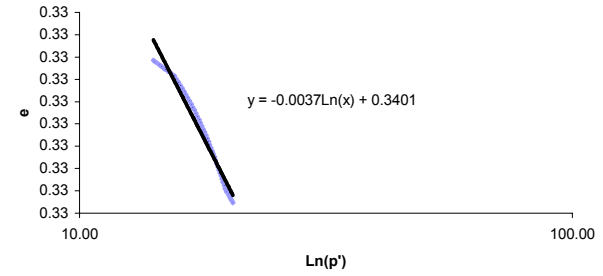
Initial p' (psi): 14

Soil Properties

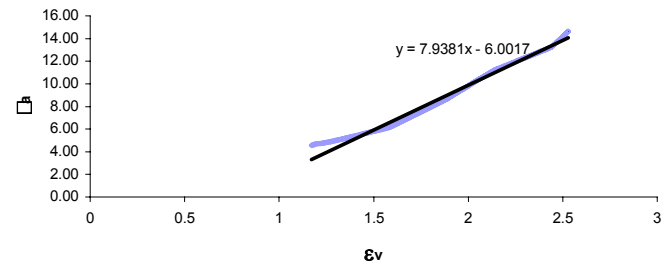
Young's Modulus (E')



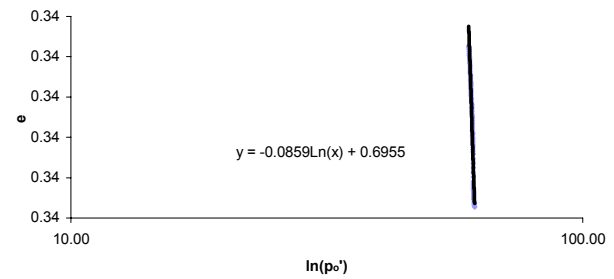
Swelling Index (κ)



ϵ_a vs ϵ_v



Expansion Index (λ_e)

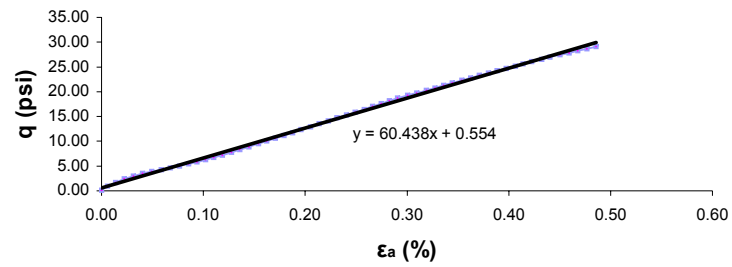


Test # : 21481

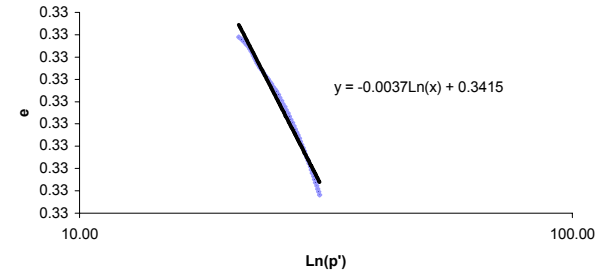
Initial p' (psi): 21

Soil Properties

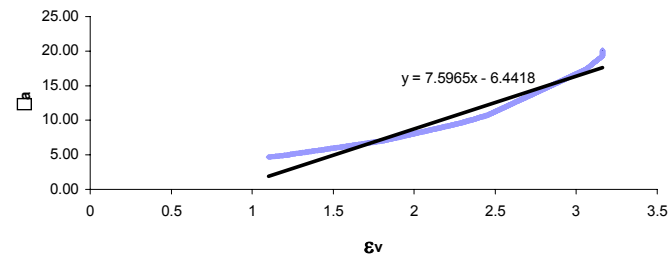
Young's Modulus (E')



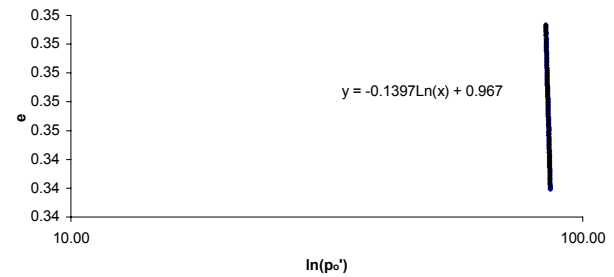
Swelling Index (κ)



ϵ_a vs ϵ_v



Expansion Index (λ_e)

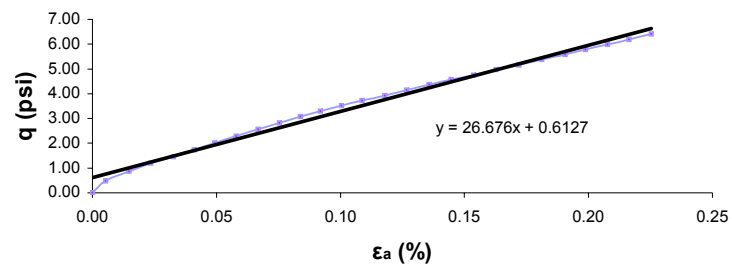


Test # : 21482

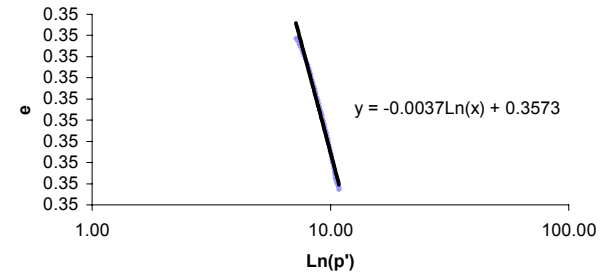
Initial p' (psi): 7

Soil Properties

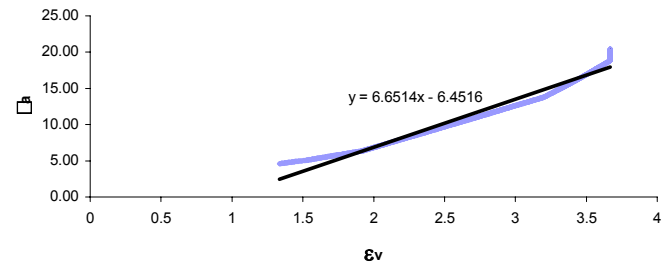
Young's Modulus (E')



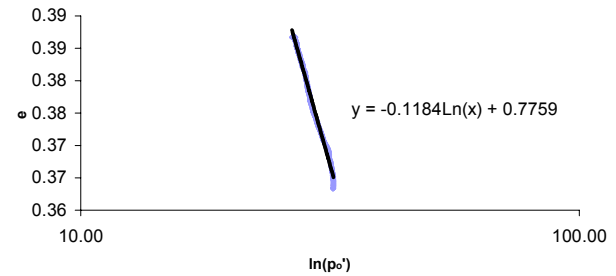
Swelling Index (κ)



ϵ_a vs ϵ_v



Expansion Index (λ_e)

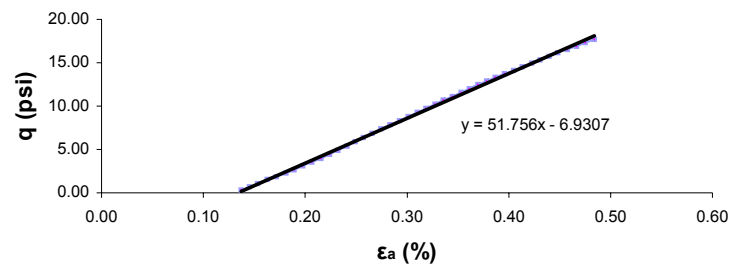


Test # : 21482

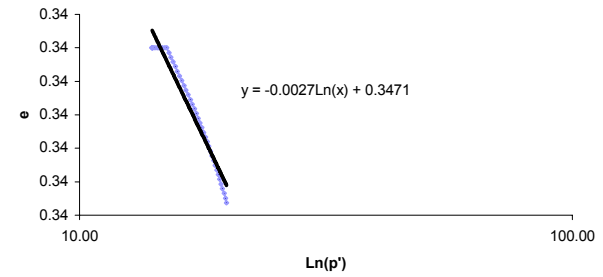
Initial p' (psi): 14

Soil Properties

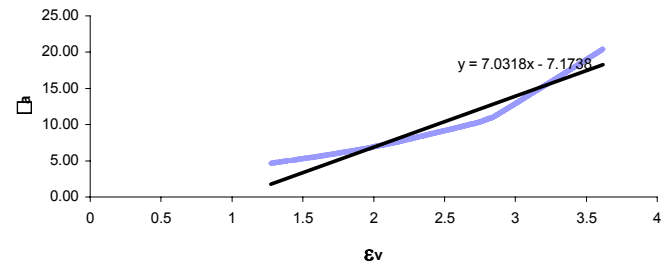
Young's Modulus (E')



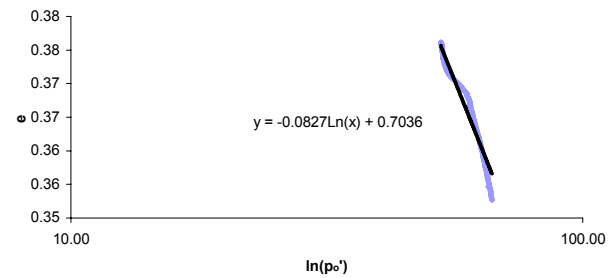
Swelling Index (κ)



ϵ_a vs ϵ_v



Expansion Index (λ_e)

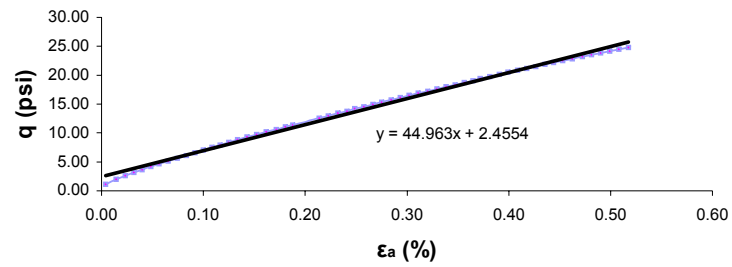


Test # : 21482

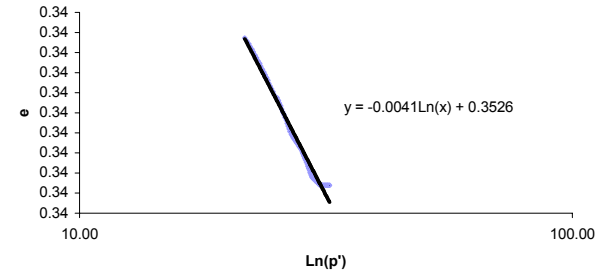
Initial p' (psi): 21

Soil Properties

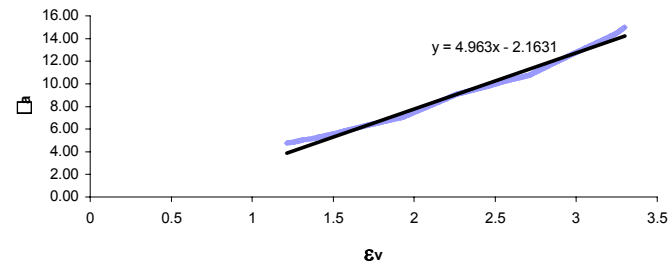
Young's Modulus (E')



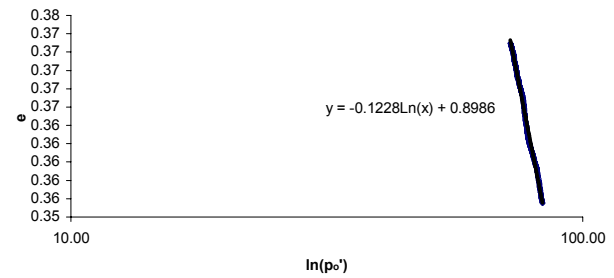
Swelling Index (κ)



ϵ_a vs ϵ_v



Expansion Index (λ_e)

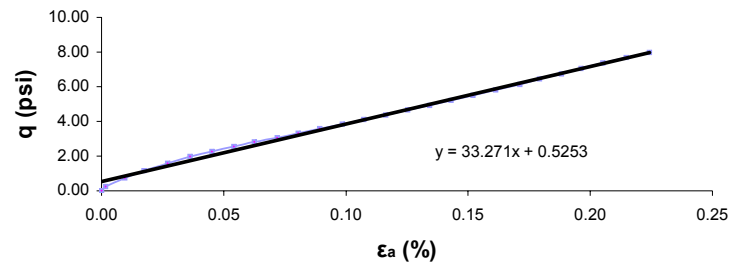


Test # : 21483

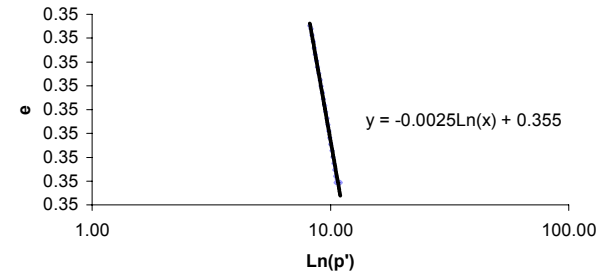
Initial p' (psi): 7

Soil Properties

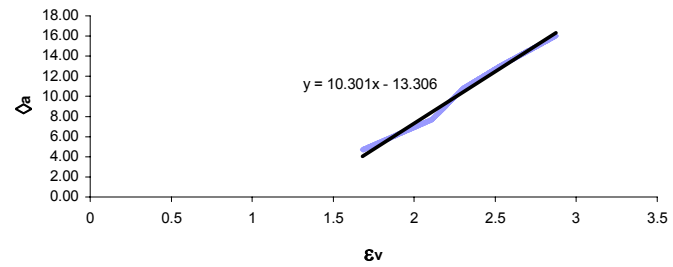
Young's Modulus (E')



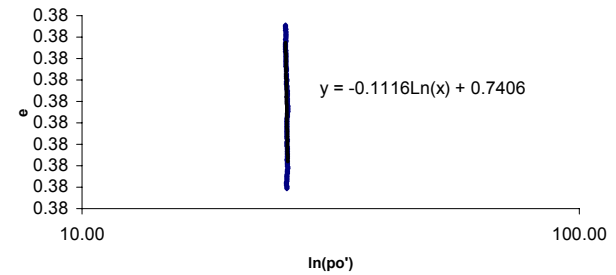
Swelling Index (κ)



ϵ_a vs ϵ_v



Expansion Index (λ_e)

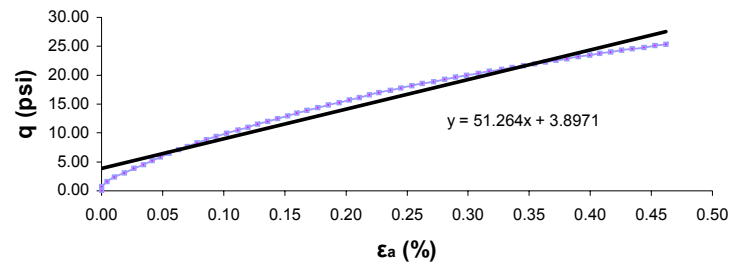


Test # : 21483

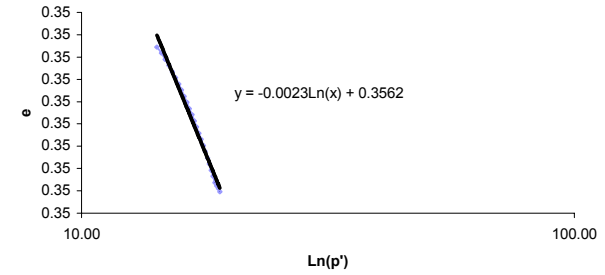
Initial p' (psi): 14

Soil Properties

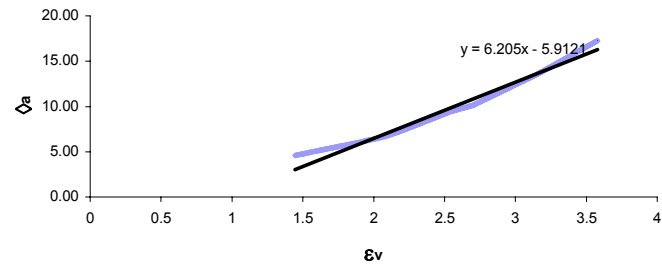
Young's Modulus (E')



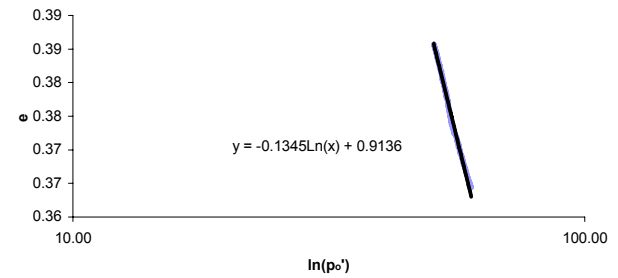
Swelling Index (κ)



ϵ_a vs ϵ_v



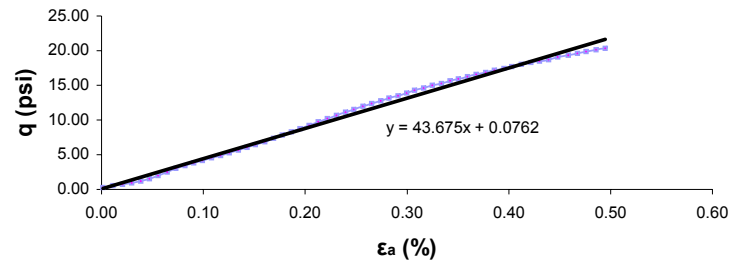
Expansion Index (λ_e)



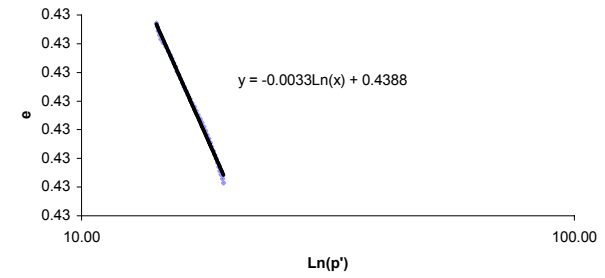
Test # : 21515
Initial p' (psi): 14

Soil Properties

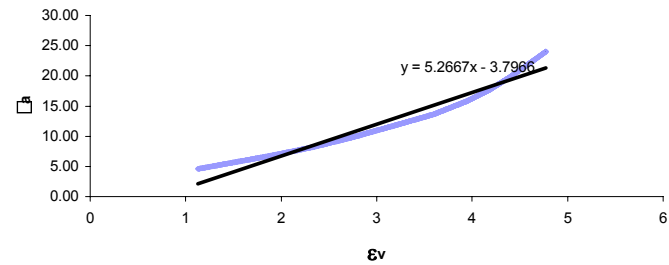
Young's Modulus (E')



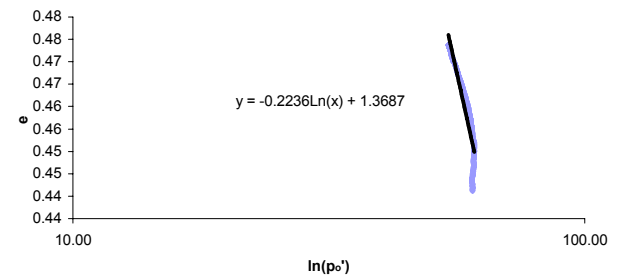
Swelling Index (κ)



ϵ_a vs ϵ_v



Expansion Index (λ_e)

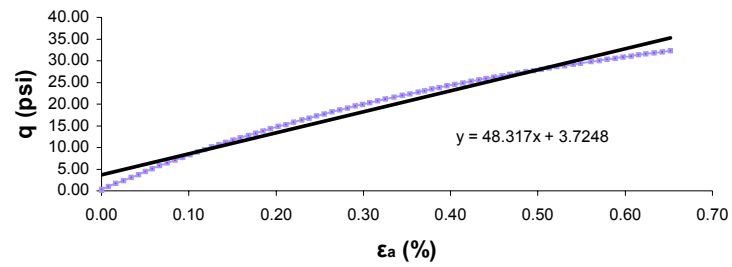


Test # : 21515

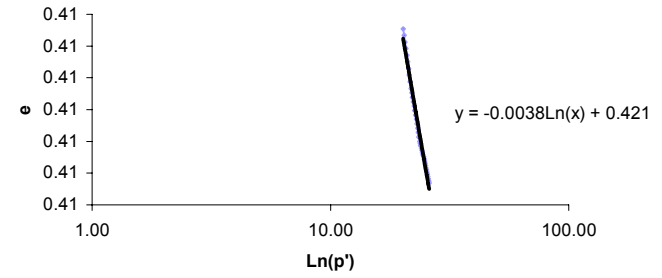
Initial p' (psi): 17

Soil Properties

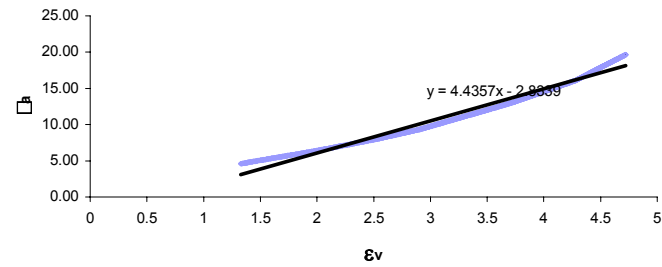
Young's Modulus (E')



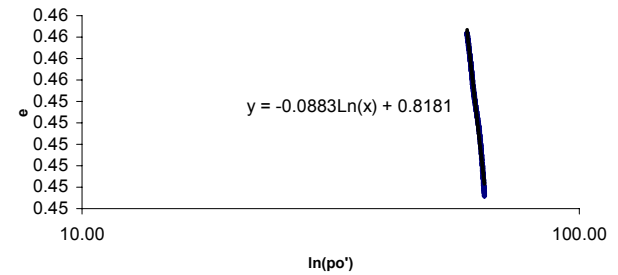
Swelling Index (κ)



ϵ_a vs ϵ_v



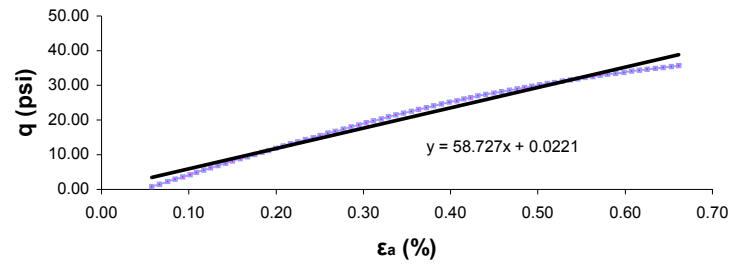
Expansion Index (λ_e)



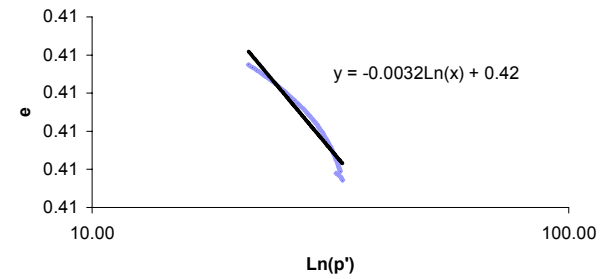
Test # : 21515
Initial p' (psi): 21

Soil Properties

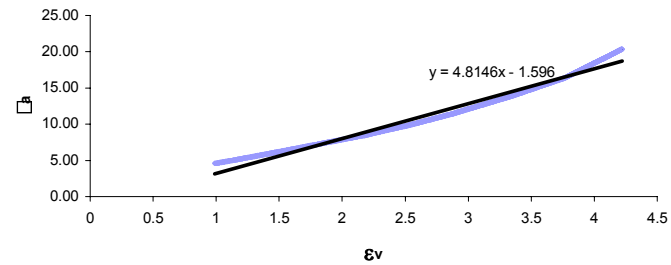
Young's Modulus (E')



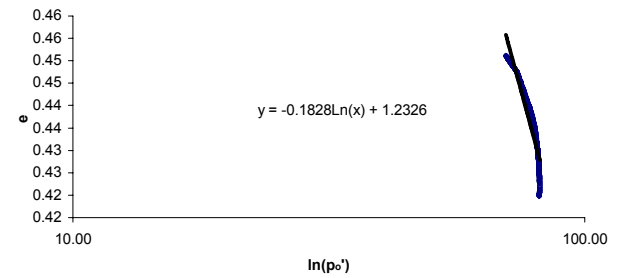
Swelling Index (κ)



ϵ_a vs ϵ_v



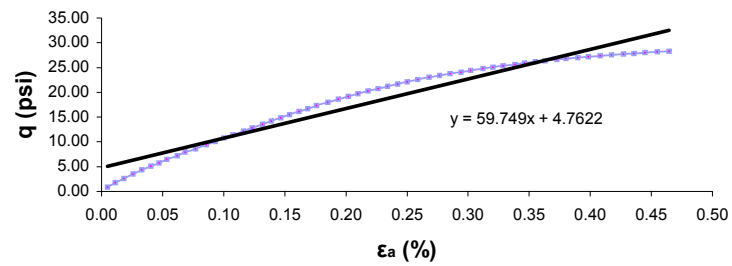
Expansion Index (λ_e)



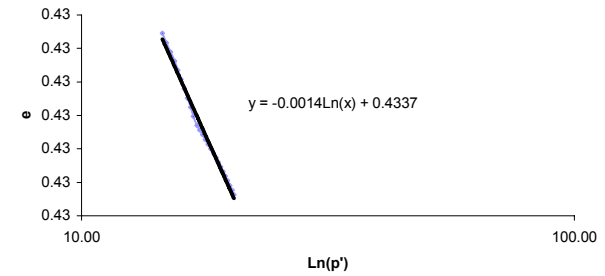
Test # : 21516
 Initial p' (psi): 14

Soil Properties

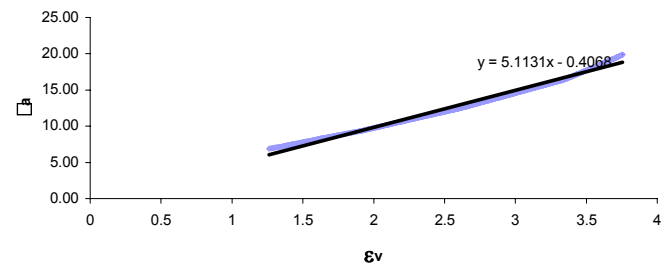
Young's Modulus (E')



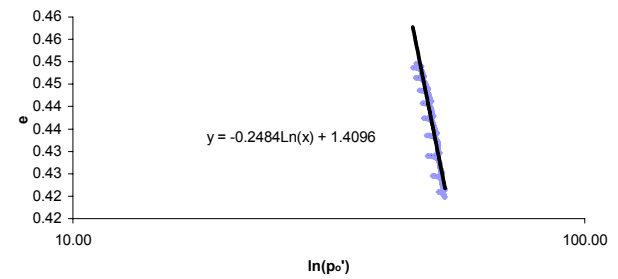
Swelling Index (κ)



ϵ_a vs ϵ_v



Expansion Index (λ_e)

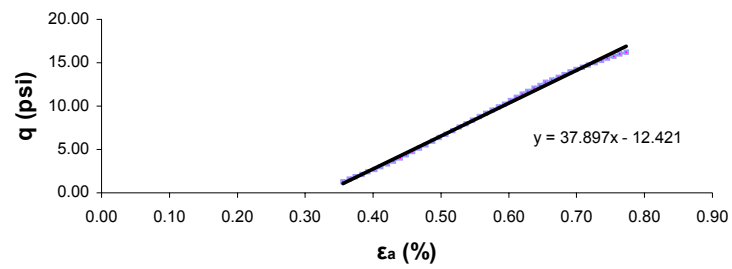


Test # : 21548

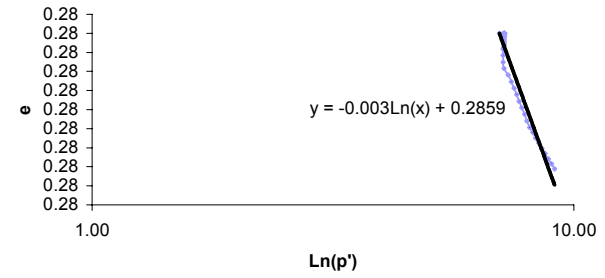
Initial p' (psi): 7

Soil Properties

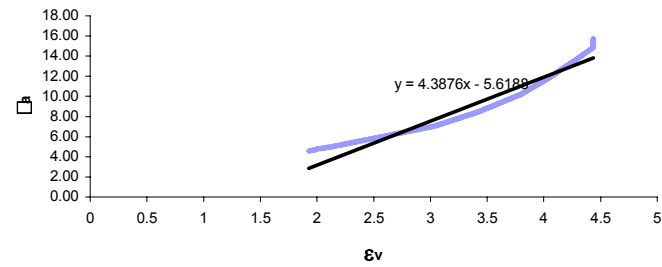
Young's Modulus (E')



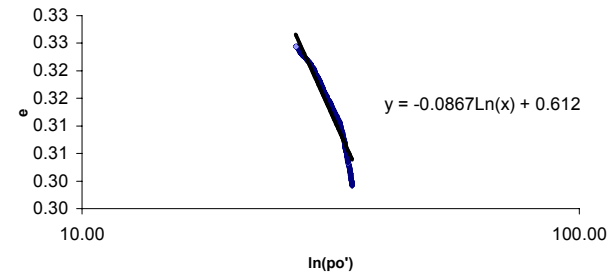
Swelling Index (κ)



ϵ_a vs ϵ_v



Expansion Index (λ_e)

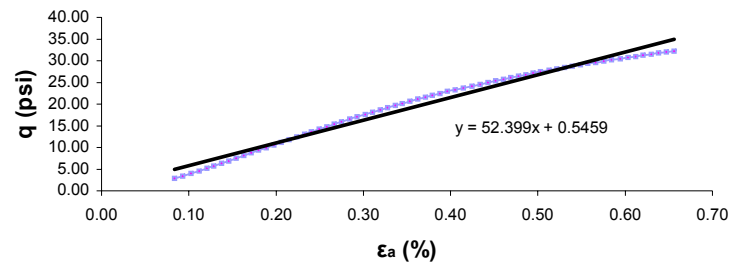


Test # : 21548

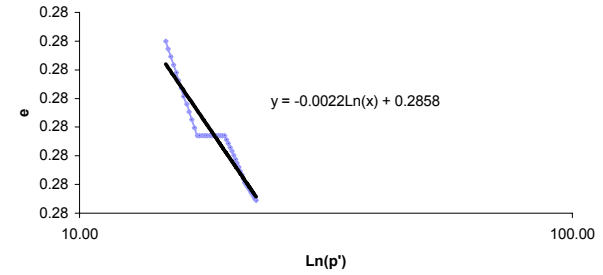
Initial p' (psi): 14

Soil Properties

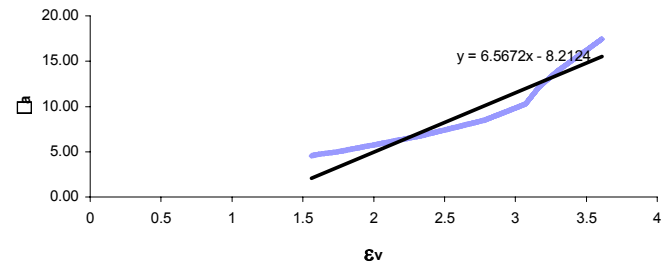
Young's Modulus (E')



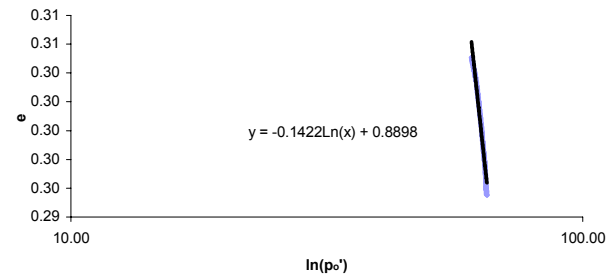
Swelling Index (κ)



ϵ_a vs ϵ_v



Expansion Index (λ_e)

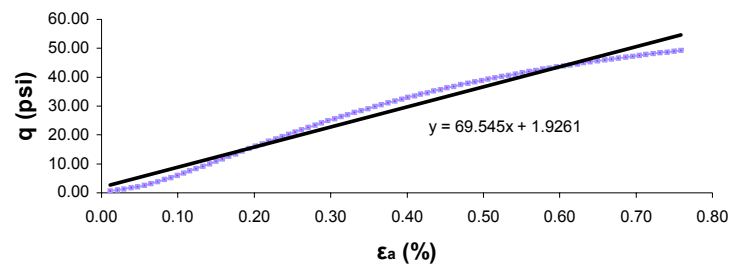


Test # : 21548

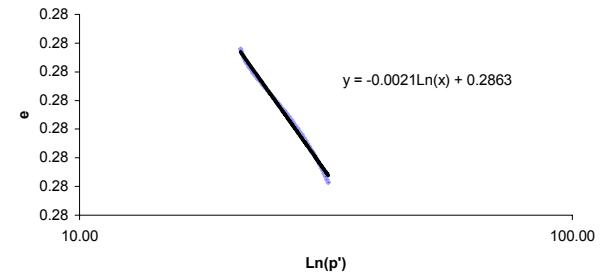
Initial p' (psi): 21

Soil Properties

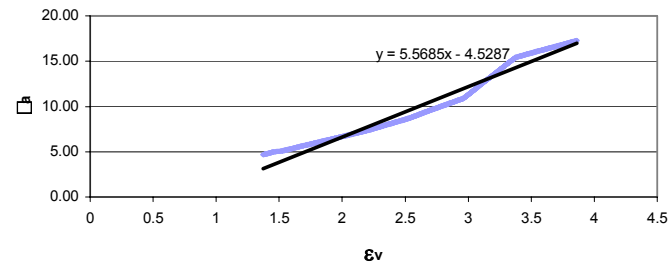
Young's Modulus (E')



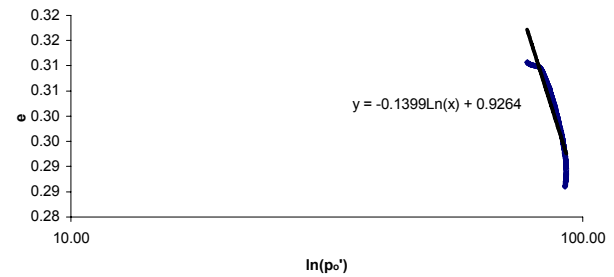
Swelling Index (κ)



ϵ_a vs ϵ_v

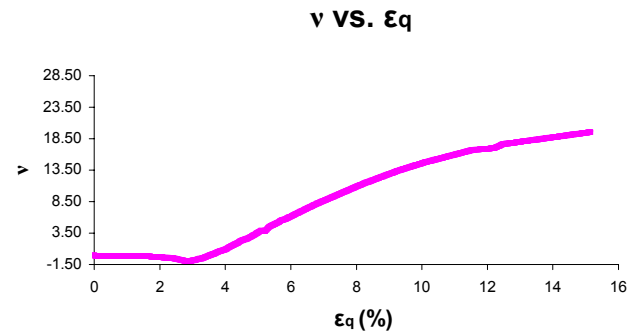
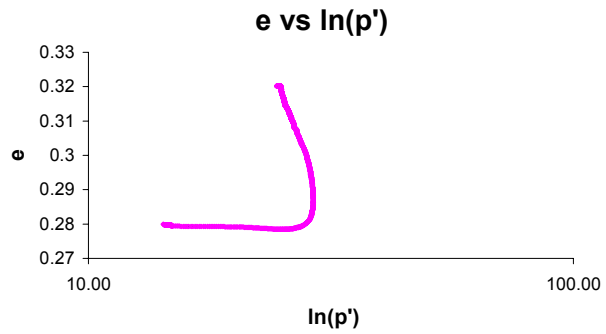
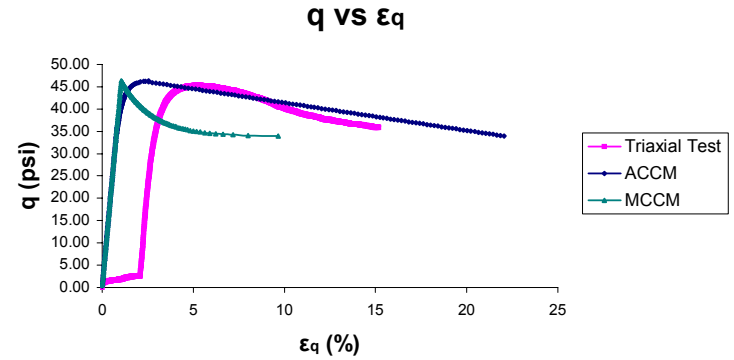
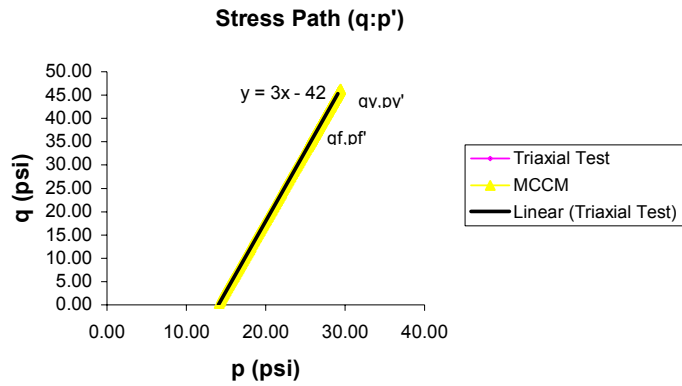


Expansion Index (λ_e)



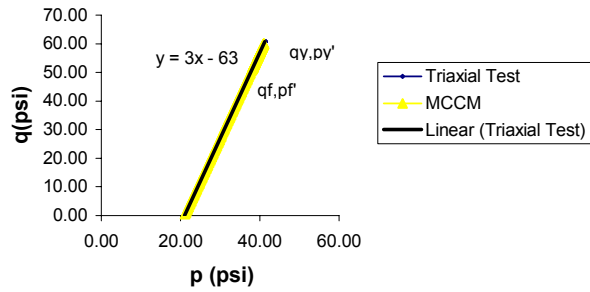
APPENDIX B

Test # : 21398
 Initial p' (psi): 14

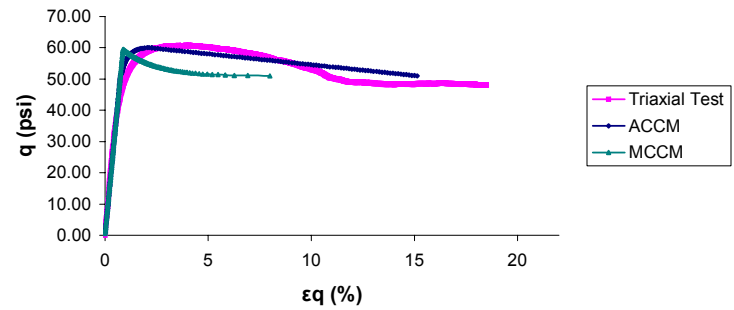


Test # : 21398
 Initial p' (psi): 21

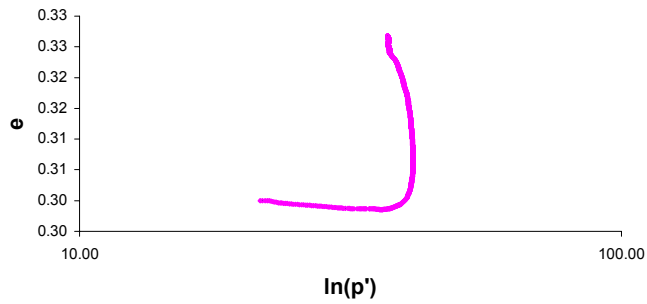
Stress Path (q:p')



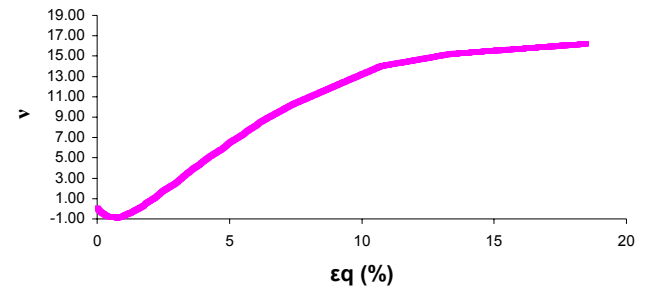
q vs ϵ_q



e vs $\ln(p')$

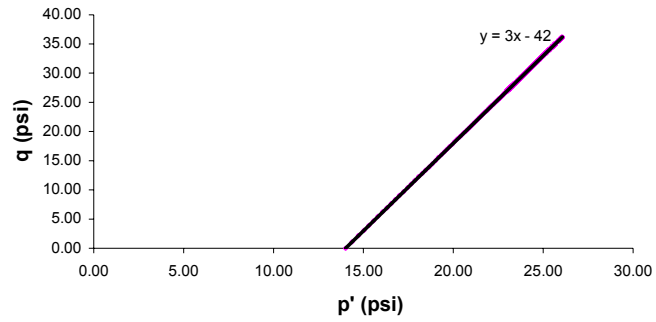


v vs. ϵ_q

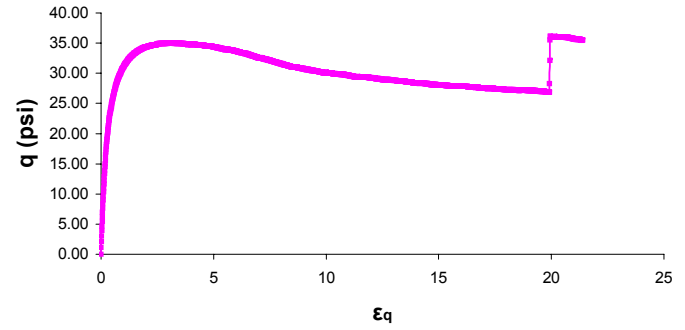


Test # : 21399
Initial p' (psi): 14

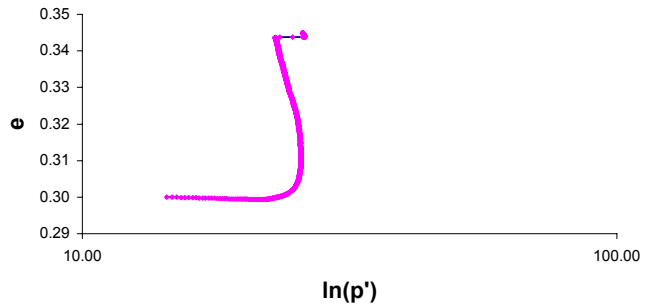
Stress Path (q:p')



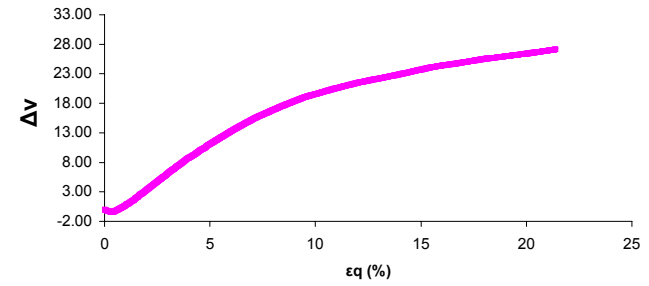
q vs ϵ_q



e vs $\ln(p')$



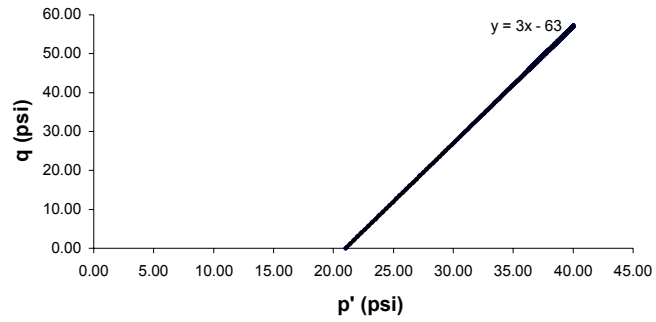
Δv vs. ϵ_q



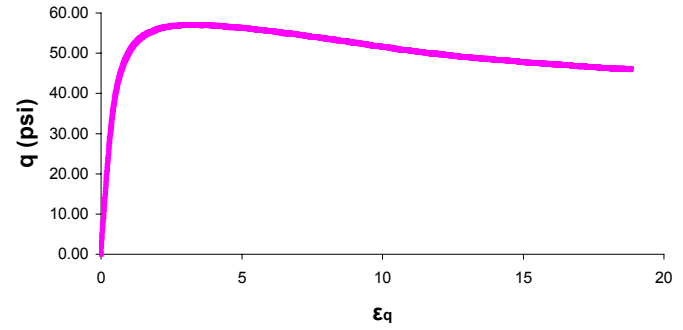
Test # : 21399

Initial p' (psi): 21

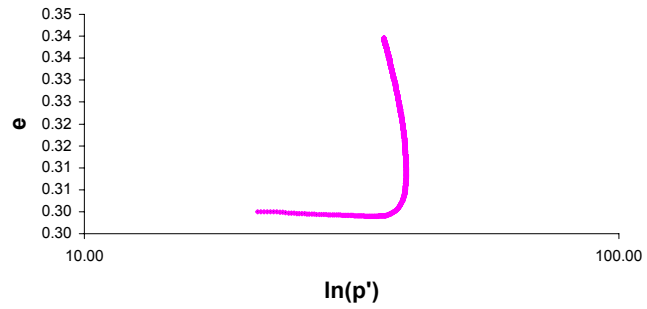
Stress Path (q:p')



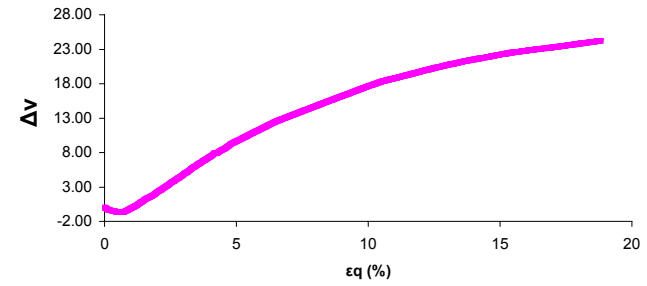
q vs ϵ_q



e vs $\ln(p')$

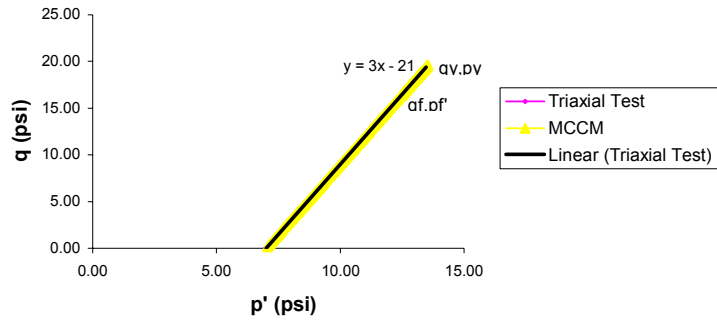


Δv vs. ϵ_q

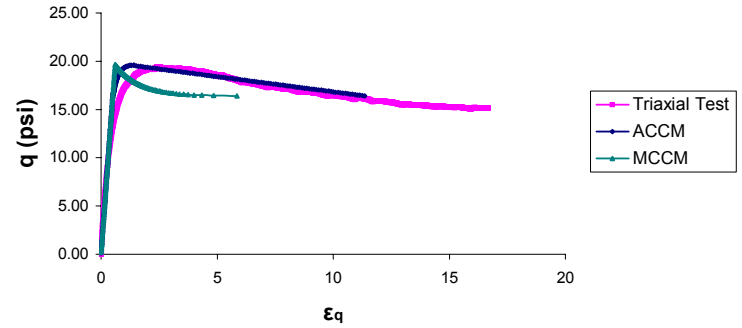


Test # : 21401
 Initial p' (psi): 7

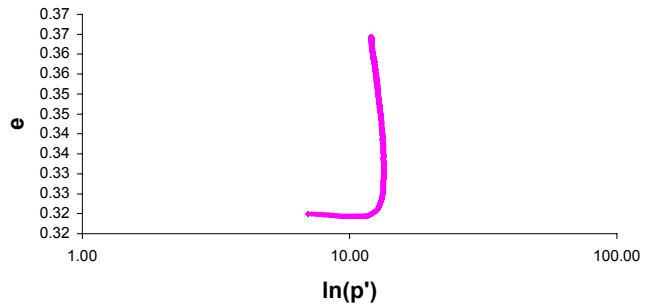
Stress Path (q:p')



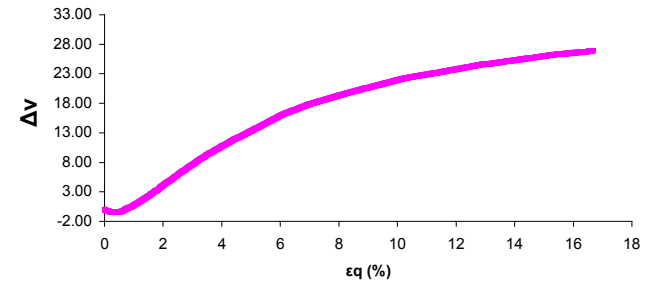
q vs ϵ_q



e vs $\ln(p')$

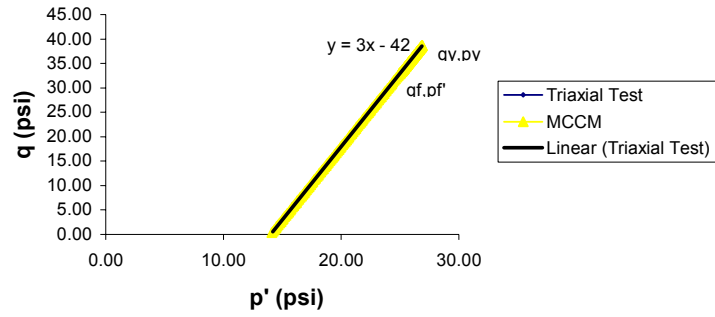


Δv vs. ϵ_q

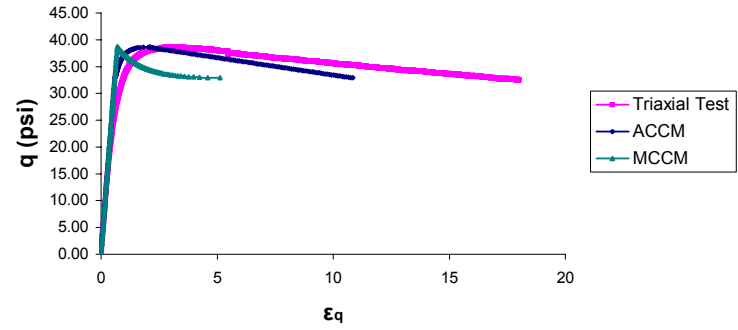


Test # : 21401
 Initial p' (psi): 14

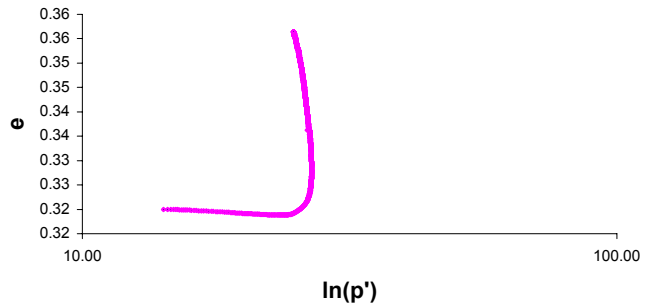
Stress Path (q:p')



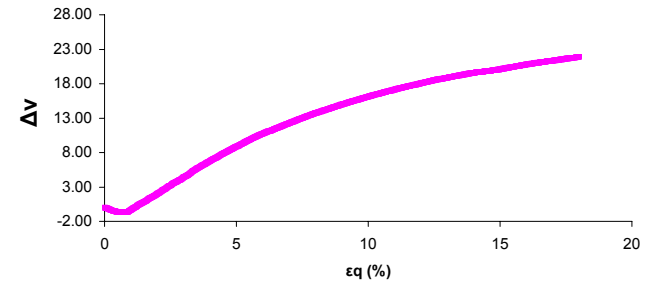
q vs ϵ_q



e vs $\ln(p')$

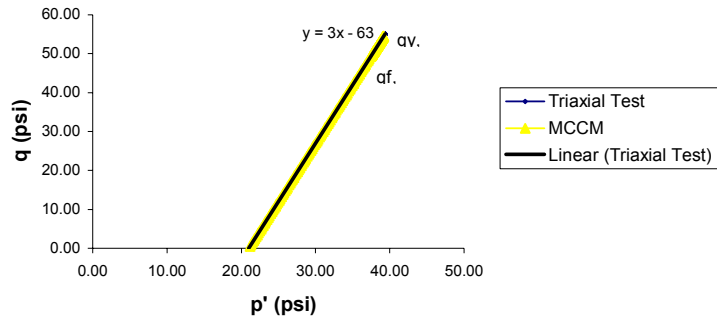


Δv vs. ϵ_q

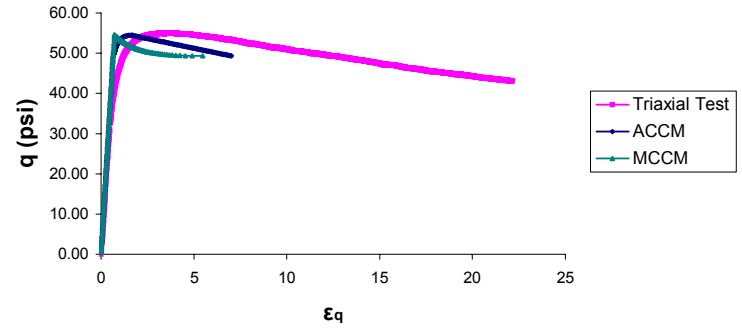


Test # : 21401
 Initial p' (psi): 21

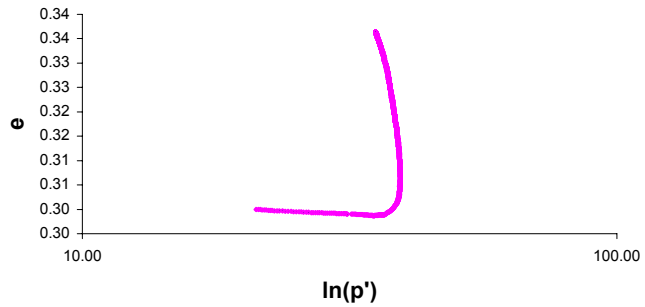
Stress Path (q:p')



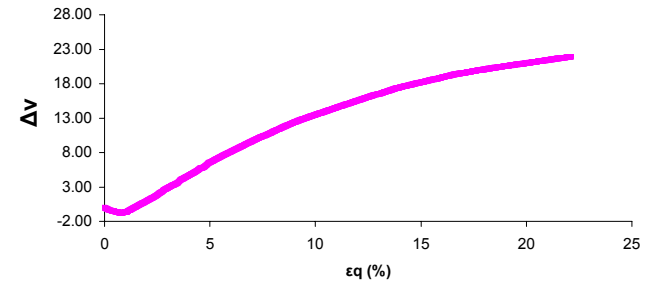
q vs ϵ_q



e vs $\ln(p')$

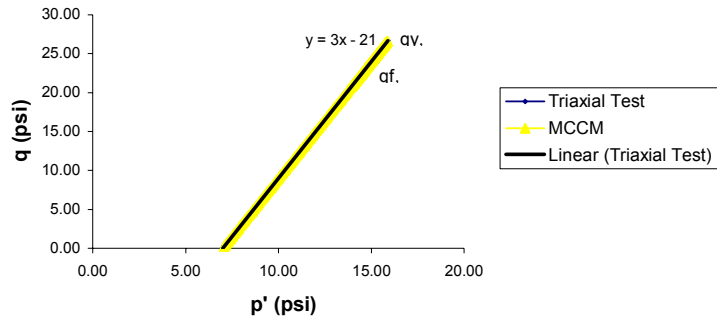


Δv vs. ϵ_q

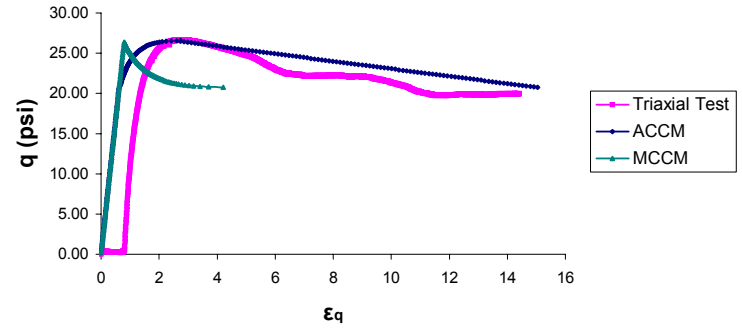


Test # : 21434
 Initial p' (psi): 7

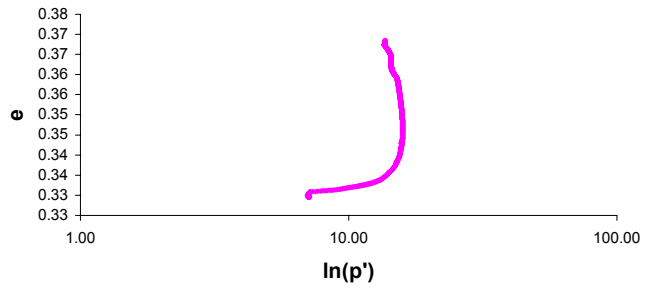
Stress Path (q:p')



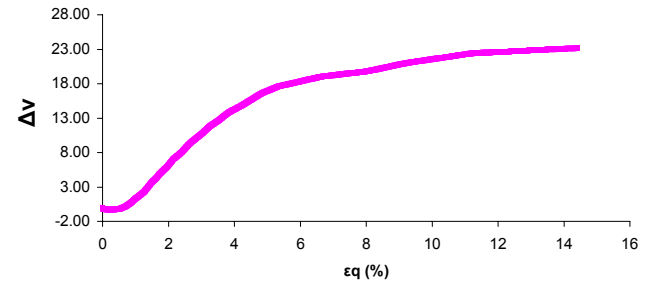
q vs ϵ_q



e vs $\ln(p')$

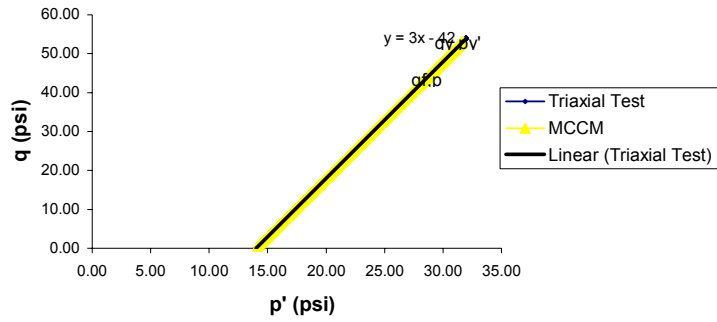


Δv vs. ϵ_q

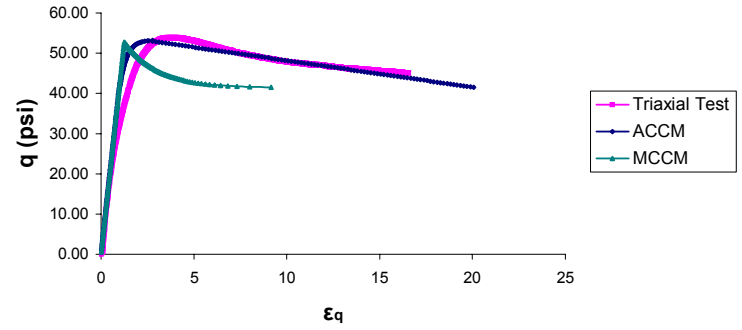


Test # : 21434
 Initial p' (psi): 14

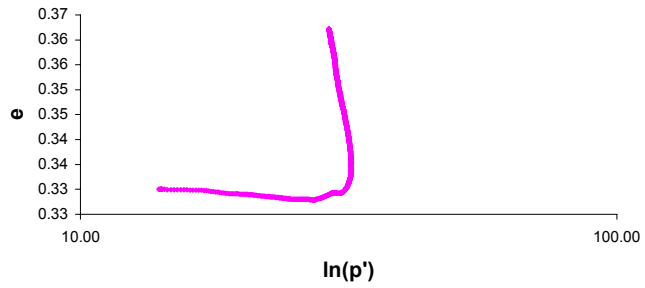
Stress Path (q:p')



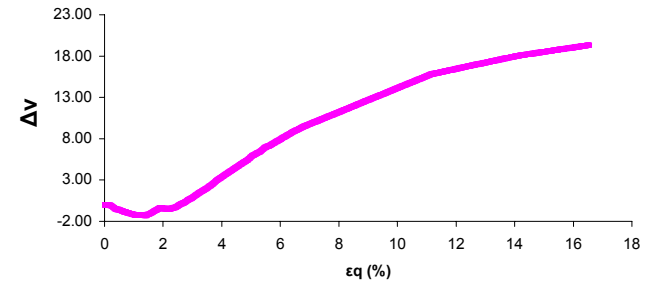
q vs ϵ_q



e vs $\ln(p')$



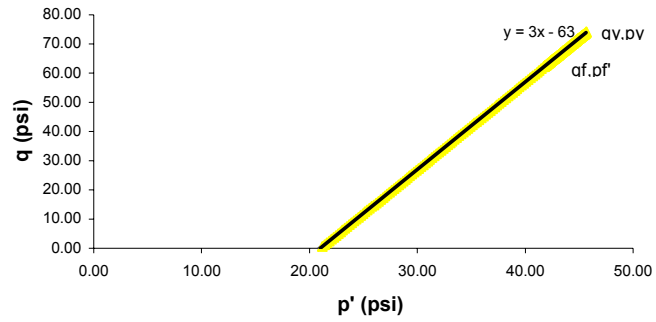
Δv vs. ϵ_q



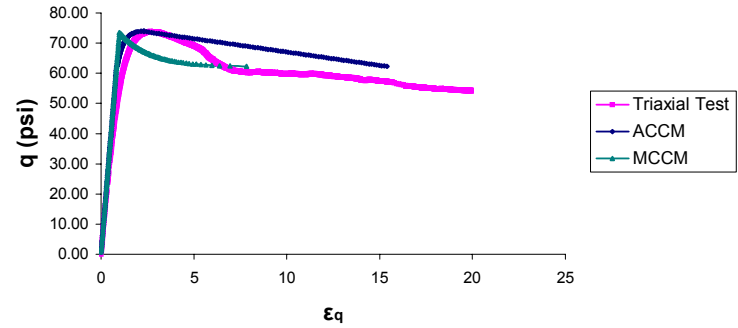
Test # : 21434

Initial p' (psi): 21

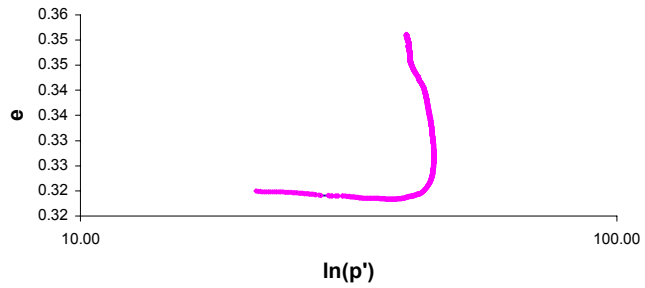
Stress Path (q:p')



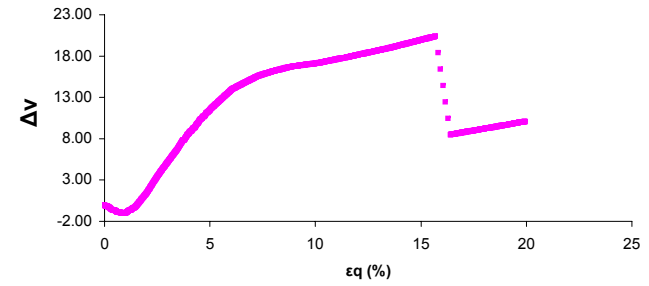
q vs ϵ_q



e vs $\ln(p')$

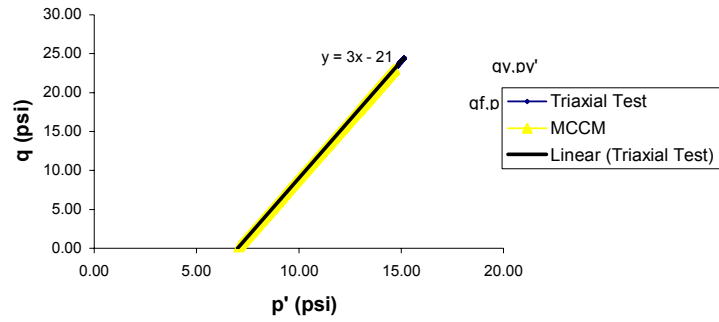


Δv vs. ϵ_q

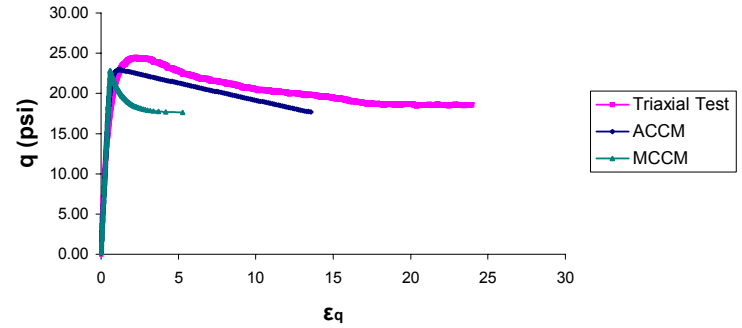


Test # : 21481
 Initial p' (psi): 7

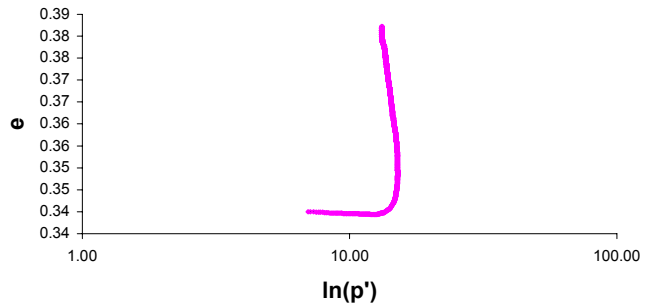
Stress Path (q:p')



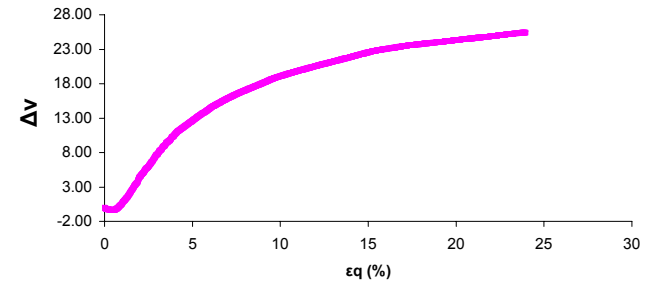
q vs ϵ_q



e vs $\ln(p')$

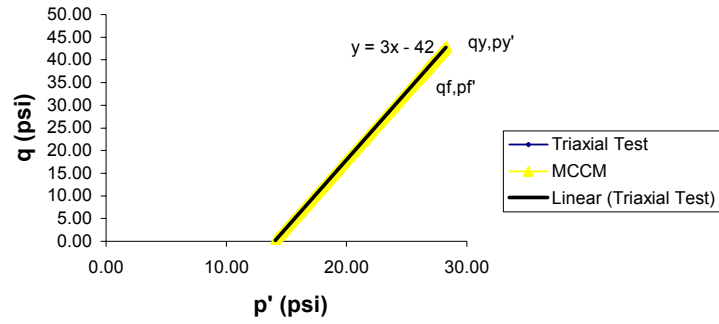


Δv vs. ϵ_q

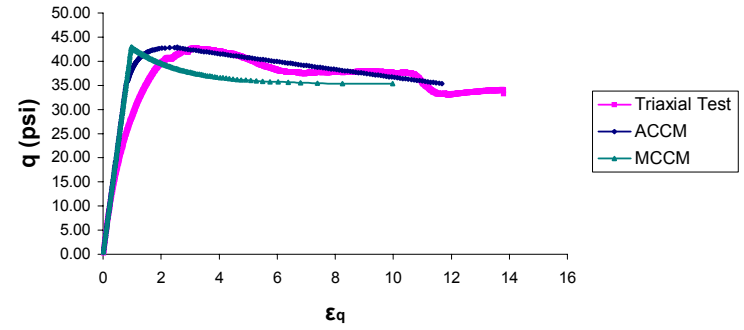


Test # : 21481
 Initial p' (psi): 14

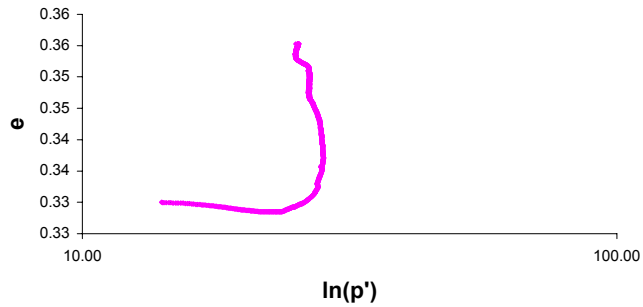
Stress Path (q:p')



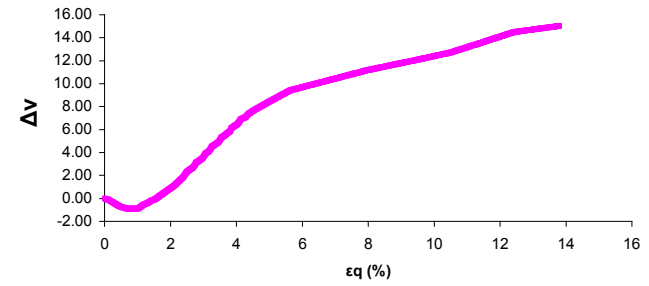
q vs ϵ_q



e vs $\ln(p')$

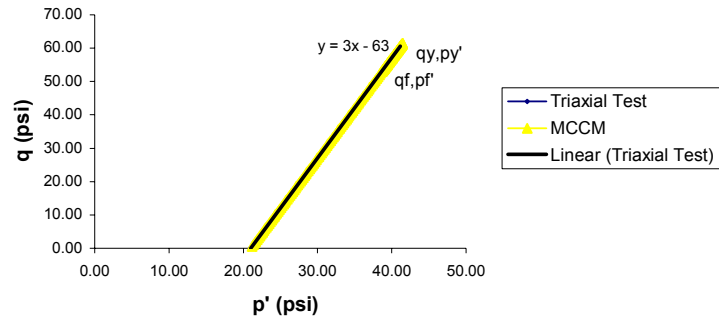


Δv vs. ϵ_q

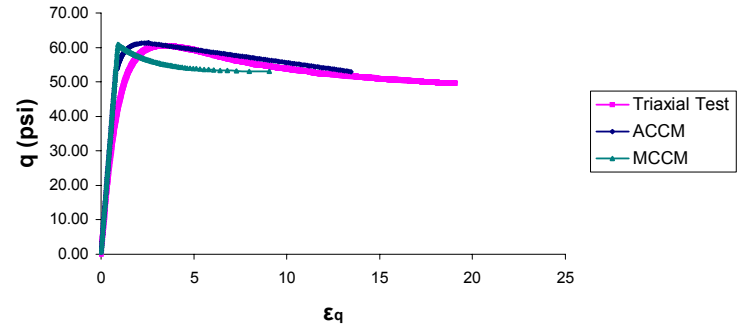


Test # : 21481
 Initial p' (psi): 21

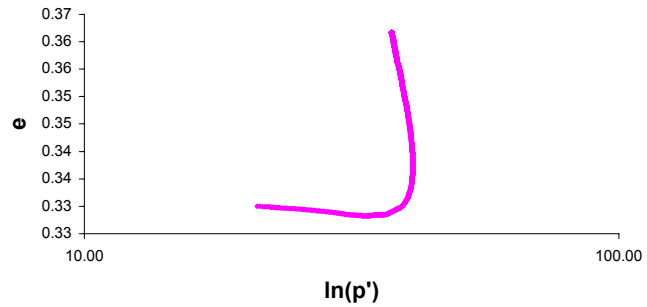
Stress Path (q:p')



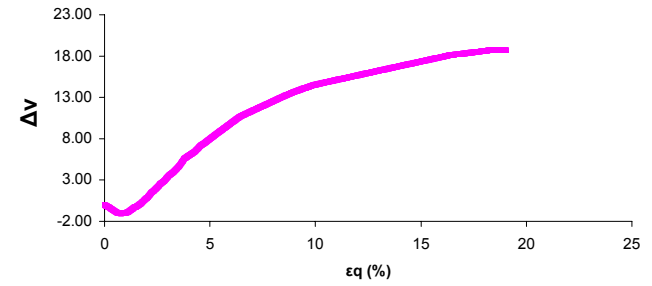
q vs ϵ_q



e vs $\ln(p')$

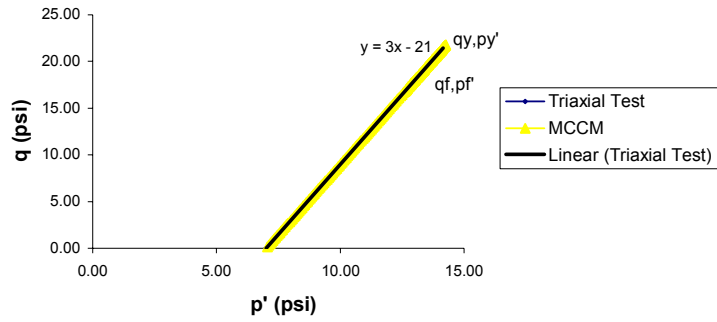


Δv vs. ϵ_q

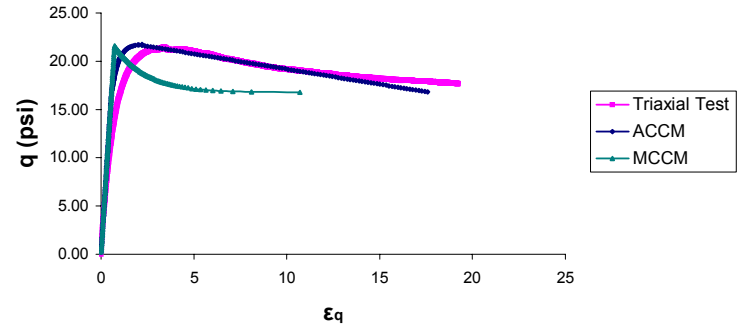


Test # : 21482
 Initial p' (psi): 7

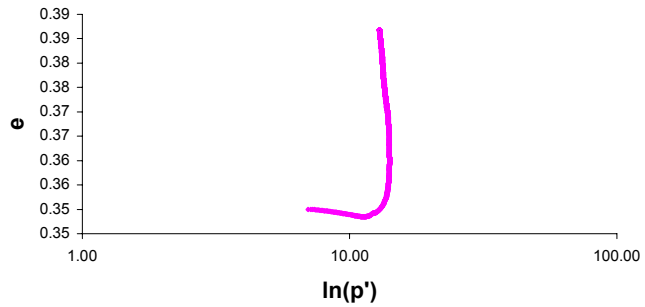
Stress Path (q:p')



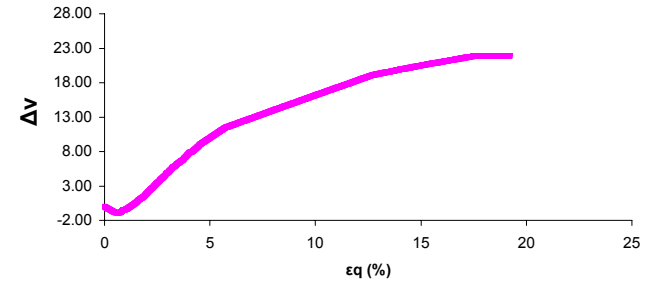
q vs ϵ_q



e vs $\ln(p')$

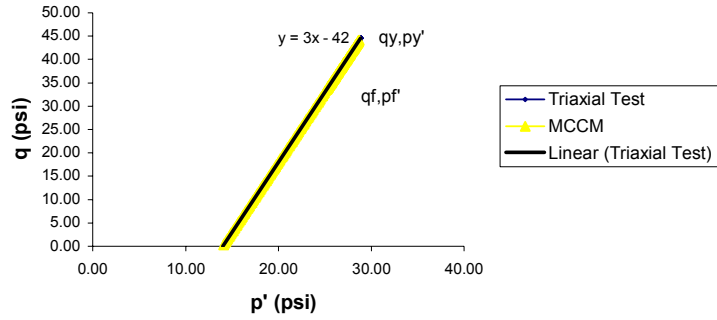


Δv vs. ϵ_q

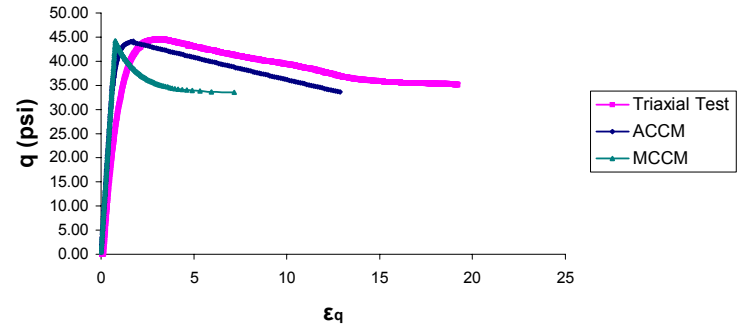


Test # : 21482
 Initial p' (psi): 14

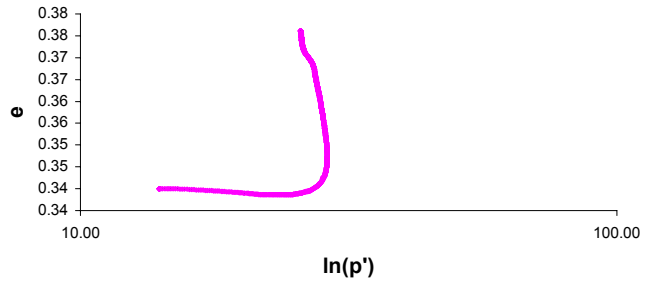
Stress Path (q:p')



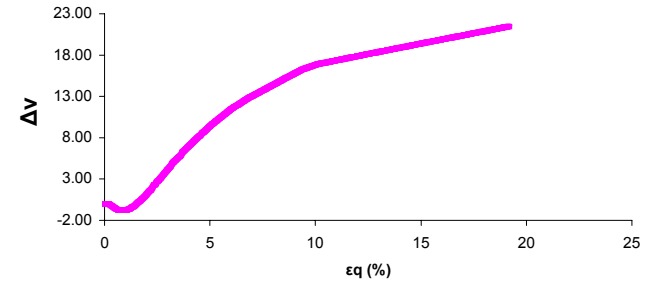
q vs ϵ_q



e vs $\ln(p')$

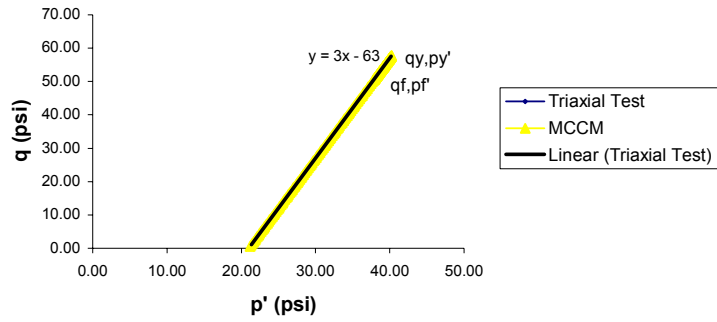


Δv vs. ϵ_q

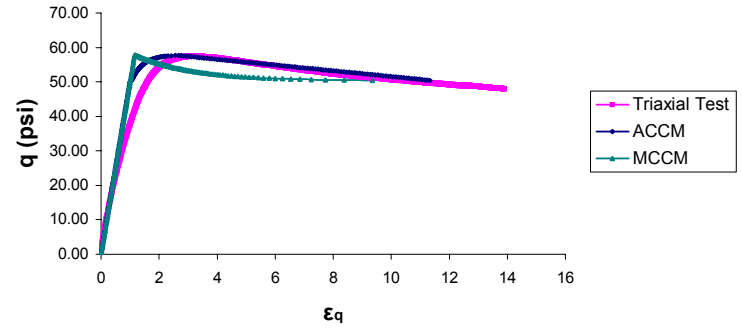


Test # : 21482
 Initial p' (psi): 21

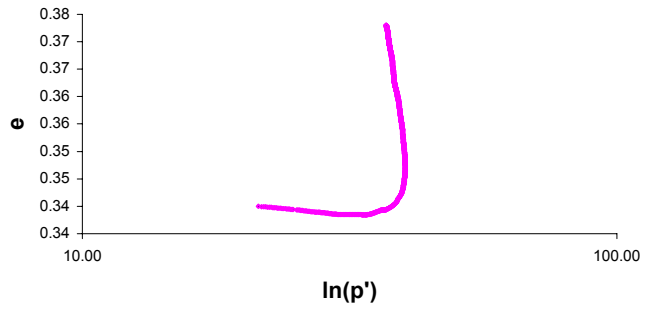
Stress Path (q:p')



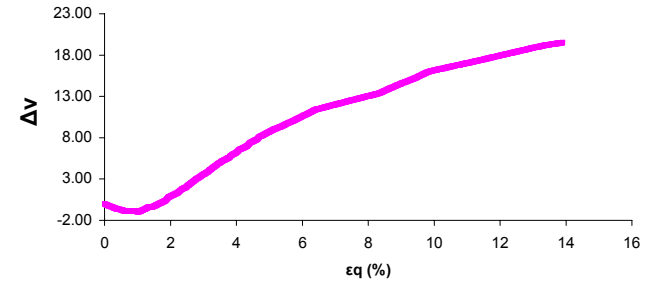
q vs ϵ_q



e vs $\ln(p')$

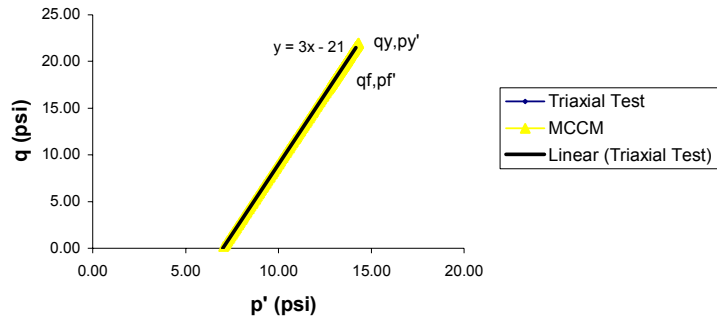


Δv vs. ϵ_q

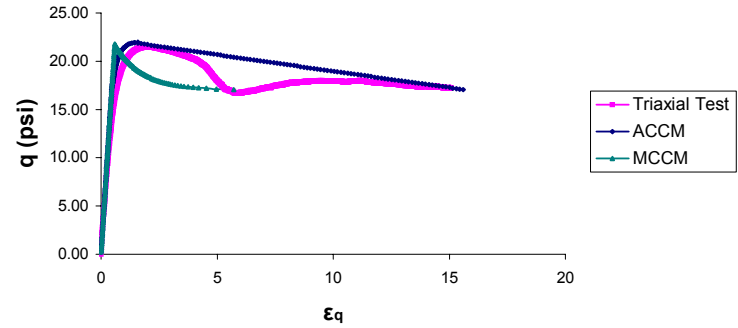


Test # : 21483
 Initial p' (psi): 7

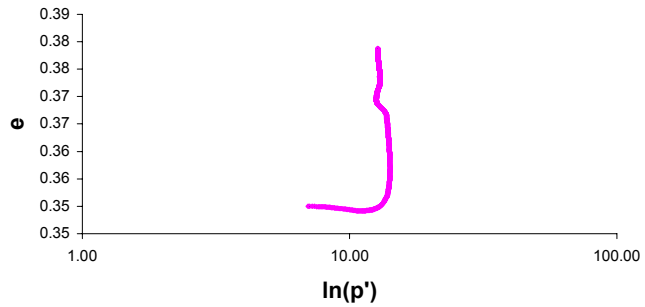
Stress Path (q:p')



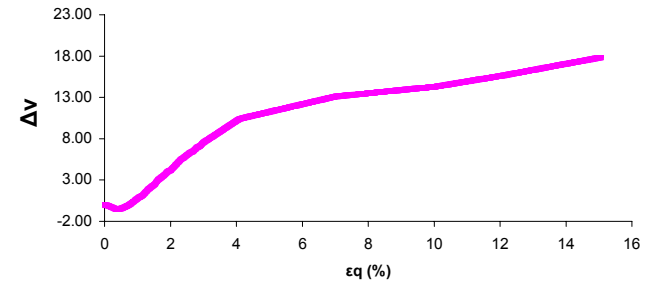
q vs ϵ_q



e vs $\ln(p')$

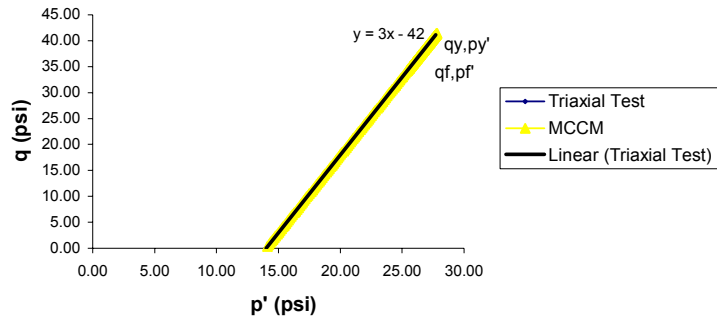


Δv vs. ϵ_q

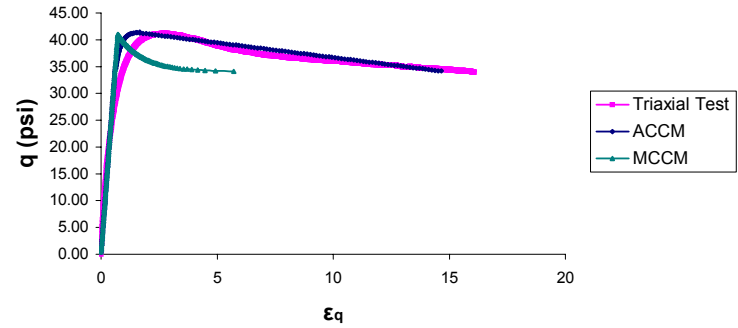


Test # : 21483
 Initial p' (psi): 14

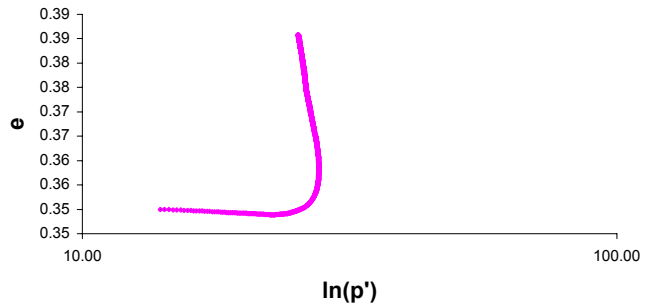
Stress Path (q:p')



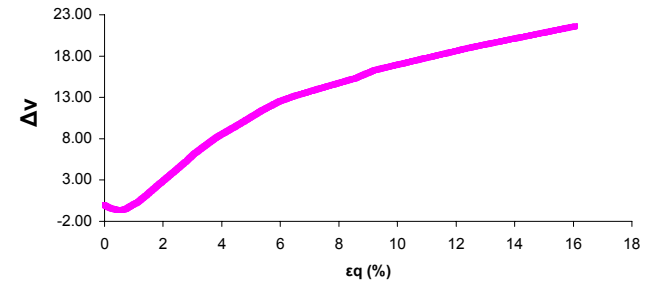
q vs ϵ_q



e vs $\ln(p')$

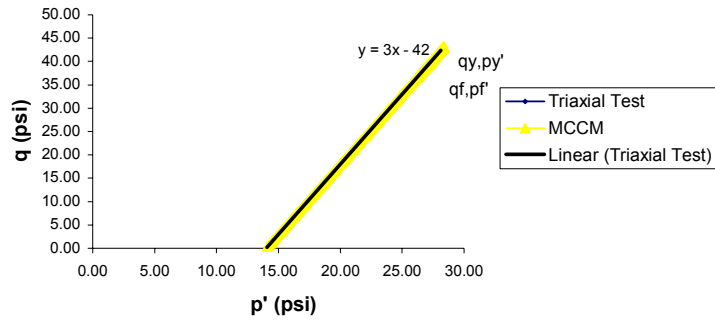


Δv vs. ϵ_q

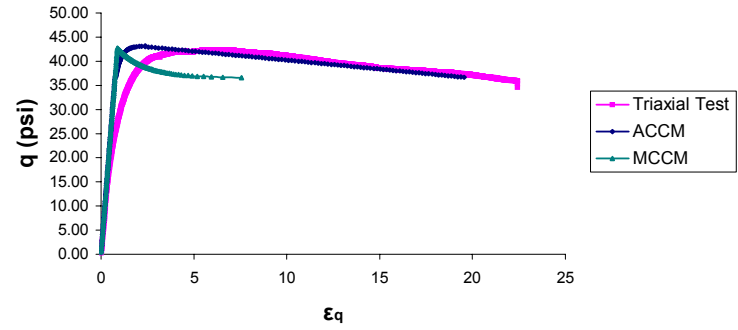


Test # : 21515
 Initial p' (psi): 14

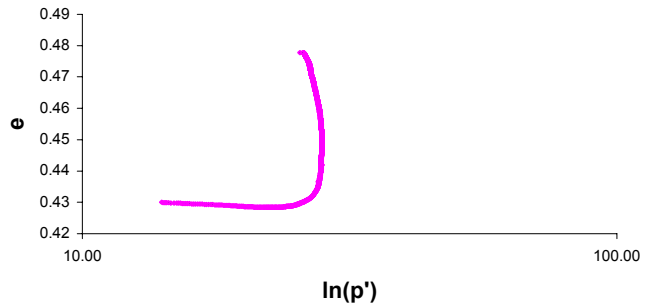
Stress Path (q:p')



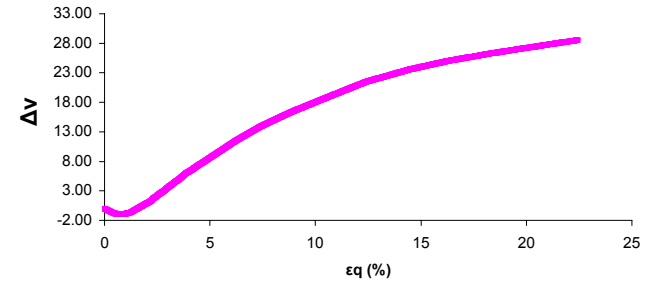
q vs ϵ_q



e vs $\ln(p')$

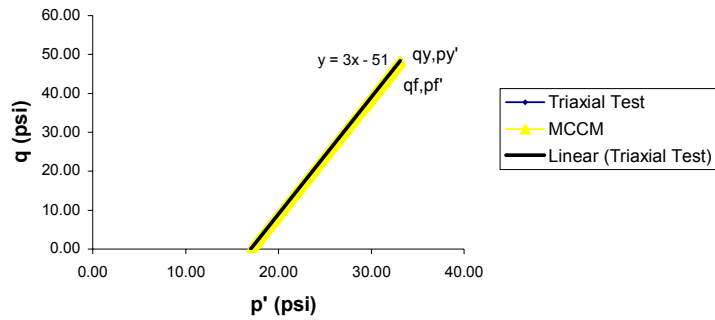


Δv vs. ϵ_q

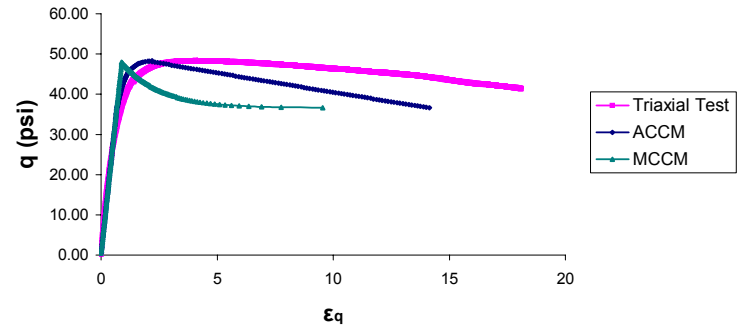


Test # : 21515
 Initial p' (psi): 17

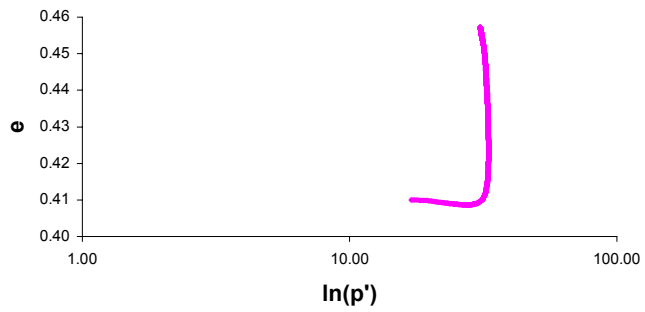
Stress Path (q:p')



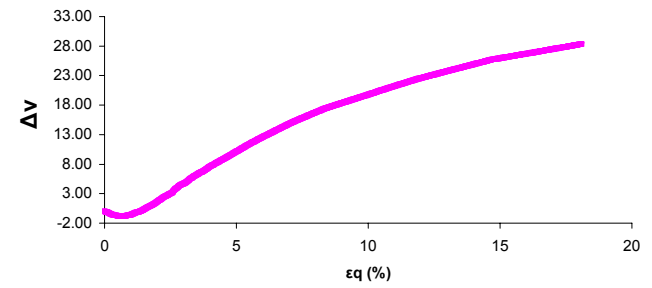
q vs ϵ_q



e vs $\ln(p')$

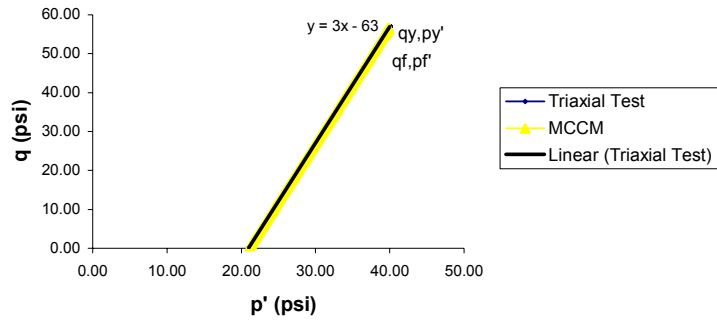


Δv vs. ϵ_q

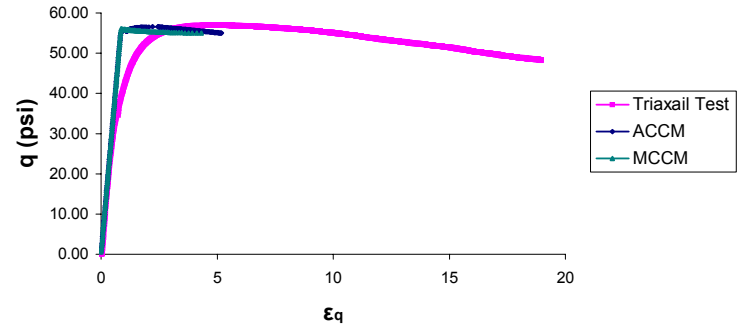


Test # : 21515
 Initial p' (psi): 21

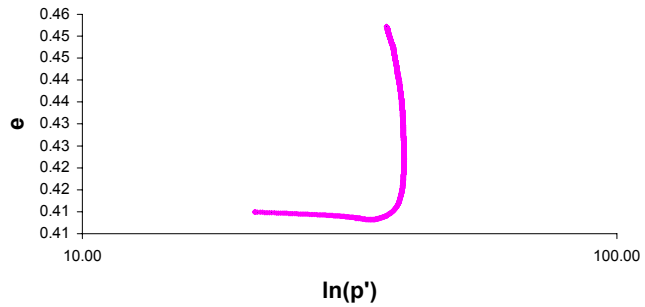
Stress Path (q:p')



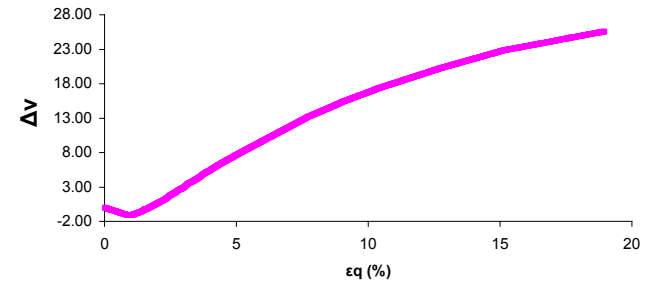
q vs ϵ_q



e vs $\ln(p')$

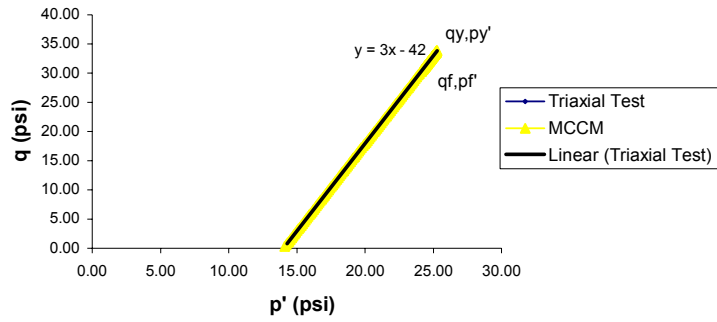


Δv vs. ϵ_q

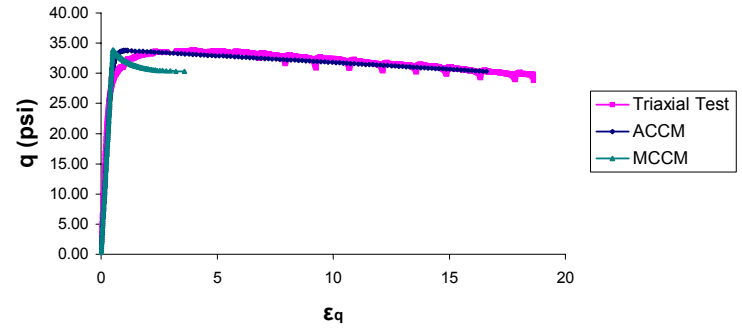


Test # : 21516
 Initial p' (psi): 14

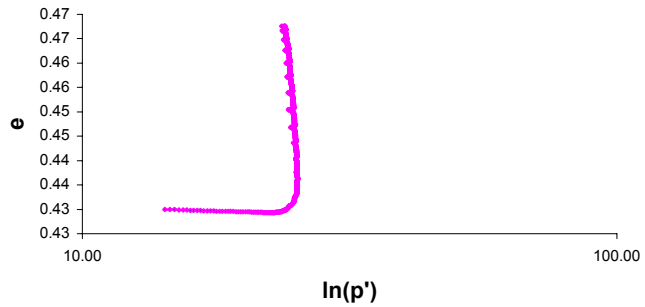
Stress Path (q:p')



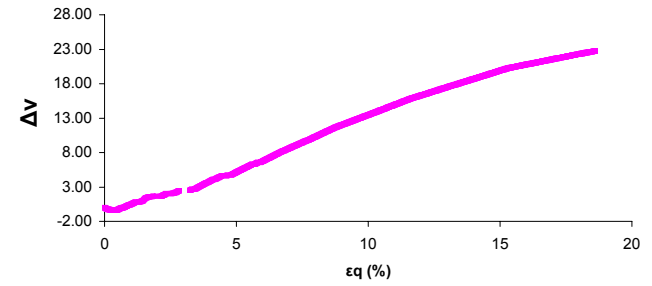
q vs ϵ_q



e vs $\ln(p')$

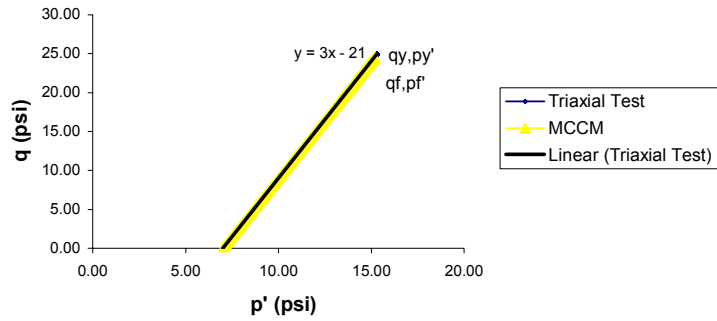


Δv vs. ϵ_q

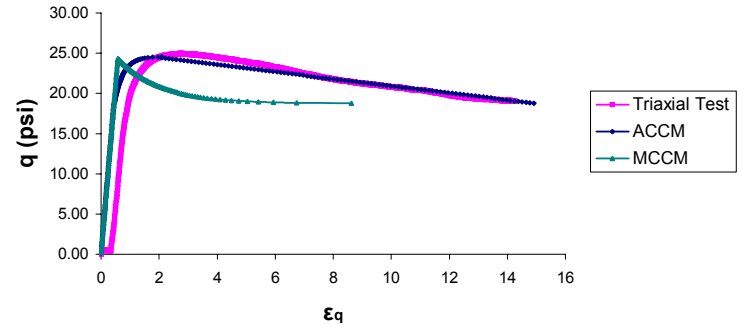


Test # : 21548
 Initial p' (psi): 7

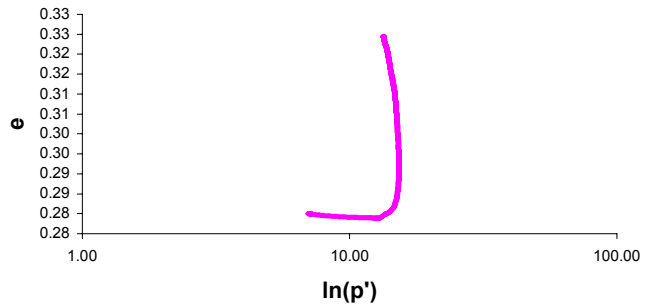
Stress Path (q:p')



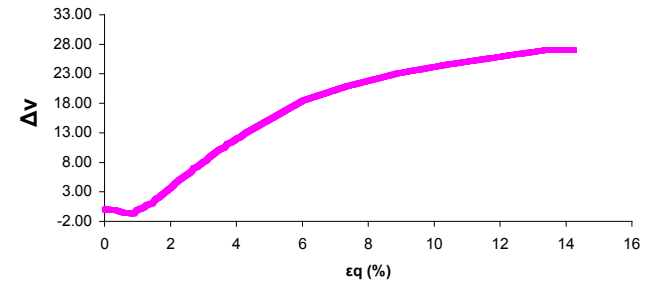
q vs ϵ_q



e vs $\ln(p')$

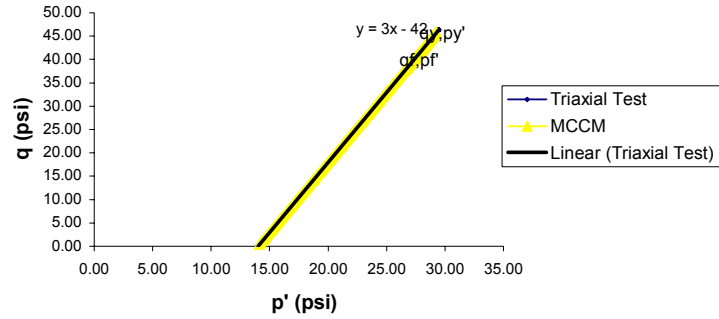


Δv vs. ϵ_q

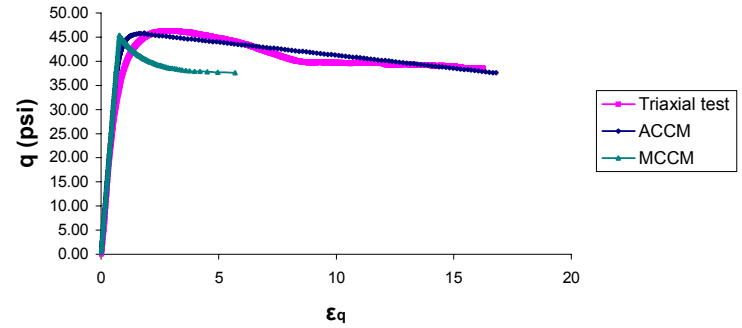


Test # : 21548
 Initial p' (psi): 14

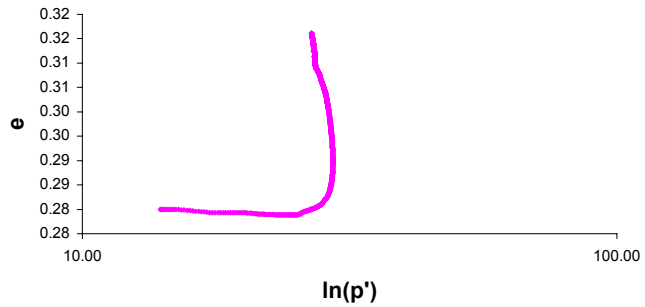
Stress Path (q:p')



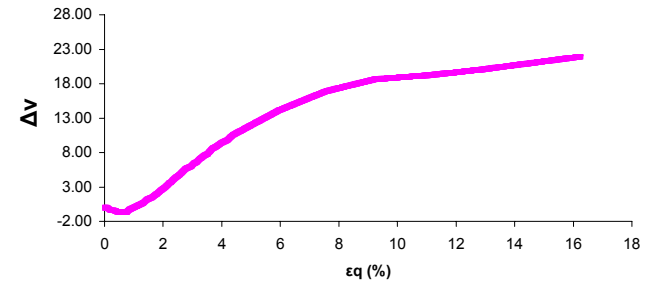
q vs ϵ_q



e vs $\ln(p')$

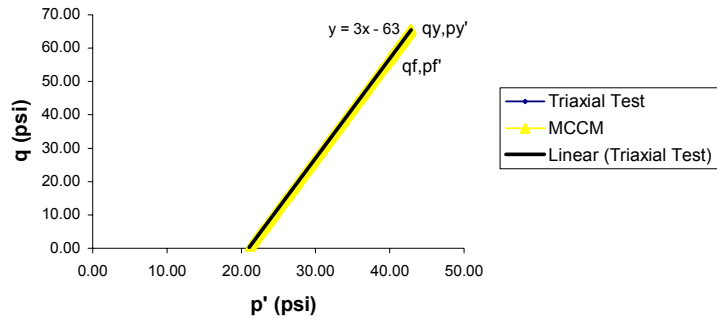


Δv vs. ϵ_q

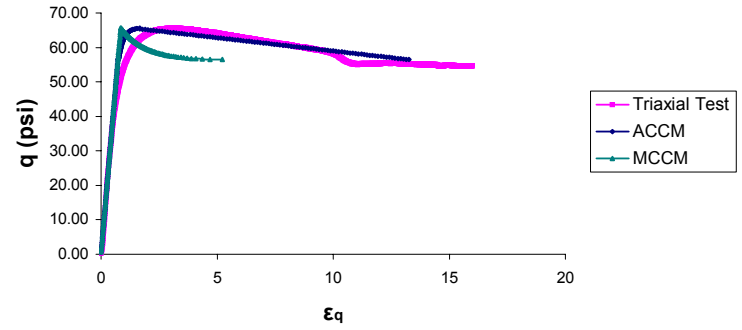


Test # : 21548
 Initial p' (psi): 21

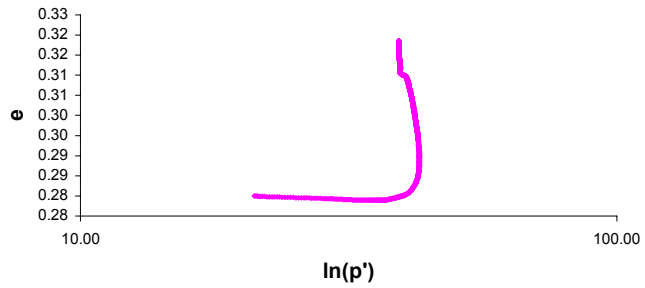
Stress Path (q:p')



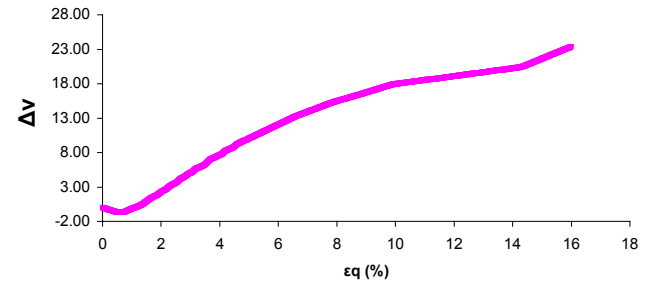
q vs ϵ_q



e vs $\ln(p')$



Δv vs. ϵ_q



APPENDIX C

Matlab Program Cofiguration for the Modified Cam Clay Model:

```
function result = CD3(phi,pemo,eo,v,E,k,lambda,sigmaeAo,pem)
```

```
MAX=100000;
```

```
disp(' ');
```

```
disp('Results');
```

```
disp(' ');
```

```
OCR=(pem)/(pemo);
```

```
fprintf('the overconsolidation ratio is, OCR=%3.2f\n\n',OCR);
```

```
sigmaA=[];
```

```
dsd=[];
```

```
dq=[];
```

```
dp=[];
```

```
dpe=[];
```

```
p=[];
```

```
pe=[];
```

```
q=[];
```

```
n=[];
```

```
Epq=[];
```

```
dEpq=[];
```

```
dEq=[];
```

```
Eq=[];
```

```
Epp=[];
```

```
dEpp=[];
```

```
Etq=[];
```

```
Eep=[];
```

```
qcsl=[];
```

```
dsd(1)=0;
```

```
dq(1)=0;
```

```
p(1)=sigmaeAo;
```

```
dp(1)=0;
```

```
dpe(1)=dp(1);
```

```
pe(1)=sigmaeAo;
```

```
peo(1)=sigmaeAo;
```

```
dpeo(1)=0;
```

```
q(1)=0;
```

```
n(1)=0;
```

```
Epq(1)=0;
```

```
qcsl(1)=0;
```



```

Eeq(1)=0;
dEpq(1)=0;
Epp(1)=0;
Eep(1)=0;
Etq(1)=0;
dEpp(1)=0;
Eap(1)=0;
dEap(1)=0;
Etq(1)=0;
v(1)=v;
qcs1(1)=0;
G=E/(2*(1+v))
M=(6*sin(phi*pi/180))/(3-sin(phi*pi/180))

%-----Yield Calculation Equation
pemy=pem;
%-----Cuadratic Equation-----
a= M^2+9;
b=-M^2*pem-18*sigmaeAo;
c=9*sigmaeAo^2;
pey1=(-b+sqrt((b^2)-(4*a*c)))/(2*a);
q1=3*(pey1-sigmaeAo);
pey2=(-b-sqrt((b^2)-(4*a*c)))/(2*a);
q2=3*(pey2-sigmaeAo);
if q1>=0
    pey=pey1
    qy=q1
else
    pey=pey2
    qy=q2
end
%-----end Cuadratic Equation
dsdy=qy;
ny=qy/pey
%----- End Yield Calculation
%-----Failure Calculation
pf=3*sigmaeAo/(3-M)
qf=M^3*sigmaeAo/(3-M)
nf=qf/pf;
ef=eo-k*log(pf/sigmaeAo)
ey=ef-(-lambda+k)*log(pey/pf)
%-----End Failure Calculation
%-----Loop
retro=0;
jump=0;

```



```

e(i)=eo-k*log(pe(i)/sigmaeAo);
Etq(i) = (Eeq(i) + Epq(i))*100;
Ety=Etq(i);
e(i)=ef+k*log(pe(i)/pf);
%-----MCC
peo(i)= pe(i)*(ny^2+n(i)^2)/ny^2;
%-----

else

e(i)=ey-15*(-lambda)*log(pey/pe(i));
%-----PLASTICAS -----
%-----MCC
peo(i)= pe(i)*(ny^2+n(i)^2)/ny^2;
%-----
dpeo(i)= peo(i)-peo(i-1);
dEpp(i)=- (lambda-k)/(1+e(i))*dpeo(i)/peo(i-1);
y=n(i-1)/(-nf^2+n(i-1)^2);
dEpq(i)=dEpp(i)*2*n(i-1)/(-nf^2+n(i-1)^2);
Eeq(i)=0;
Epq(i)=Epq(i-1)+dEpq(i);
Etq(i) =Etq(i-1) + dEpq(i)*100;
end

% escribe las tres columnas con datos
fprintf(fid, '%4.3f', Etq(i));
fprintf(fid, '%4.3f', pe(i));
fprintf(fid, '%4.3f', q(i));
fprintf(fid, '\n');

if ((n(i)<=M*1.001)&&(retro==1))
    break;
end
end
Ety=Ety
ETQ=Etq(i)
%----- End Loop

% cierra archivo
fclose(fid);

% Plots
figure, plot(Etq, q);
fprintf('comment in eq-q plot: ELASTIC and PLASTIC STRAINS PRESENT until
eq=%4.3f\n\n', Etq(i));

```

```
title('Drained Test & Heavily Overconsolidated Soil: "q vs Eq"');
xlabel('Shear Strain (eq) (%)');
ylabel('Deviator Stress "q" ');
grid;
figure,plot(pe,q);
fprintf('comment in pe-q plot:ELASTIC and PLASTIC STRAINS PRESENT until
pe=%4.3f\n\n',pe(i));
title('Drained Test & Heavily Overconsolidated Soil: "q vs p" (TSP=ESP)');
xlabel('p');
ylabel('q');
grid;
%End Plots
```

Matlab Program Cofiguration for the Adapted Model:

```
function result = CD3(phi,pemo,eo,v,E,k,lambda,sigmaeAo,pem)
```

```
MAX=100000;
```

```
disp(' ');
```

```
disp('Results');
```

```
disp(' ');
```

```
OCR=(pem)/(pemo);
```

```
fprintf('the overconsolidation ratio is, OCR=%3.2f\n\n',OCR);
```

```
sigmaA=[];
```

```
dsd=[];
```

```
dq=[];
```

```
dp=[];
```

```
dpe=[];
```

```
p=[];
```

```
pe=[];
```

```
q=[];
```

```
n=[];
```

```
Epq=[];
```

```
dEpq=[];
```

```
dEq=[];
```

```
Eeq=[];
```

```
Epp=[];
```

```
dEpp=[];
```

```
Etq=[];
```

```
Etp=[];
```

```
Eep=[];
```

```
qcsl=[];
```

```
sigmaA(1)=sigmaeAo;
```

```
dsd(1)=0;
```

```
dq(1)=0;
```

```
p(1)=sigmaeAo;
```

```
dp(1)=0;
```

```
dpe(1)=dp(1);
```

```
pe(1)=sigmaeAo;
```

```
peo(1)=sigmaeAo;
```

```
dpeo(1)=0;
```

```
q(1)=0;
```

```
n(1)=0;
```

```
Epq(1)=0;
```

```

qcsl(1)=0;
Eq(1)=0;
dEpq(1)=0;
Epp(1)=0;
Eep(1)=0;
Etq(1)=0;
dEpp(1)=0;
Etq(1)=0;
Etp(1)=0;
v(1)=v;
qcsl(1)=0;
f=0;
G=E/(2*(1+v));
M=(6*sin(phi*pi/180))/(3-sin(phi*pi/180))

%-----Yield Calculation Equation
pemy=pem;
%-----Cuadratic Equation-----
a= M^2+9;
b=-M^2*pem-18*sigmaeAo;
c=9*sigmaeAo^2;
pey1=(-b+sqrt((b^2)-(4*a*c)))/(2*a);
q1=3*(pey1-sigmaeAo);
pey2=(-b-sqrt((b^2)-(4*a*c)))/(2*a);
q2=3*(pey2-sigmaeAo);
if q1>=0
    pey=pey1
    qy=q1
else
    pey=pey2
    qy=q2
end
%-----end Cuadratic Equation
dsdy=qy;
ny=qy/pey
%----- End Yield Calculation
%-----Failure Calculation
pf=3*sigmaeAo/(3-M)
qf=M^3*sigmaeAo/(3-M)
nf=qf/pf;
ef=eo-k*log(pf/sigmaeAo);
ey=ef-(-lambda+k)*log(pey/pf);
%-----End Failure Calculation
%-----Loop
retro=0;
jump=0;

```



```

q(i)=q(i-1)+dq(i);
n(i)=q(i)/pe(i);
retro=1;
end
end
if ((q(i-1)<qy)&&(retro==0))
    if ((q(i)<=qf)&&(retro==0))
        %-----ELASTICAS -----
        %-----MCC
        peo(i)= pe(i)*(ny^2+n(i)^2)/ny^2;
        %-----
        dEq(i)=dq(i)/(3*G);
        Eq(i)=Eq(i-1)+dEq(i);
        Epq(i)=0;
        e(i)=eo-k*log(pe(i)/sigmaeAo);
        Etq(i) = (Eq(i) + Epq(i))*100;
        dpeo(i)= peo(i)-peo(i-1);
        Epp(i)=0;
        dEep(i)=(k)/(1+e(i))*dpeo(i-1)/peo(i-1);
        Eep(i)=Eep(i-1)+dEep(i);
        Etp(i) = (Eep(i) + dEep(i))*100;
        else
            e(i)=ef+k*log(pe(i)/pf);
            %-----MCC
            peo(i)= pe(i)*(ny^2+n(i)^2)/ny^2;
            %-----
            dpeo(i)= peo(i)-peo(i-1);
            dEpp(i)=(k)/(1+e(i))*dpeo(i-1)/peo(i-1);
            Epp(i)=Epp(i-1)+dEpp(i);
            dEpq(i)=dEpp(i)*2*n(i-1)/(ny^2-n(i-1)^2);
            Epq(i)=Epq(i-1)+dEpq(i);
            Eq(i)=0;
            Etq(i) = Etq(i-1) + dEpq(i)*100;
            Etp(i) = Etp(i-1) + dEpp(i)*100;
            Ety=Etq(i);
        end
    else
        %e(i)=ey+(-lambda+k)*log(pe(i)/pey);
        e(i)=ey-15*(-lambda)*log(pey/pe(i));
        %-----PLASTICAS -----

        %-----MCC
        peo(i)= pe(i)*(ny^2+n(i)^2)/ny^2;
        %-----
        dpeo(i)= peo(i)-peo(i-1);
        dEpp(i)=-(-lambda-k)/(1+e(i))*dpeo(i-1)/peo(i-1);

```



```

Epp(i)=Epp(i-1)+dEpp(i);
y=n(i-1)/(-nf^2+n(i-1)^2);
dEpq(i)=dEpp(i)*8.0;
Eqq(i)=0;
Epq(i)=Epq(i-1)+dEpq(i);
Etq(i) =Etq(i-1) + dEpq(i)*100;
Etp(i) = Etp(i-1) + dEpp(i)*100;
end

```

```

% escribe las tres columnas con datos
fprintf(fid,'%4.3f',Etq(i));
fprintf(fid,'%4.3f',pe(i));
fprintf(fid,'%4.3f',q(i));
fprintf(fid,'\n');

```

```

if ((n(i)<=M*1.001)&&(retro==1))
    break;
end
end
end
Etqy=Etq
ETQ=Etq(i)
%----- End Loop

```

```

% cierra archivo
fclose(fid);

```

```

% Plots
figure,plot(Etq,q);
fprintf('comment in eq-q plot:ELASTIC and PLASTIC STRAINS PRESENT until
eq=%4.3f\n\n',Etq(i));
title('Drained Test & Heavily Overconsolidated Soil: "q vs Eq"');
xlabel('Shear Strain (eq) (%)');
ylabel('Deviator Stress (q) ');
grid;
figure,plot(pe,q);
fprintf('comment in pe-q plot:ELASTIC and PLASTIC STRAINS PRESENT until
pe=%4.3f\n\n',pe(i));
title('Drained Test & Heavily Overconsolidated Soil: "q vs pe" (TSP=ESP)');
xlabel('pe');
ylabel('q');
grid;
%End Plot

```

REFERENCES

- Alfaro, M., Crilly, T., Graham, J. and Tanaka, M., “ Modified Cam-Clay Modelling of Temperature Effects in Clays”, *Canada Geotech Journal*, 2001, Vol. 38, pp. 608-621.
- Bardet, J.P., “Application of Soil Plasticity Theory to Soil Behavior: A New Sand Model”, Research Report, California Institute of Technology, Pasadena, California, 1983.
- Carter J.P and Liu, M.D., “A Structured Cam Clay Model”, Research Report, University of Sydney, Department of Civil Engineering , R814, 2002.
- Chopra, M. B., “A Constitutive Model for Anisotropically Consolidated Clays Under Axisymmetric, Plane Strain and General Three Dimensional Loading Conditions”, M. S. Thesis, University of New York, Buffalo, N.Y., 1988.
- Collins, I.F. and Hilder, T., “A Theoretical Framework for Constructing Elastic/Plastic Constitutive Models of Triaxial Tests”, *International Journal for Numerical and Analytical Methods in Geomechanics*, Vol. 26, 2002, pp. 1313-1347.
- Dafalias, Y.F., “An anisotropic critical state clay plasticity model”, *International Conference on Constitutive Laws for Engineering Materials: Theory and Applications*, Elsevier Science Publishing Co. Inc, pp. 513-521, 1987.
- Das, B.M., “Principles of Foundation Engineering”, Brooks/Cole- Thompson, 5th edition, 2004.

- Das, B.M., "Principles of Soil Dynamics", Brooks/Cole- Thompson, 1992.
- Evetts, J. B., "Soil Properties: Testing Measurement, and Evaluation", Prentice-Hall, Inc., Upper Saddle River, New Jersey, 2000.
- Grant, D., "Cyclic Soil Plasticity", Dissertation, Instituto Universitario di Studi Superiori di Pavia, Italy, 2002.
- Jefferies, M. G., And Shuttle, D.A., "Dilatancy in General Cambridge-Type Models", *Geotechnique*, 2002, No. 9, pp. 625-638.
- Khalili, N. and Russel, A.R., "Drained Cavity Expansion in Sands Exhibiting Particle Crushing", *International Journal for Numerical and Analytical Methods in Geomechanics*, Vol. 26, 2002, pp. 323-340.
- Lancellotta, R., "Geotechnical Engineering", Zanichelli Editore S.p.A., Bologna, Italy, 1993.
- Massoudi, M. and Mehrabadi, M.M., "A Continuum Model for Granular Material: Considering Dilatancy and the Mohr-Coulomb Criterion", *Acta Mechanica*, 2001, Vol. 152, pp.121-138.
- Muir W., D., "Soil Behavior and Critical State soil Mechanics", Cambridge University Press, 1990.
- Parry, R.H.G., "Mohr Circles, Stress Paths and Geotechnics", E & FN Spon, an imprint of Chapman & Hall, London, 1995.
- Potts, D. and Zdravkovic, L., "Some Pitfall when Using Modified Cam Clay", Imperial College, London, U.K.
- Rahim, A., "Simply Cyclic Loading Model Based on Modified Cam Clay", *CRISP Consortium Ltd*, 2002, pp. 1-11.

Roscoe, K.H., Schofield, A.N., and Wroth, C.P., “ On the yielding of Soils”,
Geotechnique, Vol.8,1958, pp. 22-53.

Schofield, A. N., “Original Cam Clay”, *Keynote Lecture for the International Conference
on Soft Soil*, University of Cambridge, U.K., 1993.